REPORT DOCUMENTATION PAGE

AFRL-SR-AR-TR-03-

0359

Public reporting burden for this collection of information is estimated to average 1 hour per response, including the tin gathering and maintaining the data needed, and completing and reviewing this collection of information. Send comme collection of information, including suggestions for reducing this burden to Department of Defense, Washington Head Reports (0704-0188), 1215 Jefferson Davis Highway, Suite 1204, Arlington, VA 22202-4302. Respondents should be person shall be subject to any penalty for failing to comply with a collection of information if it does not display a curren YOUR FORM TO THE ABOVE ADDRESS.

1. REPORT DATE (DD-MM-YYYY) 18-07-2003	2. REPORT TYPE Final Technical Report	3. DATES COVERED (From - To) 12/1/2000 to 12/31/2002

4. TITLE AND SUBTITLE Cryogenic Cycling Behavior of Polymeric Composite Materials	5a. CONTRACT NUMBER
	5b. GRANT NUMBER AFOSR Grant#F49620-00-1-0132
	5c. PROGRAM ELEMENT NUMBER
6. AUTHOR(S) Dr. James C. Seferis	5d. PROJECT NUMBER
	5e. TASK NUMBER
	5f. WORK UNIT NUMBER

7. PERFORMING ORGANIZATION NAME(S) AND ADDRESS(ES) Polymeric Composites Laboratory University of Washington Department of Chemical Engineering Box 351750 Seattle, WA 98195-1750	8. PERFORMING ORGANIZATION REPORT NUMBER

9. SPONSORING / MONITORING AGENCY NAME(S) AND ADDRESS(ES) Dr. Charles Lee AFOSR/NL 4015 Wilson Blvd., Rm. 713 Arlington, VA 22203-1954	10. SPONSOR/MONITOR'S ACRONYM(S)
	11. SPONSOR/MONITOR'S REPORT NUMBER(S)

12. DISTRIBUTION / AVAILABILITY STATEMENT

Approve for Public Release: Distribution Unlimited.

13. SUPPLEMENTARY NOTES

14. ABSTRACT
The basis of this research was an exploration of the fundamental phenomena that determine the response of fiber-reinforced composite materials to thermal cycling between cryogenic and ambient temperatures. This analysis began with a phenomenological approach that investigated the role of the processing, structure, and properties of composite materials on their behavior at cryogenic temperatures. The components of a composite material, the fibers and the matrix, were investigated along with the interaction between the fibers and the matrix to determine the effects of composite structure and properties on performance. In addition, processing and thermal ramp rate effects on internal stresses were also investigated. This approach provided an understanding of which variables influence composite behavior at cryogenic temperatures. Once this knowledge base had been established it could be extended to predict and model the performance of composite materials and develop design procedures to produce composite materials with optimized performance. Overall, this work investigated the performance of composite materials at cryogenic temperatures through a phenomenological and theoretical approach that established a fundamental understanding of the science and engineering of composite materials.

20031006 080

15. SUBJECT TERMS
Microcracking, thermal cycling, composites, fracture

16. SECURITY CLASSIFICATION OF:			17. LIMITATION OF ABSTRACT	18. NUMBER OF PAGES	19a. NAME OF RESPONSIBLE PERSON
a. REPORT	b. ABSTRACT	c. THIS PAGE			19b. TELEPHONE NUMBER (include area code)

Standard Form 298 (Rev. 8-98)
Prescribed by ANSI Std. Z39.18

CRYOGENIC CYCLING BEHAVIOR OF POLYMERIC
COMPOSITE MATERIALS

AFOSR Final Technical Report
Grant #: F49620-00-1-0132

Dr. James C. Seferis
Polymeric Composites Laboratory
University of Washington
Benson Hall 243, Box 351750
Seattle, WA 98195-1750

Submitted to
Dr. Charles Lee
AFOSR/NL
4015 Wilson Blvd., Rm. 713
Arlington, VA 22203-1954

Reference Status: Internal report
BEDR Internal No.:   03:425:AFOSR:JCS

TABLE OF CONTENTS

LIST OF FIGURES

LIST OF TABLES

PEOPLE INVOLVED

Principal investigator:
     Dr. James C. Seferis   Boeing/Steiner Professor and Director
                                        Polymeric Composites Laboratory

Research Fellows:
     Dr. Brian Hayes

Graduate Students:
     J. Timmerman, M. Tillman, M. Nobelen, A. Dharia

PUBLICATIONS

A.K. Dharia, B.S. Hayes, and J.C. Seferis, 33rd International SAMPE Technical Conference, 33, p. 120 (2001).

J.F. Timmerman and J.C. Seferis, 48th International SAMPE Symposium and Exhibition, *Accepted*, (2003).

J.F. Timmerman and J.C. Seferis, Journal of Applied Polymer Science, *Accepted*, (2003).

J.F. Timmerman, B.S. Hayes, and J.C. Seferis, Journal of Composite Materials, *Accepted*, (2003).

J.F. Timmerman, B.S. Hayes, and J.C. Seferis, Polymer Composites, 24 1, p. 132 (2003).

J.F. Timmerman, B.S. Hayes, and J.C. Seferis, 34th International SAMPE Technical Conference, 34, (2002).

J.F. Timmerman, B.S. Hayes, and J.C. Seferis, 47th International SAMPE Symposium and Exhibition 2002, 47, p. 1119 (2002).

J.F. Timmerman, B.S. Hayes, and J.C. Seferis, Composites Science and Technology, 62 9, p. 1240 (2002).

J.F. Timmerman, M.S. Tillman, B.S. Hayes, and J.C. Seferis, Composites Part A: Applied Science and Manufacturing, 33A 3, p. 323 (2002).

J.F. Timmerman, B.S. Hayes, and J.C. Seferis, 33rd International SAMPE Technical Conference, 33, p. 1597 (2001).

J.F. Timmerman, M.S. Tillman, B.S. Hayes, and J.C. Seferis, 46th International SAMPE Symposium and Exhibition 2001, 46 (2001: A Materials and Processes Odyssey, Book 2), p. 2303 (2001).

J.F. Timmerman, M.S. Tillman, B.S. Hayes, and J.C. Seferis, 59th Annual Technical Conference of the Society of Plastics Engineers, Proc. SPE ANTEC '01, May 6-10, 2, p. 2100 (2001).

M. Nobelen, B.S. Hayes, and J.C. Seferis, Journal of Applied Polymer Science, Accepted for Publication (2003).

M. Nobelen, B.S. Hayes, and J.C. Seferis, Polymer Composites, Accepted for Publication (2002).

M. Nobelen, B. S. Hayes, and J.C. Seferis, 47th International SAMPE Symposium and Exhibition, 47II, p. 1539 (2002).

M. Nobelen, B.S. Hayes, and J.C. Seferis, 33rd International SAMPE Technical Conference, 33, p. 1619 (2001).

EXECUTIVE SUMMARY

This work focused on investigating the behavior of carbon fiber/epoxy composites at low temperatures. The generation of internal stresses and the formation of microcracks during thermal cycling between cryogenic and ambient temperatures were the specific phenomena addressed. A combination of a theoretical and phenomenological approach was used to observe and predict the formation of microcracks in carbon fiber/epoxy composites at cryogenic temperatures.

The type of fibers and the polymeric matrix used in the composites played a large role in determining the propensity for microcracking as well as the microcrack morphology in symmetric cross-ply carbon fiber/epoxy composites. The microcrack density increased and larger cracks were formed when fibers with larger tensile moduli and longitudinal coefficients of thermal expansion were used. Increased flexibility of the polymeric matrix decreased the glass transition temperatures of the laminates studied and increased the microcrack density. A curing agent that led to stiffer and more regular network structures resulted in a decrease in microcrack density. The presence of a rubber interpenetrating network toughener prevented the formation of microcracks in all of the laminates studied. The fibers and the matrix used in a composite altered the thermal stresses present in a material as well as the ability of the material to resist thermal stresses, and therefore, had a direct influence on matrix microcracking at cryogenic temperatures.

Symmetric cross-ply laminates were fabricated containing fibers with different surface chemistries, and consequently, differences in fiber-matrix adhesion. The laminates with good adhesion exhibited lower microcrack densities than the laminates with poor adhesion. Surfactant sized fibers outperformed traditional epoxy sized fibers and formed composites with improved mechanical properties and resistance to microcracking.

The effect of rubber type and concentration was investigated to understand how traditional toughening techniques performed at cryogenic temperatures. Variations in rubber amount (10 and 20 phr) and compatibility (two different acrylonitrile contents) with the model resin provided different levels of phase separation in the laminates. Five

resin systems were developed and impregnated into unidirectional carbon fibers to be cured at two different temperatures. Both the glass transition temperature and the interlaminar shear strength of the laminates were depressed due to the addition of rubber, particularly when rubber with a higher acrylonitrile content was used. Symmetric cross-ply laminates were exposed to cryogenic cycling and all but the most highly rubber modified of the composite materials formed microcracks. A higher rubber concentration gave a greater crack resistance and led to a decrease in the microcrack density.

Cross-linked carboxyl functionalized preformed rubber particles, carboxyl functionalized core-shell particles, and solid carboxyl functionalized rubber were used to modify the matrices of prepreg-based composites in order to obtain various distributions: Interlayer toughening, dispersion throughout the matrix, and an interpenetrating network, respectively. The eight different systems developed included a control, each rubber separately, and every combination. Interlayer toughening did not significantly reduce the crack density, but the dispersed core-shell particles reduced it by 50%. The dissolved solid carboxyl functionalized rubber, providing an interpenetrating network, was shown to reduce the microcracking the most efficiently. The level of microcracking in an inherently brittle system was reduced substantially by the addition of various types of rubber additives; furthermore, it was shown that the microcrack density was highly dependent on the distribution and amount of rubber added to the system.

Nanoparticle fillers were used as modifiers in carbon fiber/epoxy composites at concentrations much lower than those used for traditional fillers and a significant reduction in cryogenic microcracking was observed. The concentration of the particles and their distribution in the matrix were important parameters in the optimization of the benefits of nanoparticle reinforcement. The best reinforcement was provided by exfoliated and disordered intercalated structures, with more ordered intercalated structures offering little benefit. The mechanical properties and processing characteristics of the laminates studied were not adversely influenced by the presence of the nanoparticles and the thermal expansion characteristics were improved. It was shown that the resistance of traditional fiber-reinforced composite materials to microcracking during cryogenic cycling could be enhanced using nanoparticle modification.

The following lay-up schedules were subjected to a previously established thermal cycle for Kevlar® based composites: $[0_5/90_5]_s$, $[0/90]_{10}$, 20 ply unidirectional and 20 ply woven. After 1200 thermal cycles the greatest microcrack density was found in a symmetric cross-ply laminate on the $[90_5/0_5]_s$ side where the 90° layer contacted the bag. $[90_5/0_5]_s$, $[90_4/0_4]_s$, $[90_3/0_3]_s$ and $[90_2/0_2]_s$ symmetric laminates were prepared and exposed to a thermal cycle using ramp rates of 2.5°C/min, 5°C/min, 10°C/min and 20°C/min. It was found that a certain minimum thickness of the laminate was required to generate enough internal stress for microcracks to appear. A thermal ramp rate of 2.5°C/min allowed thermal equilibrium to be reached in the thickest panels, but at higher ramp rates a skin core effect was observed that hindered microcracking. For a given composite system and a specific thermal cycle, the lay-up and thickness of the laminate can be adjusted to maximize microcrack sensitivity.

A theoretical and experimental analysis was performed on carbon fiber/epoxy symmetric cross-ply laminates to investigate microcracking and the role of cure temperature on the development of thermal stresses at low temperatures. Experimental results correlated with the theoretical predictions of the development of thermal strains in composite materials. Microcracking occurred in all of the laminates tested, but the number and morphology of the microcracks was strongly dependent on the cure temperature. Higher stress free temperatures, residual thermal strains, and glass transition temperatures of the laminates were all the results of elevated cure temperatures. The larger stress free temperatures corresponded to increased microcrack densities and residual thermal strains. A model was developed that predicted the onset temperature for microcracking in symmetric cross-ply carbon fiber/epoxy laminates based on the thermal stresses in a laminate and the yield strengths of the ply groups in a laminate at sub-ambient temperatures. The model predicted the low temperature behavior of the ply groups in a laminate based on the room temperature properties of the plies. Microcrack formation caused a discontinuity in material properties that could be detected using dynamic mechanical analysis. Four different material systems were studied, and the model was found to accurately predict the onset temperature for microcracking in three of the four cases.

Taken as a whole, this work comprised a phenomenological and theoretical investigation of cryogenic microcracking in composite materials. The results presented here furthered the understanding of the causes and mechanisms of cryogenic microcracking and will be of utility in the development of composite materials and structures that operate at low temperatures.

CHAPTER 1: INTRODUCTION

1.1 COMPOSITE MATERIALS

Composite materials are composed of two or more distinct materials, a matrix and a reinforcing phase, that are combined to create a material with improved properties and performance over the individual constituents. The matrix serves as a protecting and supporting medium that transfers any applied loads to the reinforcing phase. Typically, the matrix is ductile and tough, and the reinforcing phase is strong, stiff, and has a low density. When the matrix and reinforcing phase are combined it can result in a material that is both strong and tough [1]. Additional advantages of composite materials result from their anisotropy and heterogeneity. The components of a composite material can be combined in various volume and weight fractions as well as different orientations. This allows the properties of a material to be customized on a macroscopic and microscopic scale [1-3].

The matrix in composite materials can be metal, polymer, or ceramic. The reinforcing phase can also be metal, polymer, or ceramic-based and is commonly used in the form of particles, whiskers, or fibers. Most discussions of composites focus on mechanical properties, but materials with different properties can be combined to create composites with improved optical, thermal, electronic, magnetic, or chemical properties. Some examples that illustrate the variety of composite materials and their applications include wood, concrete, superconducting wires, boron-reinforced aluminum, silicon carbide-reinforced alumina, and fiber-reinforced plastics [1, 4, 5].

1.2 FIBER-REINFORCED POLYMERIC COMPOSITES

1.2.1 Fibers

Several different types of fibers are used as the reinforcing phase in fiber-reinforced polymeric composite materials. These fibers differ in their chemical structure as well as their microscopic structural character. The most commonly used fibers for structural applications are carbon, glass, and aramid fibers. These fibers are used in different applications depending on the desired final properties of the material. The

important factors to be considered when choosing one of these fibers include density, tensile strength and modulus, compressive strength and modulus, coefficient of thermal expansion, thermal conductivity, electrical conductivity, toughness, compatibility with matrix, fatigue resistance, environmental durability, and cost [2].

Carbon fibers are a blend of amorphous and graphitic carbon and are used because of their large specific tensile strength and moduli, fatigue resistance, and low coefficient of thermal expansion. Disadvantages of carbon fibers include their high electrical and thermal conductivity and poor impact resistance [2].

Glass fibers are the most widely used reinforcing fibers in polymeric composites because of their low cost. Additional advantages include high tensile strength, high chemical resistance, and low electrical conductivity. The disadvantages of glass fibers are low tensile modulus, susceptibility to damage during processing, high density, and low fatigue resistance [2].

Aramid fibers are highly crystalline polymer-based materials. They have very low densities, high specific tensile strengths, and good resistance to impact and abrasion. They suffer from low compressive strengths, machining difficulties, and a poor-resistance to hot-wet environments [2, 6].

Reinforcing fibers in polymeric composite materials are used in continuous, chopped, woven, or braided forms. Continuous and woven forms are most commonly used because they produce the most efficient utilization of the fiber properties. The fibers are often coated with a polymer sizing or subjected to a chemical surface treatment to ensure good adhesion to the matrix [2].

1.2.2 Matrices

The polymeric matrix can be classified as either a thermoplastic or a thermoset [2, 7, 8]. The distinction between these two types of matrices results from differences in connectivity and structure on the molecular level. Thermoplastics are composed of long chains of atoms that are held together by intermolecular forces. This results in materials that can soften and flow under repeated applications of heat [7, 8]. Typical thermoplastics used in advanced composites include polyetheretherketone (PEEK),

polyphenylene sulfide (PPS), polyetherimide, and polyamideimide [2, 9-12].
Thermosets are materials composed of small molecules that react irreversibly to form a
network structure. In this case, the polymer chains are linked together by covalent bonds
and once reacted, the material may soften but will not flow under the application of heat
[7, 8]. Typical thermosets used in advanced composites include epoxies, cyanate esters,
phenolics, bismaleimides, and vinyl esters [2, 13]. Thermosets are more widely used
than thermoplastics, largely due to easier processing for thermosets and a much larger
resistance to creep [2].

1.3 COMPOSITE PROCESSING TECHNOLOGIES

1.3.1 Prepregging

Prepregging is a fundamental operation in the production of fiber-reinforced
composite materials. It is a process by which the fibers and the matrix are combined to
form a continuous tape that can be used to produce larger composite structures [2, 14-16].
Most prepregs contain thermosetting matrices, although a few thermoplastic prepregs are
used. Prepregging is widely used because of the large volume percentages (50 %) of
fibers that can be achieved, the ease of working with the finished material, and the
excellent properties of composites made using prepreg [2, 15, 16].

Two main types of prepregging operations are used: Hot melt and solution dip.
A hot melt process is shown in Figure 1-1. The polymeric matrix is placed on a hot plate
and formed into a film on release paper. The fibers are then impregnated with the matrix
by a series of rollers. The material then passes over a cooled plate to increase the
viscosity of the matrix and stop any reaction that may be occurring. The final properties
of the prepreg are determined by the line speed, the pressure of the impregnation rollers,
the temperature of the impregnation zone, and the thickness of the polymer film [16-18].

A solution dip process is used when a low matrix viscosity is necessary to
properly impregnate the fibrous reinforcement. This situation usually occurs when
woven fabric reinforcement is used. A solution dip process is shown in Figure 1-2. The
fabric is pulled through a resin bath where capillary forces draw the polymer solution into
the fabric. Nip rolls are then used to control the resin thickness and the solvent is

removed in a drying tower. The material passes over a cooled roll to stop any reaction and raise the viscosity of the matrix before the product is wound onto a roll. Solution dip prepregging is not used as often as hot melt because of the increased processing necessary and the environmental implications of solvent use [16].

1.3.2 Autoclaving

Once the prepreg material has been produced, it is cut into the appropriate shapes and stacked to form a laminate. This stack of laminas is then subjected to heat and pressure in an autoclave to cure and consolidate the material into a composite laminate. The prepreg stack is subjected to vacuum pressure before being placed in the autoclave in order to begin consolidation of the plies and remove any air or entrapped volatiles. The stack is then placed in a vacuum bag on a tool that is used in the autoclave to provide uniform consolidation pressure and remove any gases that are evolved during cure. A schematic of a typical vacuum bag is shown in Figure 1-3. The release film ensures that the part does not stick to the mold or the vacuum bag, and the breather distributes vacuum evenly over the part. The vacuum bag itself separates the assembly from the environment of the autoclave so that vacuum can be drawn on the part [15, 19].

The cure cycle in the autoclave usually consists of a ramp to the desired pressure, a ramp to the cure temperature, a hold at the cure temperature, a ramp to room temperature, and a ramp to ambient pressure. These parameters can be varied to control the final properties of the composite laminate. In some cases a hold at a lower temperature than the cure temperature will be used to improve consolidation of the part or a post cure will be used to increase material performance while still utilizing a relatively low cure temperature. During the autoclave cycle vacuum is applied to the vacuum bag until the pressure in the autoclave has become large enough to consolidate the part on its own. At this point, the bag is vented so that any entrapped gases or volatiles produced during cure are eliminated [15, 19].

1.4 SCOPE OF RESEARCH

The primary objective of this work was to understand how the process-structure-property relationship of polymeric composite materials relates to the response of composite materials to cryogenic temperatures. The methodology developed by Seferis et al. combines the process-structure-property relationship of polymeric composite materials with performance, design, and manufacturing using scaling concepts. This approach to fiber-reinforced composite materials is shown in Figure 1-4 [3, 20]. The behavior of composite materials at cryogenic temperatures is uniquely suited to take advantage of this approach to composite analysis. The processing of composite materials has a strong influence on their structure and properties, especially internal stresses, which relate directly to failure mechanisms at cryogenic temperatures [21-23]. This then connects to material performance at cryogenic temperatures and the intelligent design of materials with improved performance during and after exposure to low temperatures.

The basis of this research was an exploration of the fundamental phenomena that determine the response of fiber-reinforced composite materials to thermal cycling between cryogenic and ambient temperatures. This analysis began with a phenomenological approach that investigated the role of the processing, structure, and properties of composite materials on their behavior at cryogenic temperatures. The components of a composite material, the fibers and the matrix, were investigated along with the interaction between the fibers and the matrix and the lay-up schedule to determine the effects of composite structure and properties on performance. In addition, processing effects on internal stresses were also investigated. This approach provided an understanding of which variables influence composite behavior at cryogenic temperatures. Once this knowledge base had been established it could be extended to predict and model the performance of composite materials and develop design procedures to produce composite materials with optimized performance. Overall, this work investigated the performance of composite materials at cryogenic temperatures through a phenomenological and theoretical approach that established a fundamental understanding of the science and engineering of composite materials.

1.5 SUMMARY OF CHAPTERS

In chapter 2 the fundamentals of thermal cycling and its effect on composite materials are outlined. Thermal cycling results in the development of internal stresses that can cause material failure. Internal stresses are discussed and the failure mechanisms of composite materials during thermal cycling are explained. The implications of composite material failure and past work on the topic are presented. This chapter deals with the fundamental phenomena that occur during cryogenic cycling that will be investigated in later chapters.

In chapter 3 the effects of matrix and fiber variations on the cryogenic microcracking of carbon fiber/epoxy composites are investigated. The fibers and the matrix make up a composite material and a fundamental understanding of their role in the performance of composite materials at cryogenic temperatures is necessary to build a foundation for further analyses. The flexibility of the polymeric backbone, the curing agent used, the network structure of the matrix, and the presence of a rubber interpenetrating network were all examined to determine the role of the matrix. The effects of fiber type, which corresponded to the fiber strength, modulus, and longitudinal coefficient of thermal expansion, were investigated.

Chapter 4 builds off chapter 3 to analyze how adhesion between the fibers and the matrix influenced the behavior of carbon fiber/epoxy composites exposed to thermal cycling at cryogenic temperatures. The properties of a composite material are determined largely by the properties of their interfaces, and composite failure at cryogenic temperatures often propagates along the fiber-matrix interface. Effective adhesion between the fibers and the matrix was therefore expected to be an important variable in preventing microcracking at cryogenic temperatures.

Chapter 5 discusses the influence of carboxyl-terminated butadiene acrylonitrile (CTBN) liquid rubbers on the microcracking response of polymeric composite materials to cryogenic cycling. Matrices of carbon fiber/epoxy prepregs were modified with different concentrations of two CTBN liquid rubbers, which formed a second phase *in situ* during cure. The glass transition temperature and the interlaminar shear strength of the laminate systems were depressed due to the presence of CTBN in the epoxy phase.

An increase in total rubber concentration and lower rubber compatibility with the continuous phase were found to decrease and in some cases eliminate microcracking in laminates exposed to cryogenic cycling.

Chapter 6 focuses on the effect of elastomer type and distribution in prepreg matrices on the cryogenic microcracking of polymeric composite materials. Carbon fiber/epoxy laminates containing three different types of rubber modifiers, separately and in combination, were developed for testing in a cryogenic environment. Preformed rubber particles, core-shell rubber, and solid carboxyl functionalized rubber in solution were incorporated into the matrices of those laminates and cryogenic microcracking and mechanical experiments were performed. These rubber additives were used to obtain interlayer toughening, dispersed particles throughout the matrix, and interpenetrating network formation, respectively. The mode I and II fracture toughness and interlaminar shear strength properties of these materials were also investigated. Fracture toughness properties were improved while the ILSS decreased due to the presence of these rubber modifiers. It was observed that the presence of these modifiers reduced the microcrack density of the laminates exposed to cryogenic cycling.

Chapter 7 deals with the modification of the polymeric matrix using nanoparticles derived from layered silicate clays. This formed a nanocomposite matrix that was expected to improve the properties of the composite material through a reduction in internal stresses and an increase in matrix strength. The design of composite matrices to perform well at low temperatures is an important area to investigate, and the role of nanostructures in the performance of composite materials was determined.

Chapter 8 examines the role of laminate geometry and thermal ramp rates on cryogenic microcracking. A series of carbon fiber/epoxy based laminates with the same thickness were prepared to study the dependence of the microcracking performance of a commercial prepreg system on the lay-up schedule. The laminates were exposed to a previously established thermal cycle for Kevlar® materials and inspected for microcracking at fixed intervals of thermal cycles. This initial assessment was used to identify the lay-up resulting in the greatest level of microcracking that was then used to

evaluate the effect of thermal ramp rates and thickness of composite materials on the microcracking performance of the chosen prepreg system.

The objective of chapter 9 was to determine how processing, in this case cure temperature, influenced the behavior of composite materials at low temperatures. A unique matrix resin was developed so that carbon fiber/epoxy composites could be cured at a variety of temperatures without any significant changes in network structure or degree of cure. The cryogenic microcracking of the laminates cured at different temperatures was determined, and the residual stresses in model laminates were calculated and compared with the experimental results. This chapter related processing to performance and presented a model of residual stress development in composite materials.

Chapter 10 expands on chapter 9 to develop a predictive model for microcracking in composite materials at cryogenic temperatures. This model accounted for the variation in material properties at low temperatures and used a stress-based failure analysis to determine what level of thermal stress would cause microcrack formation. This chapter showed that microcracking could be predicted based on the room temperature properties of a material, appropriately modified, using a straightforward modeling methodology.

Chapter 11 presents conclusions based on the presented work and describes research paths to be explored in the future.

NOTES TO CHAPTER 1

1. Schaffer, J.P., A. Saxena, S.D. Antolovich, T.H. Sanders, Jr. and S.B. Warner. 1995. The Science and Design of Engineering Materials, Irwin: Chicago, pp. 842.

2. Mallick, P.K. 1993. Fiber Reinforced Composites: Materials Manufacturing and Design, 2nd ed., Marcel Dekker: New York, pp. 566.

3. Seferis, J.C. and P.S. Theocaris, Eds. 1984. Interrelations Between Processing Structure and Properties of Polymeric Materials, Elsevier: New York, pp. 772.

4. McMurry, J. and R.C. Fay. 1995. Chemistry, Prentice Hall: Englewood Cliffs, NJ, pp. 1001.

5. Ashby, M.F. and D.R.H. Jones. 1996. Engineering Materials 1: An Introduction to Their Properties and Applications, 2nd ed., Butterworth Heinemann: Boston, pp. 306.

6. Hancox, N.L. 1984. The Environmental Response of Hybrid Composites, Journal of Materials Science, 19(6): 1969.

7. Rodriguez, F. 1996. Principles of Polymer Systems, 4th ed., Taylor and Francis: Washington D.C., pp. 732.

8. Rosen, S.L. 1993. Fundamental Principles of Polymeric Materials, 2nd ed., John Wiley and Sons, Inc.: New York, pp. 419.

9. Lawrence, W.E. 1992. Processing Induced Internal Stresses in Advanced Thermoplastic Composite Laminates, Ph. D. Dissertation, University of Washington, pp. 303.

10. Nelson, K.M., J.C. Seferis and H.G. Zachmann. 1991. Solvent-Induced Crystallization in Polyetherimide Thermoplastics and Their Carbon Fiber Composites, Journal of Applied Polymer Science, 42: 1289.

11. Ostberg, G.M.K. and J.C. Seferis. 1987. Annealing Effects on the Crystallinity of Polyetheretherketone (PEEK) and Its Carbon Fiber Composite, Journal of Applied Polymer Science, 33: 29.

12. Velisaris, C.N. and J.C. Seferis. 1986. Crystallization Kinetics of Polyetheretherketone (PEEK) Matrices, Polymer Engineering and Science, 26: 1574.

13. Goodman, H.S. 1986. Epoxy Resins, in Handbook of Thermoset Plastics, Noyes Publications: Park Ridge, NJ, p. 132.

14. Seferis, J.C. and K.J. Ahn. 1989. <u>Prepreg Processing Science and Analysis</u>, *Proceedings of 34th International SAMPE Symposium*, 34: 63.

15. Seferis, J.C., R.W. Hillermeier and F.U. Buehler. 2001. <u>Prepregging and Autoclaving of Thermoset Composites</u>, *in Polymer Matrix Composites*, Elsevier: New York, p. 701.

16. Gutowski, T.G., Ed. 1997. <u>Advanced Composites Manufacturing</u>, John Wiley and Sons: New York, pp. 600.

17. Ahn, K.J. and J.C. Seferis. 1993. <u>Prepreg Processing Science and Engineering</u>, *Polymer Engineering and Science*, 33(18): 1177.

18. Ahn, K.J. and J.C. Seferis. 1993. <u>Prepreg Process Analysis</u>, *Polymer Composites*, 14(4): 346.

19. Ciriscioli, P.R. and G.S. Springer. 1990. <u>Smart Autoclave Cure of Composites</u>, Technomic Publishing Company, Inc.: Lancaster, PA, pp. 161.

20. Seferis, J.C., S. Zeng, A.G. Miller, D.S. Krebs and C. Blohm. 1993. <u>Composite Structures in Commercial Aircraft: From Research and Development to Field Experience</u>, *Proceedings of National Academy of Athens*, Athens, 68: 275.

21. Adams, D.S., D.E. Bowles and C.T. Herakovich. 1986. <u>Thermally Induced Transverse Cracking in Graphite-Epoxy Cross-Ply Laminates</u>, *Journal of Reinforced Plastics and Composites*, 5: 152.

22. Berman, J.B. and S.R. White. 1996. <u>Theoretical Modeling of Residual and Transformational Stresses in SMA Composites</u>, *Smart Materials and Structures*, 5(6): 731.

23. Bailey, J.E., P.T. Curtis and A. Parvizi. 1979. <u>On the Transverse Cracking and Longitudinal Splitting Behavior of Glass and Carbon Fibre Reinforced Epoxy Cross Ply Laminates and the Effect of Poisson and Thermally Generated Strain</u>, *Proceedings of the Royal Society of London, Series A.*, 366: 599.

LIST OF FIGURES

Fiber Tows
Top Paper Reel
Comb
Impregnation roll
Pull Rolls
Top Paper Take-up Reel
Doctor Blade
Resin
Filming Plate
Impregnation Plate
Chill Plate
Prepreg Take-up Reel
Bottom Paper Reel
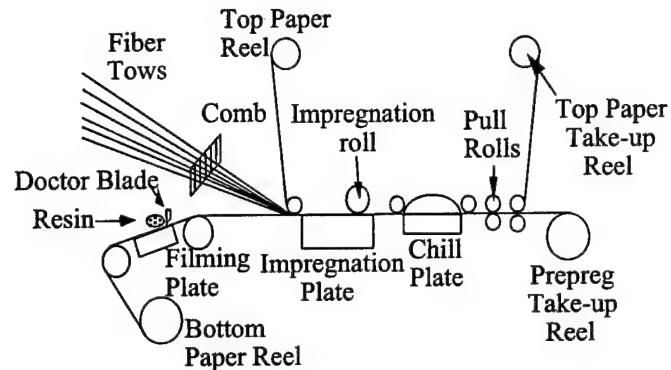
Figure 1-1. Hot melt prepregging operation

Drying Tower
Traction Unit
Unwind Roller
Wind-up Roller
Traction Unit
Nip Rollers
Carbon Fabric
Prepreg
Resin Bath
Cooling Roller
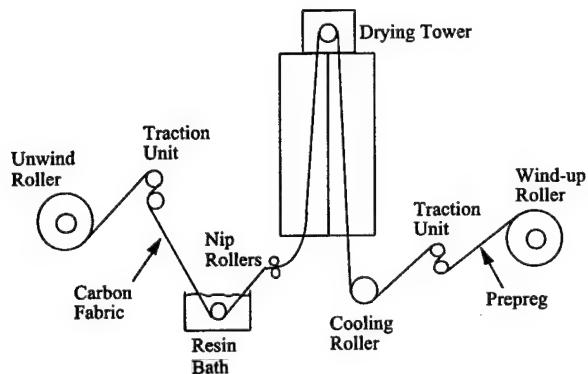
Figure 1-2. Solution dip prepregging operation

Nylon Bagging Film
Breather
Part
Vacuum Tape
Vacuum line
Tool
FEP Release Film
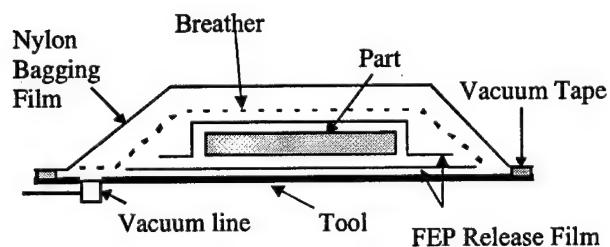
Figure 1-3. Typical vacuum bagging operation
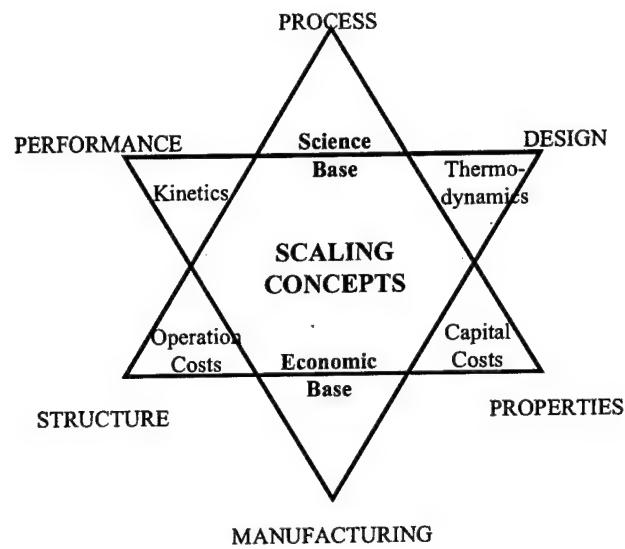
Figure 1-4. Double trinity of characterization of composite materials

CHAPTER 2: THERMAL CYCLING INDUCED STRESSES IN FIBER-
REINFORCED POLYMERIC COMPOSITES

2.1 INTRODUCTION

Fiber reinforced composites continue to be targeted for more applications in extreme environments. Work in the past focused on understanding high temperature exposure of composite materials and the mechanisms of degradation and deterioration at these conditions. While research is ongoing in this area and is still necessary, more recent uses for composites in low temperature and cryogenic applications demand increased attention [1]. Some specific uses for fiber-reinforced composites in these applications are for fuel containment of liquid oxygen and hydrogen or containment of liquid helium for cooling applications. When these tanks are filled or emptied the temperature of the composite material can change rapidly, which may damage the structure. The issue of thermal shock and rapid material cycling needs to be explored in detail to provide a fundamental understanding of composite failure caused by exposure to cryogenic temperatures.

Since designs for cryogenic fuel tanks are not specified, and the tanks are not likely to be monolithic structures, the effects of honeycomb materials and adhesives are important in the performance of composite materials used for cryogenic liquid storage. Past work by the Boeing Company identified the importance of film adhesives in these applications since rib stiffened structures may be desirable and the use of metallic bolts is not feasible [2]. In addition, as emphasized by the Boeing Company, the composite materials are never statically loaded, and therefore, should also be tested under vibration or dynamic loading for a realistic approach to investigating their utilization [3].

Over the past two decades, a significant but limited quantity of work has been performed in investigating materials that are subjected to cryogenic exposure [1]. NASA specifies that toughened thermosets are the most likely candidates for cryogenic applications in the future [4]. In their research they have focused mainly on toughened epoxy-based prepreg systems such as Hercules IM7/8551-7. Boeing/NASA has also focused on a similar material for their work on the DC-Y composite cryotank, namely Hercules 8552 [2]. Most, if not all research has been performed on commercial prepreg or composite

materials and has been typically characterization studies. Of the research that has been conducted in this area, Markley et al. were one of the only investigators to use epoxy resins of known and described compositions [5]. This work was only done for resins, but a significant amount of data was generated on many model systems; however, no explanations were given as to the findings. They found a general trend that that the compressive modulus at −196°C was constant for the systems investigated and independent of the 27°C modulus. They also determined that flexiblizing agents that greatly reduced warm temperature modulus did not affect cold temperature modulus and caused slight increases in the −196°C modulus.

In a summary of past work presented by Nettles and Biss, it is reported that cryogenic temperatures have a significant effect on thermosetting and thermoplastic resins [4]. The important findings were that all the resins tested got more brittle when at cryogenic temperatures. An interesting finding in their work was that the fracture strain was found to increase with toughened thermosets and thermoplastic matrix composites at cryogenic temperatures but decreased if the thermoset was untoughened. Similarly, the ultimate tensile strength of the entire composite increased with decreasing temperature for thermoplastics and toughened thermoset matrices but decreased for untoughened thermosets. They observed a marginal increase in matrix strength with decreasing temperature but a modest increase in matrix stiffness with decreasing temperature. Other research has shown that the tensile strength can increase by as much as two fold when cooled to −196°C, but the moduli were much less temperature dependent, increasing usually only 10-20% when cooled from 27 to -196°C [6].

Clark et al. stated that the application of polymers at low temperatures is determined by their flexibility and toughness [1]. These properties are closely linked to molecular movements in their glassy state, which are shown as specific secondary relaxations in the mechanical vibration spectrum [1]. In this pursuit, some preliminary investigations have been conducted analyzing thermal conductivity in the −272.9 to 27°C temperature range, but how these thermal conductivities translate into thermal expansion and mechanical behavior has yet to be determined [7-9].

A number of investigators have also pursued work in the development of testing methods for composite materials at cryogenic temperatures [10, 11]. Sereining and Gross developed testing methods for determining the thermal expansion/contraction of epoxies at cryogenic temperatures [8]. In addition to laboratory type testing, methods have been established for analyzing and testing sub-component structures [12-14]. Others have focused on actual fuel storage tanks [15].

In meeting ease of fabrication issues, work has been performed on skin and stringer bond line analyses for rib stiffened structures. This work is critical in manufacturing adhesively bonded structures for streamlining the production process and ultimate weight reduction [2].

There has been some research on the microcracking behavior of composite materials when exposed to cryogenic temperatures. However, this usually has focused on the construction of the laminate with nothing mentioned about the mechanisms. For example, Epstein and Ruth specified that the problem of microcracking can be mitigated by selection of materials less prone to microcracking, such as materials with ply lay-ups with low-angle orientations, laminates made from thinner plies and fabrics, composites with minimized fiber twist, and post cured composite structures [16]. While this is useful information, there is a gap in the fundamental causes of microcracking based on the composite components. Additionally, while there has been some work on cryogenic cycling, little is directly applicable to the in-service conditions experienced by composite structures [17, 18].

2.2 BACKGROUND

2.2.1 Sources of internal stresses

Increased thermal stresses are the underlying cause of microcracking in composites at cryogenic temperatures. Residual stresses develop in composite materials during cure and after cure as the temperature of the material falls below its stress free temperature. The stress free temperature is the temperature at which no residual stresses exist in the laminate. Dimensional changes in the matrix during cure usually drive the stress free temperature above the maximum processing temperature. Residual stresses are the result

of cure shrinkage of the matrix, Poisson's effects, differences in the coefficient of thermal expansion (CTE) between the fibers and the matrix, and anisotropy in the expansion of the individual plies [2, 19-22]. In a symmetric cross-ply laminate ($[0^{\circ}_{n} 90^{\circ}_{n}]_{s}$) the 0° and 90° ply groups behave differently as the temperature is reduced from the stress free temperature. When the temperature of the laminate decreases the carbon fibers that form the backbone of the composite expand in the longitudinal direction and contract in the axial direction. The resin behaves isotropically and contracts in all directions when the temperature decreases. Assuming that no slip between the matrix and the fibers occurs, a given ply will contract in the transverse direction and expand in the longitudinal direction [23]. Therefore, in a symmetric cross-ply laminate the plies are placed in a state of transverse tension and longitudinal compression when the temperature drops below the stress free temperature. Additional stresses are generated within each ply and at the fiber-matrix interface due to the mismatch in coefficient of themal expansion between the fibers and the matrix, Poisson's effects, and cure shrinkage. When a decrease in temperature occurs the matrix shrinks more than the fibers and generates a compressive hoop stress around the fiber, while the fibers expand axially and place the matrix in a state of tension. Lastly, the thickness of the laminate changes as the temperature is lowered due to contraction of the matrix and the fibers. The above factors combine to create a complex stress state in carbon fiber/epoxy composites as they are cooled to cryogenic temperatures. The ply groups in a laminate are least able to resist transverse tension and failure often occurs [24].

2.2.2 Failure mechanisms

When the internal stresses in a carbon fiber/epoxy composite exposed to low temperatures become large enough they can cause failure of the composite material. In a transverse tensile loading mode the fibers do not act as reinforcing elements; rather they behave like inclusions and stress concentrators. The fibers cause the development of local radial stresses at the fiber-matrix interface that are 50 % larger than the applied stress. In the case of fiber-reinforced composites with large fiber volume fractions (≥ 50 %), the stress fields around the individual fibers can interact and cause stress

concentrations of 75 % over the applied stress. These stresses eventually result in debonding or matrix failure that forms transverse cracks which propagate through the material [2, 25]. In some cases, other physical processes such as potholing and delamination occur as a result of internal stresses [2, 21, 22]. Chung et al. showed that the degradation of composite materials exposed to cryogenic temperatures is increased by thermal cycling between cryogenic and room temperature conditions [26].

Once a pathway for cryogenic liquids has been established in a storage tank structural failure can occur [13, 27]. Microcracking is particularly damaging for the storage of liquid hydrogen and helium as their small size allows them to diffuse through extremely small flaws. Once the escape of cryogenic liquids occurs a particularly damaging sequence of events is initiated. The released liquids can cause the condensation of liquid water and air on the tank or in the interior of sandwich tanks. Subsequent emptying and filling of the storage tank results in solid/liquid and solid/gas transformations that can ultimately result in failure of the entire structure.

NOTES TO CHAPTER 2

1. Clark, A.F., R.P. Reed and G. Hartwig. 1979. <u>Nonmetallic Materials and Composites at Low Temperatures</u>, *Proceedings of ICMC Symposium on Nonmetallic Materials and Composites at Low Temperatures*, Munich.

2. Nguyen, B. 1999. <u>Cryotank Skin/Stringer Bondline Analysis</u>, *Proceedings of 44th International SAMPE Symposium*, Long Beach, CA, 44: 856.

3. Nelson, K.M. 1999. <u>Composites in Cryogenic Fuel Tank Applications</u>, Boeing Materials Technology - Phantom Works, Seattle, WA.

4. Nettles, A.T. and E.J. Biss. 1996. <u>Low Temperature Mechanical Testing of Carbon-Fiber/Epoxy-Resin Composite Materials</u>, NASA-TP-3663, NASA.

5. Markley, F.W., J.A. Hoffman and D.P. Muniz. 1986. <u>Cryogenic Compressive Properties of Basic Epoxy Resin Systems</u>, *Advances in Cryogenic Engineering*, 32: 119.

6. Wigley, D.A. 1985. <u>Basic Cryogenics and Materials</u>, NASA-CR-177932, NASA.

7. Engeln, I. and M. Meissner. 1982. <u>Thermal Properties of Crystalline Polymers at Low Temperatures</u>, *Proceedings of Second ICMC Symposium on Nonmetallic Materials and Composites at Low Temperatures*, Geneva, 1.

8. Sereining, W. and F. Gross. 1982. <u>Method to Determine the Thermal Expansion of Epoxies, Inorganic Cements, and Polyester Resins at Cryogenic Temperatures</u>, *Cryogenics*, 22(1): 17.

9. Hust, J.G. 1975. <u>Low-Temperature Thermal Conductivity of Two Fibre-Epoxy Composites</u>, *Cryogenics*, 15(3): 126.

10. Kasen, M.B. 1988. <u>Strain-Controlled Torsional Test Method for Screening the Performance of Composite Materials at Cryogenic Temperatures</u>, *Journal of Materials Science*, 23(3): 830.

11. Oram, R.J. and E.G. Wolff. 1998. <u>Simple Guarded Hot Plate Technique for Making Thermal Conductivity Measurements of Composite Materials at Cryogenic Temperatures</u>, *Advances in Cryogenic Engineering*, 44: 349.

12. Wilkerson, C. 1996. <u>Acoustic Emission Monitoring of the DC-XA Composite Liquid Hydrogen Tank During Structural Testing</u>, NASA-TM-108520, NASA.

13. Ambur, D.R., J. Sikora, J.F. Maguire and P.M. Winn. 1996. <u>Development of a Pressure Box to Evaluate Reusable-Launch-Vehicle Cryogenic-Tank Panels</u>, NASA-TM-11406, AIAA Paper 96-1640, NASA.

14. Murphy, A.W., R.E. Lake and C. Wilkerson. 1999. <u>Unlined Reusable Filament Wound Composite Cryogenic Tank Testing</u>, NASA-TM-1999-209039, NASA.

15. Bianca, C., H.S. Greenberg and S.E. Johnson. 1996. <u>Reusable LH2 Tank Technology Demonstration Through Ground Test</u>, NASA-TM-111125, NASA.

16. Epstein, G. and S. Ruth. 1996. <u>Composites: A Key to Space Systems</u>, *SAMPE Journal*, 32(1): 24.

17. Han, K.S. and T. Ishikawa. 1983. <u>Thermal Cycling Effect on Mechanical Properties of RP/C</u>, *28th Annual Conference Preprint-Reinforced Plastics/Composites Institute*.

18. Liokhman, V.V., L.N. Kopsitskaya and V.M. Muratov. 1997. <u>Stress-Strained State of Cryogenic Vessel Under Cyclic Loading with Internal Pressure</u>, *Khimicheskoe I Neftyanoe Mashinostroenie*, 6: 22.

19. Crasto, A.S. and R.Y. Kim. 1993. <u>On the Determination of Residual Stresses in Fiber-Reinforced Thermoset Composites</u>, *Journal of Reinforced Plastics and Composites*, 12: 545.

20. Mallick, P.K. 1993. <u>Fiber Reinforced Composites: Materials Manufacturing and Design</u>, 2nd ed., Marcel Dekker: New York, pp. 566.

21. Jang, B.Z., Y.K. Lieu, S. Chang and L.R. Hwang. 1987. <u>Cryogenic Failure Mechanisms of Fiber-Epoxy Composites for Energy Applications</u>, *Polymer Composites*, 8(3): 188.

22. Bobrov, E.S., J.E.C. Williams and W. Iwasa. 1985. <u>Experimental and Theoretical Investigation of Mechanical Disturbances in Epoxy-Impregnated Superconducting Coils. Part 2. Shear-Stress-Induced Epoxy Fracture as the Principle Source of Premature Quenches and Training - Theoretical Analysis</u>, *Cryogenics*, 25(6): 307.

23. 1998. <u>Torayca Technical Reference Manual</u>, Toray Industries, Inc., Tokyo.

24. Adams, D.S., D.E. Bowles and C.T. Herakovich. 1986. <u>Thermally Induced Transverse Cracking in Graphite-Epoxy Cross-Ply Laminates</u>, *Journal of Reinforced Plastics and Composites*, 5: 152.

25. Wood, C. and W. Bradley. 1996. <u>A New Technique to Study the Interfacial Strength and Transverse Cracking Scenario in Composite Materials</u>, *in Fiber Matrix and Interface Properties, ASTM STP 1290*, ASTM: Philadelphia, p. 132.

26. Chung, K., J.C. Seferis and J.D. Nam. 1998. <u>Accelerated Aging of Polymer Composites Through Environmental Cycling Effect</u>, *Microstructural Science*, 25: 247.

27. Toth, J.M., W.J. Bailey and D.A. Boyce. 1985. <u>Fatigue at Low Temperatures</u>, *in ASTM STP 857*, ASTM: Philadelphia, p. 163.

CHAPTER 3: MATRIX AND FIBER INFLUENCES ON CRYOGENIC MICROCRACKING

3.1 INTRODUCTION

The need for high strength and low weight materials has made polymeric composites ideal for use in aerospace applications, which often require the storage and transportation of cryogenic liquids [1]. Dramatic changes in the structure and properties of composite materials can occur when they are exposed to cryogenic temperatures, particularly in a cyclical fashion [2-5]. Previous work has demonstrated the presence of structural changes and failure in composite materials after cryogenic cycling but has failed to elucidate the mechanism behind their occurrence [6-9].

Understanding the mechanisms behind thermal stress development and structural failure processes is key to preventing or controlling cryogenic microcracking. In this chapter, cryogenic cycling effects on symmetric carbon fiber/epoxy laminates were examined using model prepreg systems. The properties of the composite materials studied were altered through the introduction of variations in their structure and composition. Examination of the laminates after cycling provided insight into the mechanisms and origins of thermal stress-induced microcracking. The impact of fiber type and matrix composition on the cryogenic behavior of carbon fiber/epoxy composites was investigated. The influence of the matrix structure, morphology, and presence of an interpenetrating rubber network as well as the tensile modulus and CTE of the fibers on the low temperature behavior of model laminates was determined. It was shown that the tensile modulus and longitudinal CTE of the fibers, the curing agent chemistry, the presence of rubber toughening, the glass transition temperature of the matrix (T_g), and the flexibility of the backbone of the polymeric matrix had a direct and significant impact on the concentration, distribution, and morphology of microcracks created by thermal stresses.

3.2 EXPERIMENTAL

3.2.1 Materials

The model resins used as matrices were formulated using a mixture of commercial epoxy resins. The resins used were EPON® 828, 836, and 871 from Resolution Performance Products (formerly the Shell Chemical Company) and D.E.R. 661 from the Dow Chemical Company. The epoxy equivalent weights of these materials were 187, 315, 430, and 530 g/epoxy, respectively. D.E.R. 661 and EPON® 836 and 828 are based on diglycidyl ether of bisphenol-A and only differ in their backbone lengths. EPON® 871 is an aliphatic epoxy ester resin. Two curing agents that are common in commercial aerospace prepreg and adhesives were used. The first, 4,4'-diaminodiphenyl sulfone (DDS), HT976, was obtained from Ciba-Geigy. The second, 1-cyanoguanidine (dicy), Amicure® CG 1400 from Pacific Anchor Chemical Co., was accelerated with 3-(3,4-dichloro-phenyl)-1,1-dimethyl urea (diuron) from the Aldrich Chemical Company. Nipol 1472 from Zeon Chemicals Inc., a solid butadiene/acrylonitrile rubber with randomly distributed carboxyl functionality and 27 percent acrylonitrile content, was included in some of the formulations as a toughening agent. Chromium (2%) naphthenate, from OMG Americas Inc., was used as a catalyst for the epoxy/carboxyl esterification reaction [10].

Two resin series were prepared in this study. These series were designated 1 and 2 and their formulations can be found in Table 3-1. In series 1 EPON® 836:EPON® 871 ratios by weight of 62.5:37.5 and 50:50 were used to alter the backbone flexibility of the matrix and DDS and dicy/diuron were used as the curing agents. In series 2 a constant ratio of EPON® 828 to D.E.R 661 was used, while DDS and dicy/diuron were used as the curing agents and Nipol 1472 was used in some systems as a rubber modifier. In both series a stoichiometric amount of DDS was used. Dicy was incorporated at 5 parts per hundred resin (phr) and diuron was used at 2 phr due to their catalytic nature.

The components of each epoxy resin system were combined in an oil bath at 110°C and stirred until completely mixed. When DDS was used as the curing agent it was initially melted, added to the epoxy mixture in the oil bath, and stirred for one minute until the components were thoroughly mixed. When dicyandiamide and diuron were

used as the curing agent, a paste was made using dicyandiamide, diuron, and half of the 871 or 828 and incorporated into the epoxy mixture at 80°C. The resin was then quenched to room temperature and stored at -10°C before prepregging. For the rubber-toughened systems, the Nipol 1472 was washed with methanol to remove any surface talc and dissolved in acetone to make a 17 wt. % solution. The epoxy mixture was added to the rubber solution and mixed until it became uniform. The combination was then spread over a large surface area where the acetone was removed under vacuum at 100°C. This rubber-epoxy combination was then combined with the curing agent as detailed previously for the untoughened systems.

The resin systems were poured into molds and cured in an autoclave. The autoclave cure cycle consisted of a 2.8°C/min ramp to 177°C followed by a 90 minute hold at 177°C and a ramp down to 27°C at a rate of 2.8°C/min. The total consolidation pressure used during cure was 551 kPa. These resin plaques were machined into 0.5 x 0.5 x 0.32 cm (length x width x thickness) samples for thermal mechanical analysis testing.

This study utilized three types of carbon fibers with low, intermediate, and high tensile moduli. The fibers used were Toray T300, T800H, and M35J. Epoxy sizing was present on all of the fibers, and the filament count in each case was 12,000 filaments per tow. The tensile moduli of these fibers were 230, 294, and 343 GPa, respectively. The corresponding linear longitudinal coefficients of thermal expansion of these fibers were -0.41, -0.56, and -0.73 μm/(m°C) [11].

Three unidirectional prepregs consisting of the resins discussed previously and the fiber types described above were developed, for a total of 24 systems. The fibers were impregnated with the epoxy resin using a hot-melt prepreg machine [12]. The prepreg areal weight was set to 145 g/m² and the nominal resin content was 35±2 weight percent for all of the experiments. The filming and impregnation temperatures were 75°C and 85°C, respectively. The impregnation pressure was 275 kPa and the line speed was 1.22 m/min.

The resin content of the prepregs was determined by weighing a 5.08 x 5.08 cm square of prepreg, dissolving the resin with acetone, and weighing the dried fibers. This

technique is in accordance with ASTM D 3171-99 and Boeing Support Standard 7336 [13, 14]. Five samples from each batch of prepreg were used in the determination of resin content.

Symmetric cross-ply laminates were laid up using the above prepregs. The laminates consisted of 12 plies of prepreg in a $[0^o{}_3, 90^o{}_3]_s$ configuration. After every third ply the laminate was precompacted under vacuum pressure for two minutes during the lay-up before additional plies were positioned.

The autoclave cycle used to cure these laminates was the same as that described for the resin plaques, but the total consolidation pressure used during cure was 310 kPa. A larger pressure was used during the neat resin cure to prevent void formation. The vacuum bag was vented to the atmosphere when the autoclave pressure reached 104 kPa.

Once cured, the edges of the laminates were removed for consistency and the laminates were cut into 3.49 x 1.27 x 0.16 cm (length x width x thickness) samples for cycling studies. An additional 3.49 x 3.49 x 0.16 cm sample was prepared to compare the extent of microcracking in adjacent faces. These faces were designated 1 and 2 as demonstrated in Figure 3-1. The samples were sufficiently large to neglect edge effects. The edges of the laminates were polished prior to cycling to facilitate optical microscopy of the surfaces.

3.2.2 Analysis

Thermal mechanical analysis (TMA) was performed on the resins using a DuPont Instruments 2940 TMA controlled by thermal solutions 1.2J software. A macro-expansion probe was used with an applied force of 0.05 N. The samples were exposed to a ramp rate of 5°C/min from -150°C to 60°C in a nitrogen atmosphere.

Dynamic mechanical analysis (DMA) experiments were performed on the cured laminates with a TA instruments 2980 DMA in single cantilever mode controlled by Thermal Solutions 1.2 J software. A heating rate of 5°C/min to 300°C with a frequency of 1 Hz and an oscillation amplitude of 0.1 mm in nitrogen was used.

The cut and polished laminates were allowed to equilibrate in a desiccator at 22°C and were then placed in a liquid nitrogen bath (-195.8°C) for 10 minutes. After exposure

to liquid nitrogen, the samples were placed in the desiccator and allowed to return to room temperature. Each sample was exposed to a minimum of five cycles, or until optical microscopy revealed no further microcracking.

Optical microscopy was used to observe and document the response of the samples to cryogenic exposure. Each sample was examined prior to cycling to ensure that there were no initial cracks or defects in the surface. The samples were examined after each cycle at 50x, 100x, and 200x magnification using an optical microscope after returning to thermal equilibrium at room temperature in the desiccator. Photomicrographs were taken to document the sample response and the number of microcracks on the polished surface was counted.

The extent of microcracking in each material was quantified by dividing the total number of microcracks on the sample face by the face area to give a crack density value. Unless otherwise specified, face 1 was used in the microcracking analysis.

3.3 RESULTS AND DISCUSSION

3.3.1 Material influences on crack density

This chapter presents the results of an investigation into the trends and behaviors of composite materials when cycled between cryogenic and ambient temperatures. Optical microscopy revealed a variety of responses to cycling, such as potholing, delamination, and microcracking. Microcracking represented the majority of the structural changes in the samples, and as such, was the focus of this study.

The model resin formulations used in this analysis were chosen to provide a balance between strength and flexibility. The curing agents used were also selected to provide varying degrees of network regularity and different crosslink morphologies. These materials were selected to study the fundamental behavior of composites exposed to cryogenic cycling; however, they are not commercially viable for composite structures. EPON® 836 has an aromatic backbone that is relatively stiff and EPON® 871 has a more flexible aliphatic structure. As a result, in series 1 EPON® 836 imparts a higher modulus to the mixture while EPON® 871 provides increased backbone flexibility [15, 16]. The components of the resin in series 1 had similar epoxide equivalent weights, which

allowed alterations in the proportion of EPON® 871 in the resin to change the flexibility of the matrix backbone while maintaining a similar molecular weight between crosslinks. The incorporation of Nipol 1472 into series 2 served to toughen the system through the formation of an interpenetrating network and is representative of typical epoxy resin toughening agents [17, 18].

It should be noted that matrix 1d only formed acceptable prepreg on T300 fibers and, as such, no data exists for this system on higher modulus fibers due to the inability to fabricate laminates with these materials. Similarly, matrix 1c could not be formed into the appropriate neat resin samples and was not tested. Matrix 2a was extremely brittle and any samples formed from this material fractured during preparation.

Figure 3-2 documents the changes in the microcracking behavior of the laminates as the matrix and fibers were altered. The following general observations can be drawn from this figure. Laminates in which dicy and diuron were used as the curing agent contained more microcracks after cycling than the laminates that were cured with DDS for series 1. Raising the proportion of EPON® 871 in the resin formulation corresponded to larger levels of microcracking. Resin series 2 exhibited no cracking when toughened with Nipol 1472 and the untoughened formulation exhibited microcracking only when system 2b was combined with M35J fibers. It was observed that the laminates with lower glass transition temperatures displayed greater microcrack densities. Increased delamination and potholing of the surfaces of the laminates corresponded to increased levels of microcracking for all laminates.

The increase in microcrack density in systems 1c and 1d resulted partly from a decrease in the laminate strength as the proportion of EPON® 836 was reduced. When less EPON® 871 was used in the resin formulation, the flexible aliphatic portion of the backbone increased the ability of the laminates to resist microcracking. When larger proportions of EPON® 871 were used the overall strength of the matrix could have been degraded, which may have increased the microcrack density in laminates containing these matrices. This may have decreased the level of thermal stress at which microcracking occurred.

Increased backbone flexibility altered the response of the matrix to temperature

changes. Previous work has shown that flexible matrix segments are more mobile and occupy a greater effective volume, which raises the linear coefficient of thermal expansion (CTE) of the matrix [19]. Figure 3-3 shows the CTEs as determined by TMA for the resins studied. A small increase in the CTE at -125°C and a large increase in the CTE at 25°C between matrices 1b and 1d occurred as the proportion of 871 was increased from 37.5 to 50.0 wt.%. The disparity between the dimensional changes of the matrix and fibers, and therefore the difference between the expansion and contraction of the 0° and 90° plies, at low temperatures was enhanced as the level of EPON® 871 was raised, which in turn increased the stresses in the materials and caused more microcracking. Resin system 1a showed the largest CTE value; however, laminates containing this matrix showed the lowest levels of crack density in series 1. Laminates made with this resin contained greater thermal stresses, but it is proposed that the matrix was able to withstand greater stresses before failing, preventing extensive microcracking. Series 2 showed lower CTE values than those observed for series 1. This is partly responsible for the small microcrack density in laminates that contained series 2 as the matrix. Variations in the matrix chemistry and the incorporation of a rubber toughening agent could have altered the degree of adhesion between the fibers and the matrix. Microcracks tend to propagate along the fiber/matrix interface, and any change in the strength of adhesion in this area could have significantly altered the response of the composite materials to cryogenic cycling.

The choice of curing agent had a significant effect on the final morphology of the polymeric matrix, and as such, played a role in how the laminates responded to cryogenic cycling. DDS is a tetrafunctional amine curing agent with a rigid aromatic composition that forms a relatively regular network structure [20]. Dicyandiamide reacts through a much more complicated mechanism that can produce di, tri, and tetrafunctional reactive and catalytic species. Evidence also suggests that difunctional species produced in the reaction can act as chain extenders for epoxy resins [21]. The more irregular and flexible network created when dicy/diuron was used as a curing agent may have decreased the ability of the matrix to accommodate thermal stresses and contributed to the increase in microcrack density of the laminates. Figure 3-3 demonstrates that the use of dicy/diuron

as a curing agent caused a decrease in matrix CTE at 25°C and -125°C for series 1 and a negligible change for series 2. The fact that dicy/diuron reduced the matrix CTE and increased laminate microcracking would not be expected because lower thermal stresses were present in the laminate. The use of dicy/diuron probably weakened the matrix, reducing the level of thermal stress it could accommodate before microcracking.

The glass transition temperatures (T_g) of the laminates studied were obtained from the peak in loss modulus as determined by dynamic mechanical analysis. Increased microcracking with decreased Tg is shown in Figure 3-4. Larger EPON® 871 proportions and dicy/diuron cure increased backbone flexibility and epoxy chain length, which decreased the glass transition temperatures of the laminates [22, 23]. These same factors increased microcracking by decreasing the strength of the matrix and, in the case of EPON® 871 incorporation, increasing the CTE of the matrix.

Figure 3-2 shows the final crack density in the laminates studied as a function of the longitudinal CTE of the fiber used. The fiber tensile modulus increased by 27.8 percent from T300 to T800H and by 16.7 percent from T800H to M35J, which corresponded to a 36.6 percent increase in fiber longitudinal CTE from T300 to T800H and a 30.4 percent increase from T800H to M35J. Increasing the tensile modulus and negative longitudinal CTE of the fibers caused an increase in the crack density in all of the composite materials studied. No microcracking was observed when T300, a low modulus fiber, was used in conjunction with system 1a. The tensile modulus of the fibers influenced the microcrack morphology as well as the crack density. The microcracks typically became wider and more tortuous when higher modulus fibers were used.

Composites containing higher modulus fibers are more prone to microcracking. A higher tensile modulus corresponds to increasing crystallinity and orientation of the crystallographic basal planes parallel to the fiber axis [24]. This increases the negative longitudinal CTE of the fibers [24]. When the temperature was decreased the fibers contracted in the radial direction and expanded along the longitudinal axis while the matrix contracted in all directions [24]. Larger differences in the CTE between the fibers and the matrix increased the thermal stresses at low temperatures and caused a corresponding increase in microcracking. In addition, it has been shown for transverse

tensile mechanical testing that as the ratio of the fiber modulus to the matrix modulus increases the stress concentration at a fiber increases [24]. More total crack surface needed to be created and more material displaced in order to relieve the larger thermal stresses that were created in laminates containing fibers with high tensile moduli and CTEs. The change in aspect ratio of the fibers at low temperatures could have altered the physical properties of the laminates and their ability to resist internal stresses. Differences in fiber diameter and surface irregularities could have played a role in the cryogenic behavior of the laminates studied. M35J fibers have a diameter of 5 μm while T800H fibers have a diameter of 7-8 μm [24]. This difference could have changed the wetting and adhesion of the matrix to the fibers and altered the microcracking propensity of the materials studied.

3.3.2 Cryogenic microcracking

Microcracks propagated through the epoxy matrix transverse to the fibers in the x-direction as shown in Figure 3-1 and ended at the interface between the plies with different orientations. Figure 3-5 presents optical photomicrographs that document these phenomena in three representative laminates. Figure 3-5A presents a typical microcrack in face 1 of a model laminate. Delamination occurred in some cases when the microcracks encountered the interface between cross plies. This is illustrated well in Figure 3-5B. Examination of face 1 showed microcracks initiating at the laminate surface and propagating in the x-direction towards the interior of the specimen. For these laminates, the crack density was always larger on the bag side than the tool side. This can be attributed to the greater surface roughness on the bag side, which would provide more locations for crack initiation.

Investigation of faces 1 and 2 of a 3.49 x 3.49 x 0.16 cm laminate revealed that microcracking occurred in the central and outer plies of a $[0^{\circ}_3 \ 90^{\circ}_3]_s$ laminate. In face 2 microcracks initiated at the interface between the 0° and 90° plies and propagated across the central plies of the laminate in the x-direction, transverse to the fibers. Figure 3-5C contains an example of microcracking in the central plies. However, the crack density in the central plies of face 2 was lower than the crack density observed in the outer plies of

face 1. Microcracking in the central plies could provide a pathway for liquid to flow through the laminate. This could be disastrous for the storage of cryogenic liquids, particularly liquid hydrogen or helium [1].

All of the materials that microcracked in response to cryogenic cycling showed a large initial increase in the crack density, which generally leveled off after three or four cycles and reached a constant value. A representative example of this behavior is illustrated in Figure 3-6 for matrix 1a. Microcracking began soon after cyclic exposure to low temperatures was initiated, and once the stress was relieved to a level below the yield stress of the fiber/matrix interface, no more cracking occurred. This data indicated that the probability and severity of microcracking in a material can be determined after only a few cycles.

3.4 CONCLUSIONS

This chapter examined the propagation and distribution of microcracks in cryogenically cycled symmetric cross-ply carbon fiber/epoxy composites. Microcracks formed in some of the materials studied as a response to thermal stresses generated through cryogenic cycling. Cracking occurred in the polymeric matrix transverse to the fibers in both the inner and outer plies of autoclave cured $[0°_3 90°_3]_s$ laminates. The type of fibers and the polymeric matrix used in the composites played a large role in determining the propensity for microcracking as well as the microcrack morphology. Higher fiber tensile moduli resulted in increased microcrack density and larger cracks. Increased backbone flexibility caused an increase in microcrack density and decreased the glass transition temperatures of the laminates studied. The curing agent used in the matrix formulation also played a key role in the response of the resulting material to cryogenic cycling. The presence of a rubber interpenetrating network toughener prevented the formation of microcracks in all of the laminates studied. Collectively, it was shown that the fibers and the matrix used in a composite play an important role in determining the response to cryogenic cycling by altering the thermal stresses present in a material as well as the ability of the material to resist thermal stresses.

NOTES TO CHAPTER 3

1. Toth, J.M., W.J. Bailey and D.A. Boyce. 1985. Fatigue at Low Temperatures, in *ASTM STP 857*, ASTM: Philadelphia, p. 163.

2. Clark, A.F., R.P. Reed and G. Hartwig. 1979. Nonmetallic Materials and Composites at Low Temperatures, *Proceedings of ICMC Symposium on Nonmetallic Materials and Composites at Low Temperatures*, Munich.

3. Engeln, I. and M. Meissner. 1982. Thermal Properties of Crystalline Polymers at Low Temperatures, *Proceedings of Second ICMC Symposium on Nonmetallic Materials and Composites at Low Temperatures*, Geneva, 1.

4. Nguyen, B. 1999. Cryotank Skin/Stringer Bondline Analysis, *Proceedings of 44th International SAMPE Symposium*, Long Beach, CA, 44: 856.

5. Chung, K., J.C. Seferis and J.D. Nam. 1998. Accelerated Aging of Polymer Composites Through Environmental Cycling Effect, *Microstructural Science*, 25: 247.

6. Epstein, G. and S. Ruth. 1996. Composites: A Key to Space Systems, *SAMPE Journal*, 32(1): 24.

7. Han, K.S. and T. Ishikawa. 1983. Thermal Cycling Effect on Mechanical Properties of RP/C, *28th Annual Conference Preprint-Reinforced Plastics/Composites Institute*.

8. Liokhman, V.V., L.N. Kopsitskaya and V.M. Muratov. 1997. Stress-Strained State of Cryogenic Vessel Under Cyclic Loading with Internal Pressure, *Khimicheskoe I Neftyanoe Mashinostroenie*, 6: 22.

9. Nettles, A.T. and E.J. Biss. 1996. Low Temperature Mechanical Testing of Carbon-Fiber/Epoxy-Resin Composite Materials, NASA-TP-3663, NASA.

10. Martin, C.J. and J.C. Seferis. 1998. Effect of Prepreg Resin Composition on Honeycomb Core Crush, *Proceedings of 43rd International SAMPE Symposium*, Long Beach, CA, 43: 366.

11. 1998. Torayca Technical Reference Manual, Toray Industries, Inc., Tokyo.

12. Putnam, J.W., B.S. Hayes and J.C. Seferis. 1996. Prepreg Process-Structure-Property Analysis and Scale-Up for Manufacturing and Performance, *Journal of Advanced Materials*, 27(4): 47.

13. 1996. Resin Content and Fiber Areal Weight of Prepreg Fabric and Tape, Test Method For, BSS 7336, Boeing Materials Technology, Boeing Commercial Aircraft

Group, Renton, WA.

14. 1999. <u>Standard Test Methods for Constituent Content of Composite Materials</u>, ASTM D 3171-99, ASTM, West Conshohocken, PA.

15. <u>Heloxy Modifier 71</u>, Shell Chemicals, Houston, TX.

16. <u>EPON Resin 836</u>, Shell Chemicals, Houston, TX.

17. Drake, R. and A. Siebert. 1975. <u>Elastomer-Modified Epoxy Resins for Composite Applications</u>, *SAMPE Quarterly*, 6(4): 11.

18. Drake, R.S., D.R. Egan and W.T. Murphy. 1983. <u>Elastomer-Modified Epoxy Resins in Coating Applications</u>, *in Epoxy Resin Chemistry 2*, Washington, DC: American Chemical Society, p. 1.

19. Chompff, A.J. 1971. <u>Glass Points of Polymer Networks</u>, *in Polymer Networks: Structure and Mechanical Properties*, Plenum Press: New York, p. 145.

20. Keenan, J.D. and J.C. Seferis. 1979. <u>Effects of Moisture and Stoichiometry on the Dynamic Mechanical Properties of a High-Performance Structural Epoxy</u>, *Journal of Applied Polymer Science*, 24: 2375.

21. Gilbert, M.D., N.S. Schneider and W.J. McKnight. 1990. <u>Mechanism of the Dicyandiamide/Epoxide Reaction</u>, *Macromolecules*, 24: 360.

22. Gan, S. and J.C. Seferis. 1991. <u>A Viscoelastic Description of the Glass Transition-Conversion Relationship for Reactive Polymers</u>, *Journal of Thermal Analysis*, 37: 463.

23. Madsen, P.A. and R.T. Foister. 1989. <u>Network Structure and Properties of Imidazole-Cured Epoxy Novolac Adhesives</u>, *Journal of Applied Polymer Science*, 37: 1931.

24. Mallick, P.K. 1993. <u>Fiber Reinforced Composites: Materials Manufacturing and Design</u>, 2nd ed., Marcel Dekker: New York, pp. 566.

LIST OF TABLES

Table 3-1. Formulation of model resins

Series 1	Wt. Percent EPON® 836	Wt. Percent EPON® 871	phr[1] DDS	phr Dicyandiamide	phr Diuron
a	62.5	37.5	17.5	-	-
b	62.5	37.5	-	5	2
c	50.0	50.0	16.6	-	-
d	50.0	50.0	-	5	2

Series 2	Wt. Percent EPON® 828	Wt. Percent D.E.R. 661	phr Nipol 1472	phr DDS	phr Dicyandiamide	phr Diuron	phr Chromium Naphthenate
a	45.0	50.0	-	16.9	-	-	-
b	45.0	50.0	-	-	5	2	-
c	45.0	50.0	5.3	16.9	-	-	0.1
d	45.0	50.0	5.3	-	5	2	0.1

[1] phr: parts per hundred resin

LIST OF FIGURES
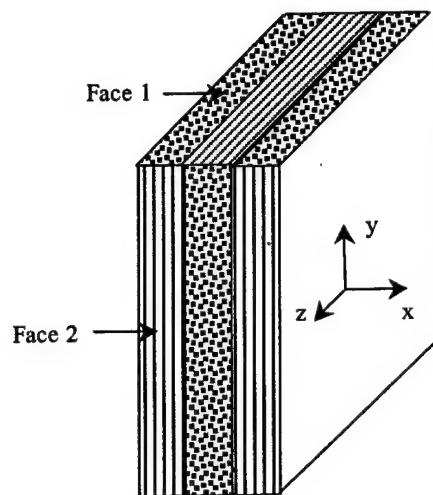
Figure 3-1. Polished faces of model laminates
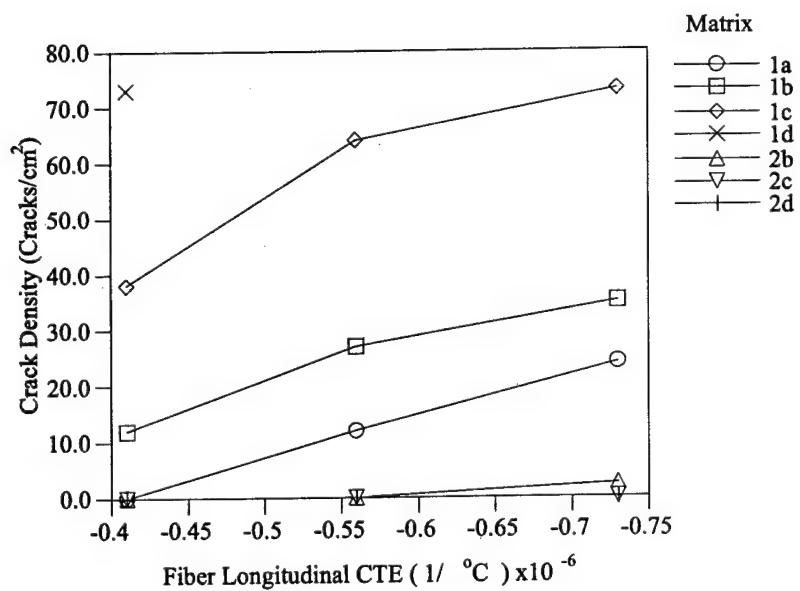
Figure 3-2. Crack density variation with fiber longitudinal CTE
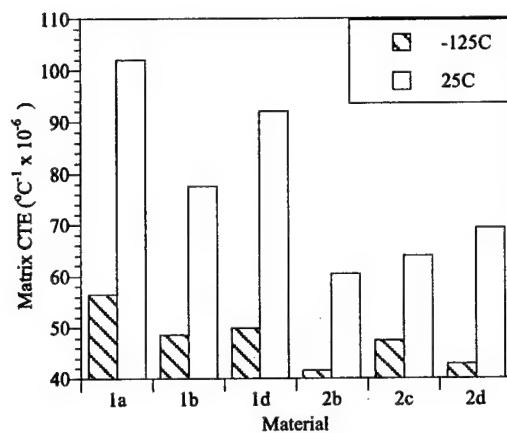
Figure 3-3. Matrix CTE variation with resin composition
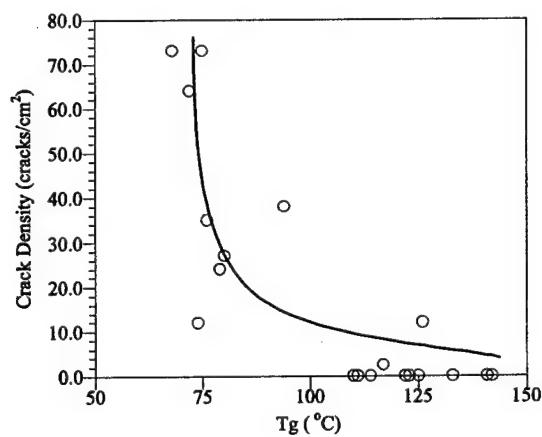
Figure 3-4. Crack density variation with laminate glass transition temperature as reported from the peak in dynamic loss modulus
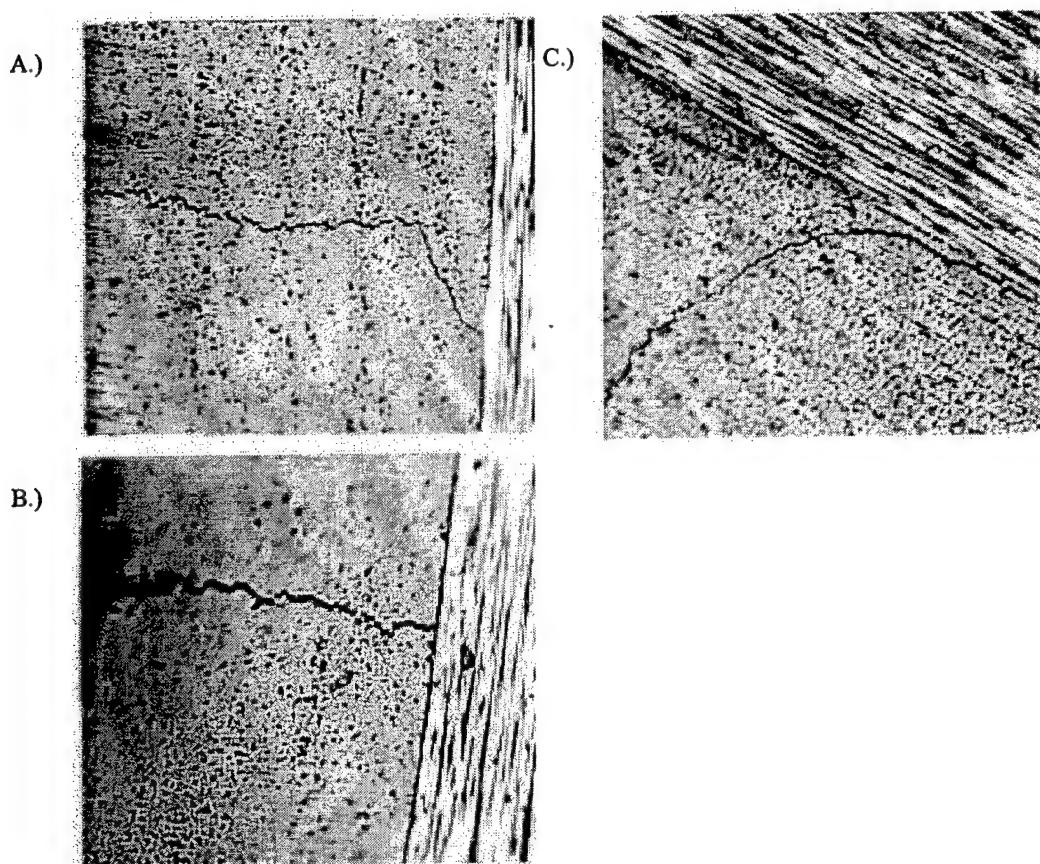
Figure 3-5. Optical photomicrographs of cryogenically cycled laminates containing M35J fibers. A: System 1c. B: System 1b. C: System 1a, central plies in face 2 of laminate. 200x magnification
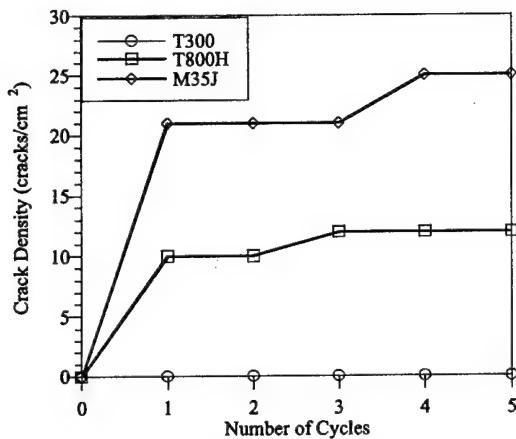
Figure 3-6. Microcracking progression with cryogenic cycling in system 1a

CHAPTER 4: EFFECTS OF FIBER-MATRIX ADHESION ON CRYOGENIC MICROCRACKING

4.1 INTRODUCTION

Traditional composite materials combine a strong, stiff reinforcing phase with a second phase that serves to transfer loads to the reinforcing phase. In the case of fiber-reinforced polymeric composites, the polymeric matrix allows applied stresses to be transferred to the fibers [1]. In chapter 3, the effects of variations in the matrix and the fibers on cryogenic microcracking were investigated. This chapter extends the work in the last chapter to examine how interactions between the fibers and the matrix influence the behavior of carbon fiber/epoxy composites at low temperatures. Stress transfer between the matrix and the fibers plays a large role in determining the ability of a composite material to support applied loads, and the properties of the fiber-matrix interface control matrix-fiber stress transfer [1-5]. Therefore, the final mechanical properties of composite materials are determined, to a large extent, by the properties of the interface and the quality of adhesion between the fibers and the matrix.

Carbon fiber/epoxy composites are often used to store cryogenic liquids, and good thermal characteristics and mechanical properties are essential for these materials to perform effectively [6]. Carbon fiber/epoxy laminates, particularly symmetric cross-ply laminates, develop thermal stresses during cryogenic cycling that place the ply groups in a state of transverse tension. Repeated applications of these loads can cause structural failure [7, 8]. Debonding and matrix cracking occur in response to these stresses and eventually combine to form transverse cracks that propagate through the material [9]. Better fiber-matrix adhesion makes it more difficult to debond the fibers from the matrix; therefore, transverse microcracking should be reduced if the quality of adhesion in a laminate is increased [10].

In this chapter the impact of fiber/matrix adhesion on the transverse microcracking of fiber reinforced polymeric materials thermally cycled at cryogenic temperatures was investigated using symmetric cross-ply carbon fiber/epoxy laminates containing fibers with different surface treatments. Three fiber surfaces were used:

Unsized but exposed to an oxidative surface treatment, epoxy sized, and surfactant sized. Modifications of the fiber surfaces changed the adhesion of the matrix to the fibers as determined by interlaminar shear strength and dynamic mechanical analysis. The extent of microcracking in the laminates exhibited a dependence on fiber/matrix adhesion, with high levels of adhesion corresponding to decreased microcracking.

4.2 EXPERIMENTAL

4.2.1 Materials

A mixture of commercial epoxies was used as the base resin for the polymeric matrix. The resins used were EPON® 828 from Resolution Performance Products and Araldite MY 9512 from Vantico Inc. The structural details of EPON® 828 are given in chapter 3. Araldite MY 9512 is a tetraglycidyl methylene dianiline (TGMDA) derivative. HT 976, diaminodiphenyl sulfone (DDS), from Ciba was used as the curing agent.

The epoxy resins were combined in a 66:34 ratio by weight of MY 9512: EPON® 828 in an oil bath at 120°C and stirred until they were completely mixed. A stoichiometric amount of DDS was melted and added to the epoxy mixture in the oil bath. The epoxy/DDS mixture was blended for two minutes in the oil bath at 120°C after which the resin was quenched to room temperature and stored at −10°C until it was prepregged.

Unidirectional prepregs were developed consisting of the resin discussed above and Hexcel AS4C PAN-based carbon fibers. Fibers with three different proprietary surfaces were used. The first, referred to as U, was unsized but exposed to an oxidative surface treatment. The second, referred to as GP, was coated with 0.3 wt. % epoxy sizing. The third, referred to as S, was coated with 0.3 wt. % surfactant sizing. The filament count for all of the fibers was 12,000 per tow [11]. A laboratory-scale hot-melt prepreg machine was used to impregnate the fibers with the epoxy resin [12]. The prepreg fiber areal weight was set to 160 g/m^2 and the nominal resin content was 30±3 wt. % for all of the experiments. The filming and impregnation temperatures were 70°C and 85°C, respectively. Two rollers were used to apply the impregnation pressure. The pressure on the first roller was 69 kPa and the pressure on the second was 241 kPa. The line speed was 1.5 m/min and the gap height for resin filming was 0.25 mm.

The resin content of the prepregs was determined in accordance with ASTM D 3171-99 and Boeing Support Standard 7336 using the technique outlined in chapter 3 [13, 14].

Symmetric 15.24 x 15.24 cm and 20.32 x 15.24 cm unidirectional laminates were laid up using the above prepregs. The symmetric laminates consisted of 12 plies of prepreg in a $[0^o_3, 90^o_3]_s$ configuration, and the unidirectional laminates consisted of 20 plies. After every third ply for the symmetric laminates and every fourth ply for the unidirectional laminates the prepreg stack was precompacted under vacuum pressure for two minutes before additional plies were positioned.

The autoclave cure cycle consisted of a 2.8^oC/min ramp to 177^oC followed by a two hour hold at 177^oC and a ramp down to 27^oC at a rate of 2.8^oC/min. The total consolidation pressure used during cure was 310 kPa. The vacuum bag was vented to the atmosphere when the autoclave pressure reached 104 kPa.

Once cured, the symmetric laminates were cut into 3.49 x 1.27 x 0.16 cm (length x width x thickness) samples for cycling studies and the unidirectional laminates were cut into 2.54 x 1.27 x 0.32 cm (length x width x thickness) samples for interlaminar shear strength testing and dynamic mechanical analysis. The edges of the symmetric laminates were polished prior to cycling to facilitate optical microscopy of the surfaces.

4.2.2 Analysis

X-ray photoelectron spectroscopy (XPS) was performed on the surfaces of the fibers to determine the differences in surface chemistries between the fibers. For each sample, survey spectra were taken from five different locations on the fiber to determine the surface composition. Once the surface composition was obtained, C 1s and O 1s spectra were acquired from the surface of each sample.

Inverse gas chromatography (IGC) was used to characterize the surface energies of the fibers. The experiments were conducted using a Varian Star 3400 gas chromatograph equipped with a 1 m stainless steel column and a flame ionization detector. The column temperature was 30^oC and the detector temperature was 250^oC for all runs. 3.2 g of fibers were packed in the column in all cases. Before each fiber was

tested, the column was purged with nitrogen for 20 minutes at 30°C. A series of normal hydrocarbon probes (methane, n-hexane, n-heptane, n-octane, and n-nonane) were injected into the column at concentrations of 10^{-3} to 10^{-4} ppm to ensure practically zero surface coverage. A minimum of five retention time (t_R) data points was recorded for each probe and the mean values were used in all subsequent calculations. The retention times of the probes were then used to calculate the dispersive component of the surface energy for each of the fiber types using the following equations.

$$RT \ln(V_n) = 2a\sqrt{\sigma_S \sigma_L} + C \qquad (4\text{-}1)$$

$$V_n = f t_N \qquad (4\text{-}2)$$

$$t_N = t_R - t_{CH4} \qquad (4\text{-}3)$$

Where R is the universal gas constant, T is the column temperature, V_n is the net retention volume, a is the molar area of the probe, σ_S is the surface energy of the fibers, σ_L is the surface energy of the probe, and C is a constant. The net retention volume was calculated from the flow rate (f) and the net retention time (t_N), which was calculated from the observed retention time (t_R) and the retention time for methane (t_{CH4}).

Dynamic mechanical analysis (DMA) experiments were performed on the cured unidirectional laminates using the technique described in chapter 3 with an amplitude of 0.01 mm.

Interlaminar shear strength (ILSS) tests were conducted on the unidirectional laminates using the short beam shear (SBS) technique. An Instron 4505 screw-testing frame controlled by Instron series IX software was used in these experiments. Five samples of each material were tested and the average value reported. The interlaminar shear strength tests were performed in accordance with ASTM D2344-84 [15].

The cut and polished symmetric laminates were tested using the cryogenic cycling procedures described in chapter 3. Three samples of each material were tested and the average crack density value reported.

4.3 RESULTS AND DISCUSSION

4.3.1 Fiber characterization

The fibers studied in this chapter were analyzed using XPS in order to determine if any differences in surface chemistry existed that may have influenced the cryogenic microcracking of laminates containing these fibers. XPS allows high-resolution analyses to be performed on the outer 25Å of a solid material and is widely used to determine the chemical composition of solid surfaces [16]. As expected, significant differences were found between the fibers, which were unsized (U), epoxy sized (GP), and surfactant sized (S). Table 4-1 summarizes the surface chemistry of the fibers studied. Values in parentheses represent one standard deviation. The atomic percentage of oxygen on the surface of the fibers increased from the unsized to the epoxy sized to the surfactant sized fibers. This was paralleled by a decrease in the atomic percentage of carbon and nitrogen on the fiber surfaces.

It was found that the oxygen on the surface of the fibers was located in hydroxyl or ether groups. The unsized fibers showed an almost equal distribution of oxygen between ether and hydroxyl functionalities, with slightly more C-O-C linkages than C-OH groups. In contrast to this, both the sized fibers showed significantly larger percentages of C-OH groups than C-O-C groups. No significant difference in the oxygen chemistry was observed between the two sized fibers. Carbon atoms on the surface of the fibers were found to be either graphitic carbon (C-C bonds) or carbon atoms bonded to oxygen atoms. The surface carbon of the unsized (U) fibers was mostly graphitic carbon, with a small percentage of C-O bonds. The epoxy (GP) sized fiber surfaces contained more than 50 % graphitic carbon, but a smaller percentage than in the unsized fibers. The surfactant (S) sized fibers exhibited a larger percentage of C-O bonds than C-C bonds, which was markedly different from the other fibers.

Figure 4-1 illustrates how the dispersive component of the surface energies of the fibers, as determined using IGC, changed with surface treatment. The surface energy decreased dramatically from the unsized to the sized fibers. It should be noted that this was only the dispersive component of the surface energy and reflected only van der Waals interactions with the fibers. The surface energy of the surfactant sized fibers was

slightly less than that for the epoxy sized fibers, paralleling the differences in surface chemistry of the fibers. A decrease in surface energy occurred as the percentage of carbon in C-C bonds decreased because it became more difficult for normal hydrocarbons to interact favorably with the fiber surface. The GP and S sized fibers showed increasing atomic percentages of oxygen on the fiber surface and increasing amounts of oxygen located in hydroxyl groups when compared with the unsized fibers. Larger amounts of oxygen on the fiber surfaces could have reduced the interaction of hydrocarbons with the fibers and lowered the observed dispersive component of the surface energies. While the dispersive component of the surface energy was seen to decrease with increasing atomic percentages of oxygen and hydroxyl groups, it was likely that the acid-base component of the surface energy increased with the greater concentration of polar groups on the fiber surface. An increase in the acid-base component of the surface energy could have resulted in an overall increase in the fiber surface energy that would have promoted good adhesion between the fibers and the matrix [2-4, 17]. It has been observed that the presence of groups that can participate in electron acceptor-donor relationships can decrease the observed dispersive component of surface energy, while increasing fiber-matrix adhesion [17].

4.3.2 Composite properties

Figure 4-2 displays how the interlaminar shear strength of unidirectional laminates varied with the sizing type. The error bars represent one standard deviation. The unsized and GP-sized fibers had ILSS values that were statistically the same, but a significant increase was observed for the S-sized fibers. This can be attributed to greater fiber-matrix adhesion in the laminates containing S-sized fibers [1, 2]. Poor adhesion, as evidenced by low ILSS values, was observed in the laminates containing the epoxy coated fibers. This could have been the result of the epoxy sizing dissolving into the matrix during prepregging and cure, which may have left behind a fiber surface that interacted poorly with the surrounding material. The GP sizing also often achieves less than complete coating of the fiber, which would significantly reduce fiber-matrix adhesion [18]. The S sized fibers had a larger percentage of C-O bonds on the surface

than the other fibers and a larger percentage of C-OH groups than the unsized fibers. It has been shown that the presence of groups that can participate in acid-base or hydrogen bonding interactions, such as hydroxyl or carboxylic acid groups, will increase fiber-matrix adhesion and interlaminar shear strength [17, 19].

Scanning electron microscopy (SEM) was used to examine the failure surfaces of the SBS specimens. All SEM samples were gold sputtered and examined using a working distance of 48 mm with a 15 kV potential. Figure 4-3 presents scanning electron micrographs of representative failure surfaces from laminates containing different fibers. Failure was primarily adhesive for the laminates containing unsized and GP sized fibers, as seen in Figures 4-3 A and B, but Figure 4-3 C shows cohesive failure in the laminates fabricated using S sized fibers. This provided evidence for increased adhesion when the S sized fibers were used and was supported by the interlaminar shear strength results. When the fiber-matrix bond was sufficiently strong failure shifted from the fiber-matrix interface to the bulk matrix. Other researchers have observed this and correlated the switch from interfacial to matrix failure in short beam shear testing to direct measurements of increased fiber-matrix adhesion [2].

Dynamic mechanical analysis was performed to determine if different levels of adhesion and interfacial damping would manifest themselves as differences in the dynamic bulk properties of the laminates. Previous research has shown that dynamic mechanical analysis can be used to characterize interfacial adhesion in composite materials [20-22]. Larger amounts of energy can be dissipated by poor interfacial bonding than by good bonding, and this is observed as a change in the viscous response $(\tan(\delta))$ of a material [20]. Increased interfacial damping, which corresponds to poor adhesion, has been shown to correlate with a decrease in static transverse tensile strength [21].

As shown in Figure 4-4, the shapes and peak temperatures of the $\tan(\delta)$ peaks for the unsized and GP sized fibers were similar, but were significantly different from the peak for the laminates containing S sized fibers. This suggests that the unsized and GP sized fibers resulted in laminates that had different adhesion and interfacial properties than the laminates that contained S sized fibers. The surface energies and chemistries of

the fibers as well as the observation of lower ILSS values for the systems that contained U and GP fibers supported this result.

4.3.3 Laminate microcracking

Microcracking occurred in all of the laminates studied and representative optical photomicrographs of the microcracks are shown in Figure 4-5. The microcracks propagated towards the interior of the samples normal to the fibers when the fibers were viewed along their length. Crack termination occurred when the interface between the 0° and 90° ply groups was reached. In some cases delamination occurred at the $0^o/90^o$ interface as shown in Figure 4-5 B. Generally, the microcracks propagated along the fiber-matrix interfaces, but in some cases fiber splitting was observed as is shown in Figure 4-5 B. No significant variation in individual crack morphology was observed as the fiber type was varied.

Significant variations in the crack density, shown in Figure 4-6, were observed as the fiber type was varied. The error bars indicate one standard deviation. There was no statistical variation in microcrack density between the laminates fabricated using U and GP fibers, but a significant decrease was observed for the laminates containing S sized fibers. When viewed in light of the adhesion results it can be concluded that as the fiber-matrix adhesion increased the microcrack density resulting from cryogenic cycling decreased. It is also interesting to note that the traditional epoxy sizing showed no improvement over the unsized material, while the surfactant sizing increased the microcrack resistance. Room temperature static tests have shown similar decreases in the transverse crack density in composite materials when increasing levels of surface treatment were used [10].

4.4 CONCLUSIONS

Fiber reinforced composite materials were prepared using fibers with different surface chemistries. Variations in the fiber surface chemistry changed the fiber-matrix adhesion in laminates containing these fibers. The fiber-matrix adhesion had a direct impact on the formation of transverse microcracks in symmetric, cross-ply carbon

fiber/epoxy laminates as a response to cryogenic cycling. Reduced microcrack density relative to laminates with poor adhesion was seen in laminates with good adhesion, and it was observed that improved mechanical properties and microcrack resistance occurred when surfactant sized fibers were used instead of traditional epoxy sized fibers.

NOTES TO CHAPTER 4

1. Mallick, P.K. 1993. <u>Fiber Reinforced Composites: Materials Manufacturing and Design</u>, 2nd ed., Marcel Dekker: New York, pp. 566.

2. Madhukar, M.S. and L.T. Drzal. 1991. <u>Fiber-Matrix Adhesion and Its Effect on Composite Mechanical Properties: I. Inplane and Interlaminar Shear Behavior of Graphite/Epoxy Composites</u>, *Journal of Composite Materials*, 25: 932.

3. Madhukar, M.S. and L.T. Drzal. 1992. <u>Fiber-Matrix Adhesion and Its Effect on Composite Mechanical Properties: IV. Mode I and Mode II Fracture Toughness of Graphite/Epoxy Composites</u>, *Journal of Composite Materials*, 26(7): 936.

4. Herrera-Franco, P.J. and L.T. Drzal. 1991. <u>Comparison of Methods for the Measurement of Fiber/Matrix Adhesion in Composites</u>, *Composites*, 23(1): 2.

5. Tandon, G.P. and R.Y. Kim. 1997. <u>Test Methods for Estimation of Interfacial Normal Strength in Unidirectional Fiber Reinforced Composites</u>, *Journal of Reinforced Plastics and Composites*, 16(17): 1550.

6. Nguyen, B. 1999. <u>Cryotank Skin/Stringer Bondline Analysis</u>, *Proceedings of 44th International SAMPE Conference*, Long Beach, CA, 44: 856.

7. Adams, D.S., D.E. Bowles and C.T. Herakovich. 1986. <u>Thermally Induced Transverse Cracking in Graphite-Epoxy Cross-Ply Laminates</u>, *Journal of Reinforced Plastics and Composites*, 5: 152.

8. Spain, R.G. 1971. <u>Thermal Microcracking of Carbon Fibre/Resin Composites</u>, *Composites*, March: 33.

9. Wood, C. and W. Bradley. 1996. <u>A New Technique to Study the Interfacial Strength and Transverse Cracking Scenario in Composite Materials</u>, *in Fiber Matrix and Interface Properties, ASTM STP 1290*, ASTM: Philadelphia, p. 132.

10. Pithkethly, M.J. 1996. <u>The Use of Interfacial Test Methods in Composite Materials Development</u>, *in Fiber Matrix and Interface Properties, ASTM STP 1290*, ASTM: Philadelphia, p. 34.

11. 2000. <u>AS4C Carbon Fiber Product Data</u>, HCF-610-001, Hexcel Carbon Fibers, Salt Lake City, UT.

12. Putnam, J.W., B.S. Hayes and J.C. Seferis. 1996. <u>Prepreg Process-Structure-Property Analysis and Scale-Up for Manufacturing and Performance</u>, *Journal of Advanced Materials*, 27(4): 47.

13. 1996. Resin Content and Fiber Areal Weight of Prepreg Fabric and Tape, Test Method For, BSS 7336, Boeing Materials Technology, Boeing Commercial Aircraft Group, Renton, WA.

14. 1999. Standard Test Methods for Constituent Content of Composite Materials, ASTM D 3171-99, ASTM: West Conshohocken, PA.

15. 1995. Standard Test Method for Apparent Interlaminar Shear Strength of Parallel Fiber Composites by Short-Beam Method, ASTM D 2344-84, ASTM: West Conshohocken, PA.

16. Skoog, D.A. and J.L. Leary. 1992. Principles of Instrumental Analysis, 4th ed., Harcourt Brace College Publishers: San Diego, pp. 700.

17. Schultz, J., L. Lavielle and C. Martin. 1987. The Role of the Interface in Carbon Fiber-Epoxy Composites, *Journal of Adhesion*, 23: 45.

18. Palmese, G.R. May 17th, 2002. Personal communication.

19. Drzal, L.T., M. Rich, J. and P.F. Lloyd. 1982. Adhesion of Graphite Fibers to Epoxy Matrices: 1. The Role of Fiber Surface Treatment, *Journal of Adhesion*, 16: 1.

20. Kennedy, J.M., D.D. Edie, A. Banerjee and R.J. Cano. 1992. Characterization of Interfacial Bond Strength by Dynamic Analysis, *Journal of Composite Materials*, 26(6): 869.

21. Wu, H.F., W. Gu, G.-Q. Lu and S.L. Kampe. 1997. Non-Destructive Characterization of Fibre-Matrix Adhesion in Composites by Vibration Damping, *Journal of Materials Science*, 32: 1795.

22. Perret, P., J.F. Gerard and B. Chabert. 1987. A New Method to Study the Fiber-Matrix Interface in Unidirectional Composite Materials: Application for Carbon Fiber-Epoxy Composites, *Polymer Testing*, 7: 405.

LIST OF TABLES

Table 4-1. Characterization of fiber surface chemistry using XPS

	U	GP	S
Atomic Percentage Oxygen (1s)	8.05 (0.22)	14.63 (1.05)	27.94 (3.01)
Atomic Percentage Carbon (1s)	87.46 (0.88)	83.72 (1.96)	71.11 (2.70)
Atomic Percentage Nitrogen (1s)	3.28 (0.46)	0.87 (0.80)	0.82 (0.58)
Percentage of Total Carbon as C-C	87.00	69.00	41.00
Percentage of Total Carbon as C-O	13.00	31.00	59.00
Percentage of Total Oxygen as C-O-C	54.00	35.00	33.00
Percentage of Total Oxygen as C-OH	46.00	65.00	67.00

LIST OF FIGURES
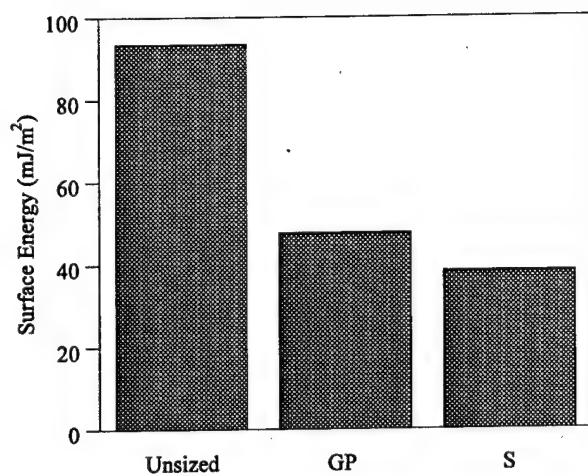
Figure 4-1. Surface energy variation with fiber type
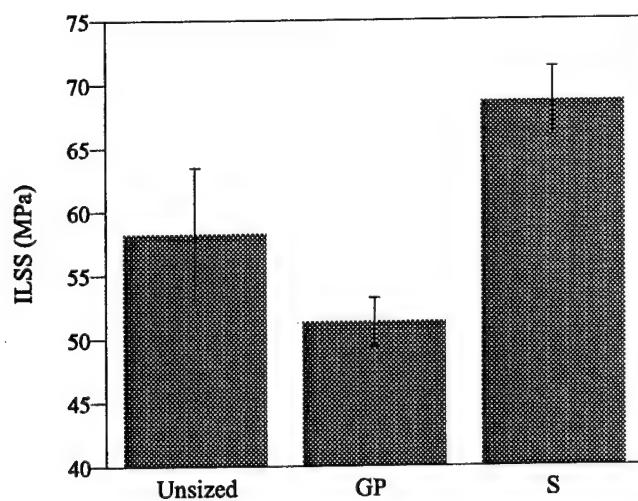
Figure 4-2. Interlaminar shear strength variation with fiber type
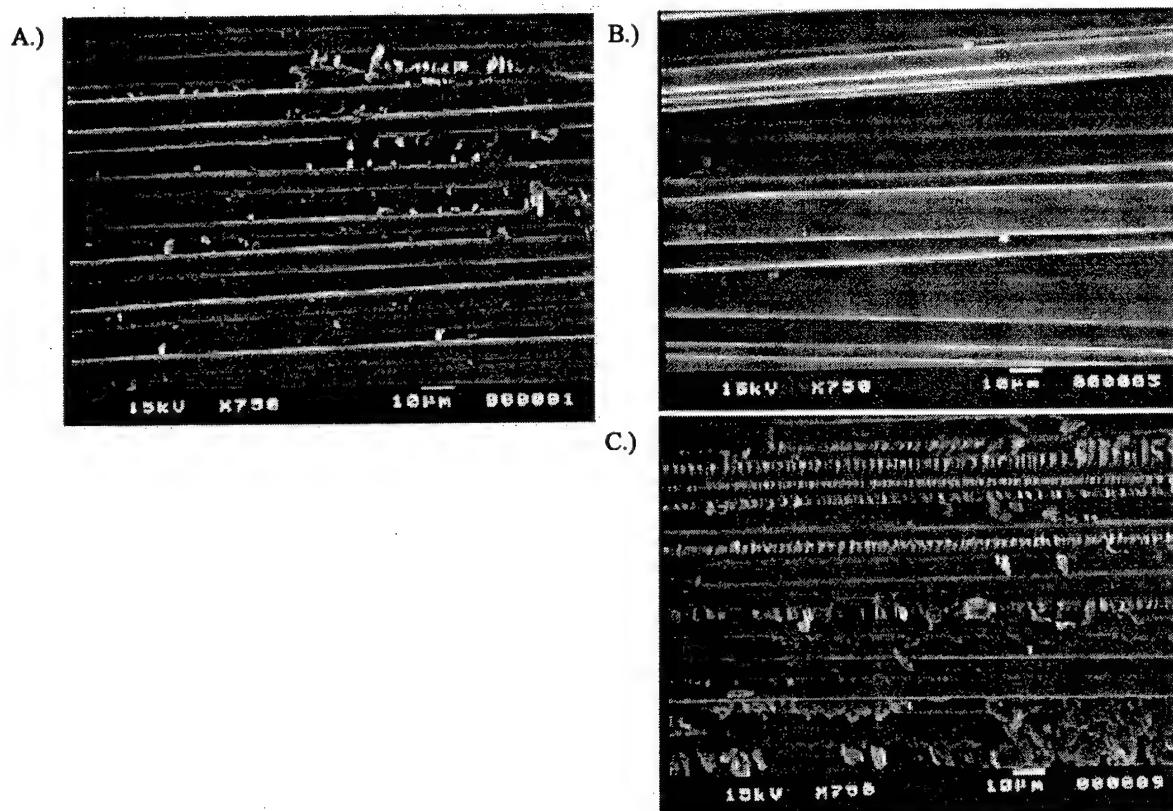
Figure 4-3. SEM images of SBS failure surfaces. A: Unsized and surface treated, B: GP sized, C: S sized. All images 750x
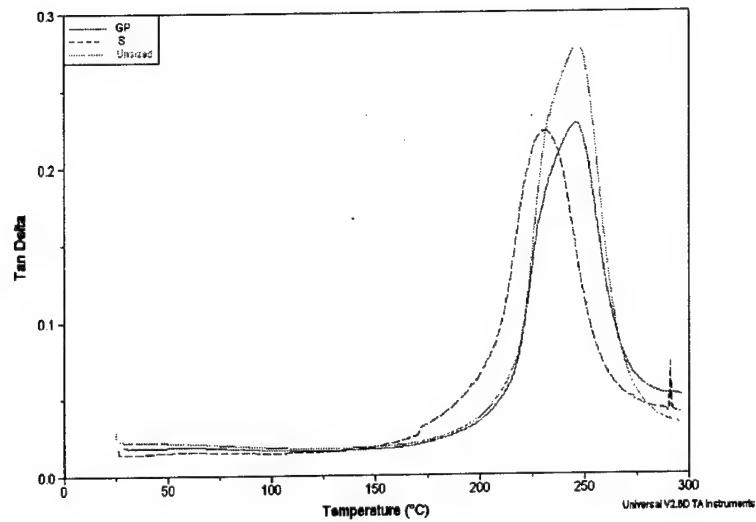
Figure 4-4. Tan(δ) variation with fiber type
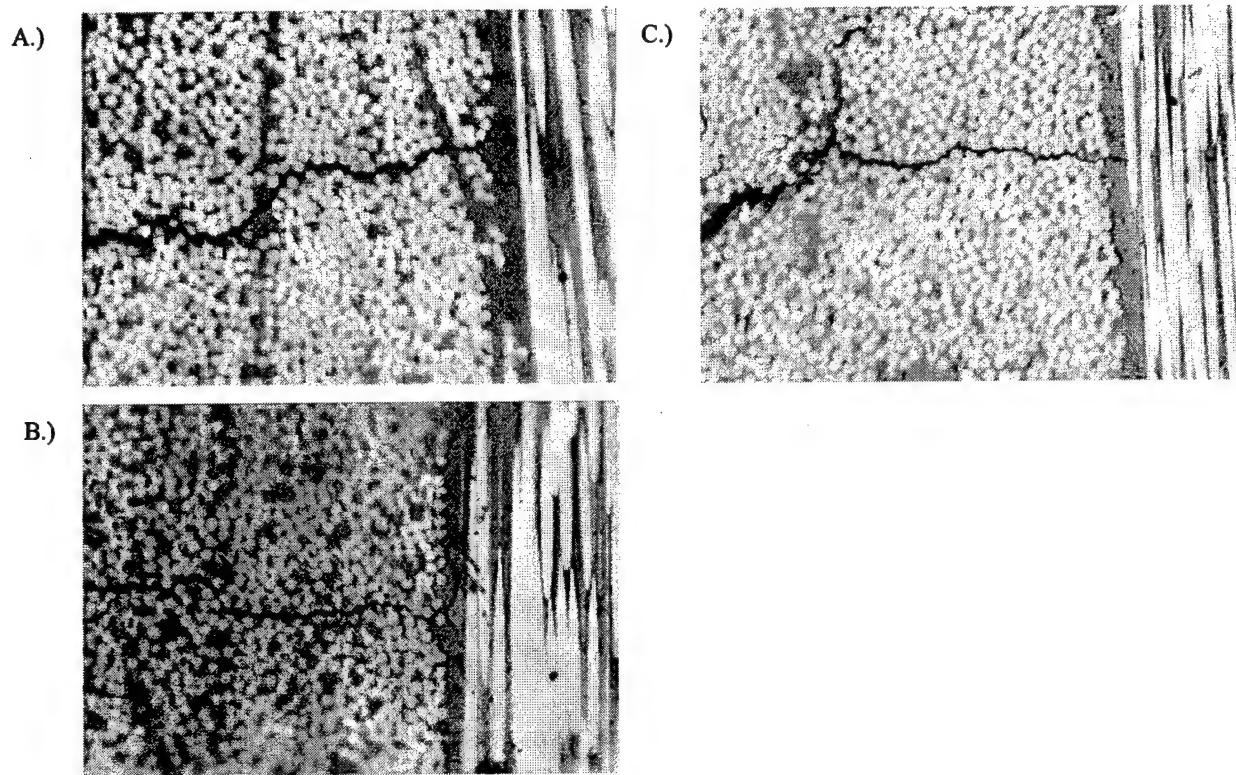
Figure 4-5. Optical photomicrographs of microcracks formed in response to cryogenic cycling. A: Unsized and surface treated, 200x, 2 cycles, B: GP sized, 200x, 5 cycles, C: S sized, 200x, 5 cycles
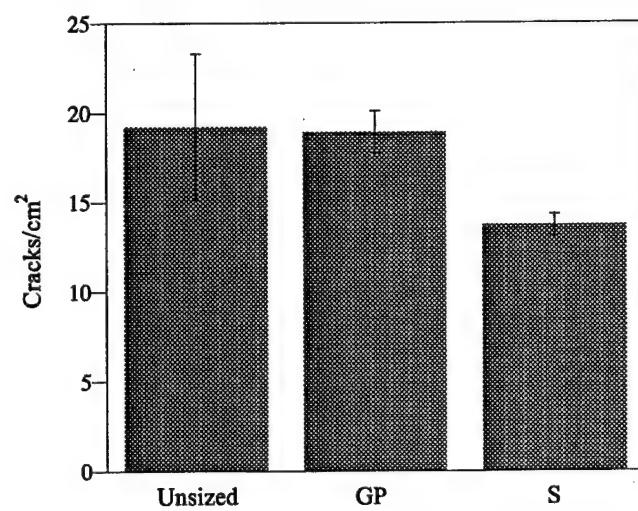
Figure 4-6. Crack density variation with fiber type

CHAPTER 5: CRYOGENIC MICROCRACKING OF RUBBER TOUGHENED COMPOSITES

5.1 INTRODUCTION

One well-studied method for toughening epoxy resins is through the use of a dispersed second phase. This morphology can be obtained by adding either liquid rubber additives or preformed particles dispersed in the unreacted system. Reactive liquid butadiene-acrylonitrile copolymers have been thoroughly studied and are the most widely used liquid rubber additives for epoxy resin systems [1-9]. These modifiers are initially miscible in epoxy resins and phase separate during polymerization to form a dispersed rubber-rich second phase. The final properties of the toughened matrix are affected by the second phase morphology developed during the curing process [4, 6-11].

An earlier study has also shown that the molecular structure of epoxy systems can be engineered to improve their fracture toughness in cryogenic environments [12]. However, little work has been performed detailing the effects of liquid rubber tougheners on the low-temperature microcracking of polymeric composite materials. In this chapter, the cryogenic microcracking of carbon fiber/epoxy composites was investigated and correlated with the morphology and concentration of dispersed rubber as well as processing conditions.

5.2 EXPERIMENTAL

5.2.1 Resin Formulation

The base epoxy resin was formulated using a mixture of the following commercial epoxy resins: Araldite® MY 9512 from Vantico Inc., D.E.N.® 431 and D.E.N.® 438 from the Dow Chemical Company, EPON® 828 from Resolution Performance Products, and 4,4'-Isopropylidenediphenol (Bisphenol-A) from Aldrich Chemical Co. EPON® 828 and Araldite® MY9512 are described in chapters 3 and 4. D.E.N.® 431 and D.E.N.® 438 are epoxy novolac resins with different functionalities [13]. The formulation was cured with dicyandiamide, Amicure® CG 1400 from Pacific Anchor Chemical Co. The system was also accelerated with diuron from Aldrich Chemical Co. One unmodified and four rubber modified resins were formulated. Two

CTBN rubbers, HYCAR® 1300x8, 18 wt% acrylonitrile, and HYCAR® 1300x13, 26 wt% acrylonitrile, from B.F. Goodrich, were used to toughen the resin at concentrations of 10 and 20 phr.

The base resin formulation consisted of 34 wt% Araldite® MY9512, 25.5 wt% D.E.N.® 438, 17 wt% D.E.N.® 431, 8.5 wt% EPON® 828, 8.5 wt% Bisphenol A, 4.6 wt% Amicure® CG 1400, and 1.9 wt% diuron. The CTBN materials were first prereacted with the epoxy resins and epoxy novolacs, except DGEBA, in an oil bath at 160°C for 30 minutes to epoxy-functionalize the carboxyl terminated rubber compounds using triphenylphosphine. Bisphenol-A was then added to the system as a chain extender, and mixed for 90 minutes at the same temperature. To facilitate the incorporation of the curing agents, a paste was made, using a high-shear mixer, consisting of all the EPON® 828, dicyandiamide, and diuron. The curing agent paste was added to the resin after it cooled to 70°C and mixed thoroughly by hand until a uniform system was obtained.

5.2.2 Prepreg Development

Unidirectional prepregs developed in this study consisted of low tensile modulus carbon fibers (Toray T300HB 12K epoxy sized fibers) and the previously described epoxy resins. The fibers were impregnated with the epoxy resin using a commercial scale hot-melt prepreg machine [14]. The fiber areal weight was set to 145g/m^2 and the nominal resin content was 35±2 wt% for all the experiments. Resin filming was performed at 71°C and the impregnation temperature was 104°C. Two press rolls were used in the impregnation zone set to 69 and 276 kPa with the pressure increasing in the direction of the material flow. The line speed was 0.91 m/min for all experiments.

5.2.3 Laminate Fabrication

Both cross-ply and unidirectional laminates were laid up using the model prepregs. The cross-ply laminates, developed for the cryogenic cycling study, consisted of 12 15 x 15 cm plies in a $[0_3/90_3]_s$ configuration, as shown in Figure 5-1. After every third ply was positioned, the plies were precompacted under vacuum pressure for two minutes during the lay-up before additional plies were positioned. The unidirectional laminates,

developed for mechanical testing, consisted of 22 plies that were 15 x 7.5 cm (L x W). For this second set of laminates, the plies were precompacted under vacuum pressure after each ply was positioned for two minutes before the lay-up was continued.

Two autoclave cure cycles were used to manufacture the cross-ply laminates. The first cycle consisted of a 2.8°C/min ramp to 121°C followed by a two-hour hold at 121°C and a ramp down to 27°C at a rate of 2.8°C/min. The second cycle consisted of a 2.8°C/min ramp to 177°C followed by a two-hour hold at 177°C and a ramp down to 27°C at a rate of 2.8°C/min. All laminates used for mechanical testing were cured using the higher temperature cycle. A total consolidation pressure of 310 kPa was applied to the panels and the vacuum bag was vented to the atmosphere when the autoclave pressure reached 103.5 kPa for both cure cycles. A labeling system, shown in Table 5-1, was developed for the laminates based on rubber type, rubber concentration, and cure temperature. Once cured, the cross-ply laminates were cut into 3.50 x 1.27 x 0.16 cm (length x width x thickness) samples for cryogenic cycling studies. The face $[0_3/90_6/0_3]$ of the samples was polished prior to cycling in order to view microcracks using optical microscopy.

5.2.4 Laminate Characterization

Dynamic Mechanical Analysis (DMA) experiments were performed on the cured cross-ply laminates as described in chapter 3 with an amplitude of 0.05 mm.

The interlaminar shear strength (ILSS) of the specimens was measured as described in chapter 4.

Reflected light microscopy was used to investigate the phase separation of the laminate matrices at 400x magnification.

5.2.5 Cryogenic Cycling Procedure

The laminates studied were subjected to the cryogenic cycling procedure outlined in chapter 3.

5.3 RESULTS AND DISCUSSION

The unmodified resin system was based on a prior understanding of cross-linked epoxy formulations in cryogenic environments. This resin was not based on a commercial system, but instead was specifically designed to better understand the microcracking in composites exposed to cryogenic cycling. It contained epoxy novolac resins that produced a tightly crosslinked system upon cure [13] and a tetrafunctional epoxy to obtain a brittle system expected to develop microcracks under low temperature exposure.

Figures 5-2 (a), (b), and (c) show examples of the cross-sections of laminates cured at 177°C that were modified with 10 and 20 phr of HYCAR® 1300x8 and 10 phr of HYCAR® 1300x13, respectively.

In these figures, the carbon fibers appear white. The dark domains in Figure 5-2 (a), the large gray circles in Figure 5-2 (b), and the black pinpoints in Figure 5-2 (c) are the rubber-rich domains resulting from phase separation of the HYCAR® materials during cure. These photomicrographs, representative of all systems, show void free laminates with an evenly distributed discontinuous rubber-rich phase. Most importantly, Figure 5-2 demonstrates that these systems resulted in widely variant phase separation morphologies. The systems containing 20 phr of HYCAR® 1300x8 were noted to present the greatest rubber domain sizes followed by the systems containing 10 phr of the same rubber as shown in Figure 5-2 (a) and (b). Figure 5-2 (c) shows that the laminate containing 10 phr of HYCAR® 1300x13 had much smaller rubber-rich domains. Interestingly, no phase separation could be detected in the laminates modified with 20 phr of HYCAR® 1300x13, this may have been due to increased rubber / epoxy compatibility. These figures demonstrate the difference in phase separation that was obtained with the addition of different types of rubber. Figure 5-2 (a), (b), and (c) show that as the compatibility of the rubber modifier increased the domain sizes were reduced significantly. This has been noted in previous work where it was shown that the phase separation was dependent on the acrylonitrile content of the rubber (18 wt% for 1300x8 vs. 26 wt% for 1300x13) [4]. No differences could be detected in the phase separation between the laminates cured at 121°C or at 177°C.

The glass transition temperatures (T_g) of the different laminates cured at 121°C and 177°C were determined using DMA and are shown in Figure 5-3. It was observed that the T_gs of systems cured at 121°C were on average 21°C lower than the equivalent system cured at 177°C. The systems containing rubber displayed lower glass transition temperatures, and at both high and low rubber concentrations the T_gs of the laminates modified with HYCAR® 1300x8 were higher than those modified with HYCAR®1300x13.

As shown in Figure 5-3, the T_g of the unmodified system was found to be 156.5°C for the laminate cured at 121°C and 178.7°C for the one cured at 177°C, which was at least 3°C and 7°C higher than that of the rubber modified laminate systems, respectively. These results suggested that a proportion of the rubber may have remained in the epoxy-rich phase upon cure [15].

The effect of the rubber concentration and the rubber type on the interlaminar shear strength (ILSS) is shown in Figure 5-4.

ILSS testing was only performed on the higher cure temperature materials because of material constraints. The ILSS of the unmodified system was found to be 78.6 MPa. As shown in this figure, the rubber toughened systems all displayed lower ILSS values than the unmodified laminate, the ILSS of the laminates decreased as the rubber concentration increased, and at both 10 and 20 phr rubber, the system modified with HYCAR® 1300x8 was stronger than the system modified with HYCAR® 1300x13. ILSS of fiber-reinforced laminates is affected by a variety of parameters such as the presence of voids and the modulus of the matrix. The lower ILSS values of the toughened materials most likely resulted from the lower moduli of the toughened resins due to the presence of rubber in the first phase, which should have been lower for the HYCAR® 1300x13 systems [16].

Figure 5-5 shows different optical photomicrographs illustrating examples of the microcrack morphology developed as a result of cryogenic cycling. Microcracks initiated at the outer edge of the laminates and then propagated towards the midplane, normal to the fibers. These cracks terminated at the interface between the 0° and 90° ply groups.

Figures 5-5 (a) and (b) show examples of microcracks in the unmodified laminates. The density and the morphology of the microcracks varied with the cure conditions as well as the type and concentration of rubber utilized. It was noted that for the untoughened resin system, a higher cure temperature resulted in wider microcracks as shown in Figure 5-5 (b). Delamination was observed at the 0°/90° ply interface of the unmodified systems. Previous work has shown that cure conditions have a direct effect on the microcrack density and morphology; higher cure temperatures resulted in higher stress free temperatures and residual strains in the laminates. The rubber-modified laminates, shown in Figures 5-5 (c) and (d), exhibited narrower microcracks than the unmodified laminates, in Figures 5-5 (a) and (b). It should be noted that the laminates cured at 121°C modified with 20 phr of rubber, for both HYCAR® 1300x8 and HYCAR® 1300x13, did not display microcracks as a response to thermal cycling. It was also observed that more microcracks formed on the bag side of the composite part.

The effect of the rubber type and concentration as well as cure temperature on the response of the laminates to cryogenic cycling is displayed in Figure 5-6. Higher cure temperatures increased the microcrack density. It was also seen that when the level of CTBN was increased, the average crack density decreased. It is to be noted that the laminate modified with the maximum amount of rubber (20 phr) and cured at the lower temperature displayed no microcracks. The presence of liquid rubber most likely improved the thermal shock resistance of the laminates, which decreased both the level of thermal stresses generated and the resulting average crack density. More phase separation was seen with the less compatible HYCAR® 1300x8, which indicated that phase morphology and rubber chemistry as well as the concentration of rubber played a role in microcrack resistance.

5.4 CONCLUSIONS

Unidirectional prepregs were made to investigate the effect of rubber type and concentration on microcrack formation in cryogenically cycled laminates. Two types of rubber with different levels of compatibility at two concentrations were combined with the base epoxy resin. These resins were impregnated into unidirectional carbon fibers and

cured at two temperatures. Different levels of phase separation were observed in the laminates resulting from variations in rubber concentration and rubber type. The addition of rubber also resulted in significant reductions of both the glass transition temperatures and the interlaminar shear strength of the laminates. The systems containing the more compatible rubber demonstrated lower T_gs, lower ILSS values and very little phase separation relative to the other rubber modified systems. Cross-ply laminates were exposed to cryogenic cycling and all but the most highly rubber modified of the composite materials formed microcracks in response to thermal stresses generated during exposure to low temperature. Systems containing more rubber demonstrated greater crack resistance. In this work, it was shown that an increase of CTBN concentration in carbon fiber/epoxy based laminates led to a decrease in the microcrack density resulting from cryogenic cycling.

NOTES TO CHAPTER 5

1. Riew, C.K., E.H. Rowe and A.R. Siebert. 1976. Rubber Toughened Thermosets, *in Toughness and Brittleness of Plastics*, American Chemical Society: Washington, D. C., p. 326.

2. Verchere, D., H. Sautereau, J.P. Pascault, S.M. Moschiar, C.C. Riccardi and R.J. Williams. 1990. Rubber-modified Epoxies. I. Influence of Carboxyl-terminated Butadiene Acrylonitrile Random Copolymers (CTBN) on the Polymerization and Phase Separation Processes, *Journal of Applied Polymer Science*, 41(3): 467.

3. Klug, J.H. and J.C. Seferis. 1999. Phase Separation Influence on the Performance of CTBN-toughened Epoxy Adhesives, *Polymer Engineering and Science*, 39(10): 1837.

4. Manzione, L.T., J.K. Gillham and C.A. McPherson. 1981. Rubber-modified Epoxies. I. Transitions and Morphology, *Journal of Applied Polymer Science*, 26(3): 889.

5. Manzione, L.T., J.K. Gillham and C.A. McPherson. 1981. Rubber-modified Epoxies. II. Morphology and Mechanical Properties, *Journal of Applied Polymer Science*, 26(3): 907.

6. Romanchick, W.A., J.E. Sohn and J.F. Geibel. 1983. Synthesis, Morphology, and Thermal Stability of Elastomer-modified Epoxy Resins, *in Epoxy Resin Chemistry 2*, American Chemical Society, Washington, D. C., p. 85.

7. Bussi, P. and H. Ishida. 1994. Composition of the Continuous Phase in Partially Miscible Blends of Epoxy Resin and Epoxidized Rubber by Dynamic Mechanical Analysis, *Polymer*, 35(5): 956.

8. Chen, D., J.P. Pascault, H. Sautereau, R.A. Ruseckaite and R.J. Williams. 1994. Rubber-modified Epoxies: III. Influence of the Rubber Molecular Weight on the Phase Separation Process, *Polymer International*, 33(3): 253.

9. Lee, H.S. and T. Kyu. 1990. Phase Separation Dynamics of Rubber/Epoxy Mixtures, *Macromolecules*, 23(2): 459.

10. Gilbert, E.N., B.S. Hayes and J.C. Seferis. 2000. Standardization of Phase Separation in Rubber Toughened Epoxy Matrices: Discontinuous Phase Functionality, *Proceedings of the 45th International SAMPE Symposium and Exhibition*, Long Beach, CA, 45: 1507.

11. Verchere, D., H. Sautereau, J.P. Pascault, S.M. Moschiar, C.C. Riccardi and R.J.J. Williams. 1993. <u>Rubber-modified Epoxies: Analysis of the Phase-separation Process</u>, *in Toughened Plastics I*, American Chemical Society, Washington, D. C., p. 335.

12. Ueki, T., K. Nojima, K. Asano, S. Nishijima and T. Okada. 1998. <u>Toughening of Epoxy Resin Systems for Cryogenic Use</u>, *Advances in Cryogenic Engineering*, 44(1): 277.

13. 1998. <u>Epoxy Novolac Resins</u>, The Dow Chemical Company, Midland, MI.

14. Putnam, J.W., B.S. Hayes and J.C. Seferis. 1996. <u>Prepreg Process-Structure-Property Analysis and Scale-up for Manufacturing and Performance</u>, *Journal of Advanced Materials*, 27(4): 47.

15. Gordon, M. and J.S. Taylor. 1952. <u>Ideal Copolymers and the Second-order Transitions of Synthetic Rubbers. I. Non-Crystalline Copolymers</u>, *Journal of Applied Chemistry*, 2(9): 493.

16. Ting, R.Y. 1988. <u>Elastomer-modified Epoxy Resins</u>, *in Epoxy Resins; Chemistry and Technology, 2nd ed.*, Marcel Dekker, Inc., New York, p. 551.

LIST OF TABLES

Table 5-1.   Resin systems developed

Resin System	Rubber Type	Rubber Level (phr)	Cure Temperature (°C)
0-L	None	n/a	121
0-H	none	n/a	177
8-10 L	x8	10	121
8-10 H	x8	10	177
8-20 L	x8	20	121
8-20 H	x8	20	177
13-10 L	x13	10	121
13-10 H	x13	10	177
13-20 L	x13	20	121
13-20 H	x13	20	177

LIST OF FIGURES
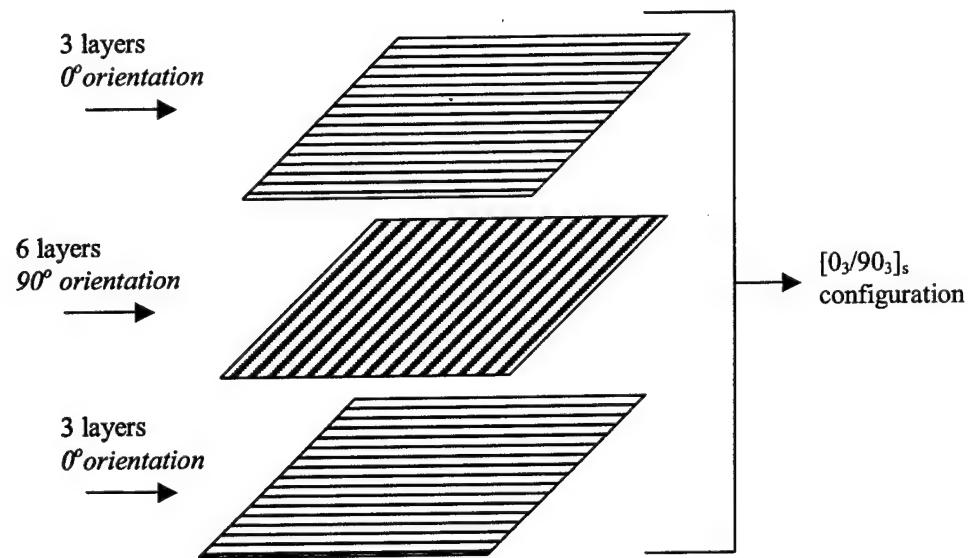
Figure 5-1.   Schematic of cross-ply $[0_3 / 90_3]_s$ configuration prepreg lay-up

A.
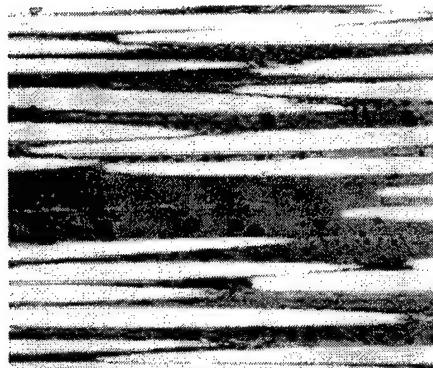
B.
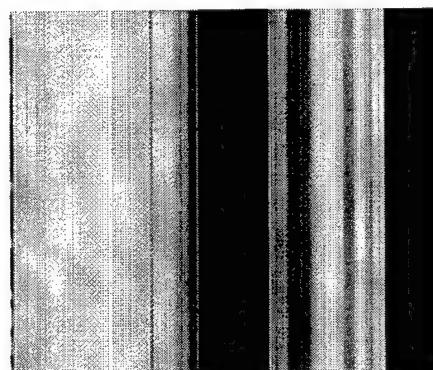
C.
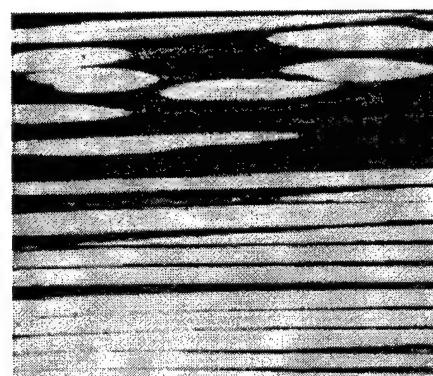
Figure 5-2.   Photomicrographs at 400x magnification of cross-sectioned laminates: (a) 8-10 H, (b) 8-20 H, and (c) 13-10 H
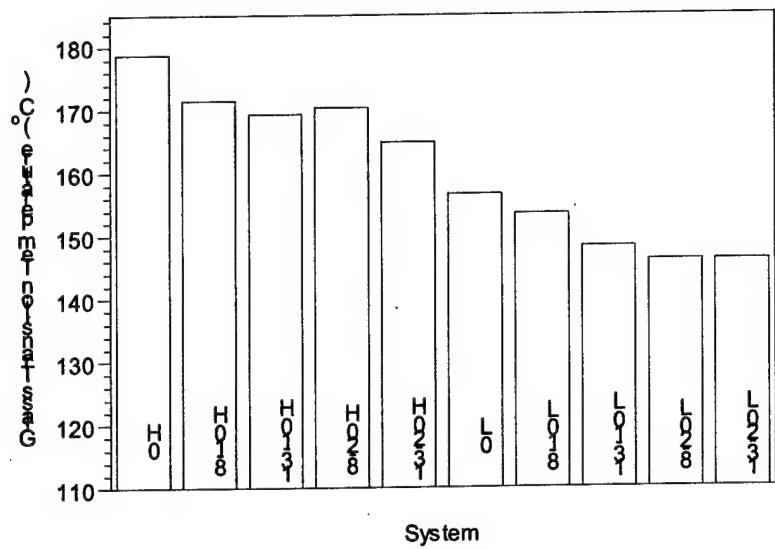
Figure 5-3.   Glass transition temperatures of all laminates
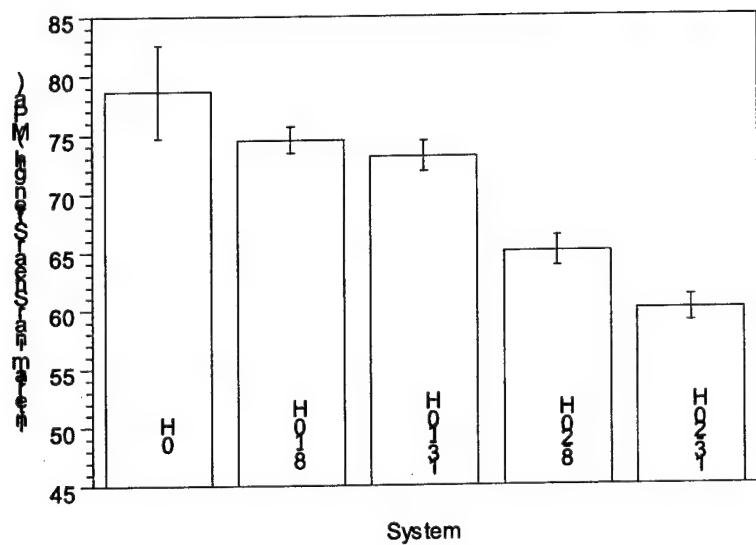
Figure 5-4.   Interlaminar shear strength of the composite laminates cured at 177°C
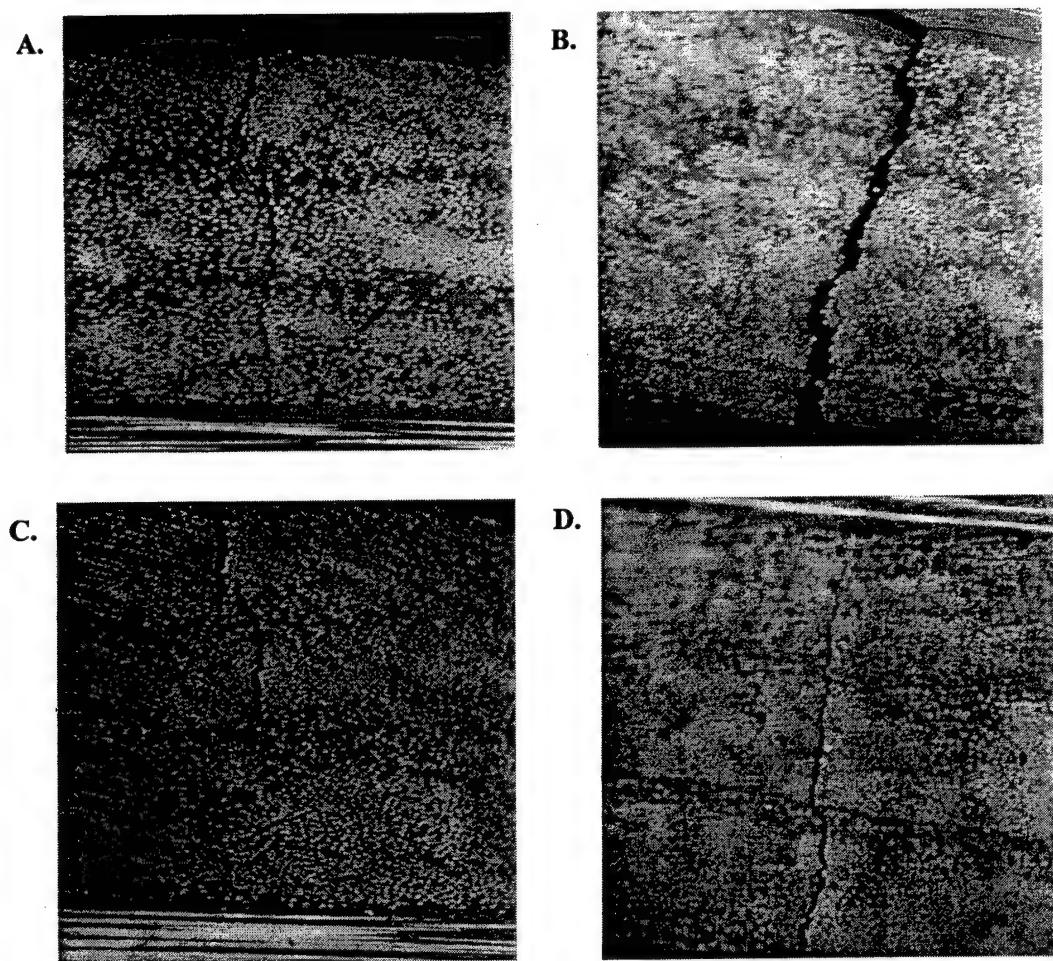
Figure 5-5.   Optical photomicrographs at 100x magnification of cryogenically
cycled laminates: (a) 0-L, (b) 0-H, (c) 8-20 H, and (d) 13-10 H
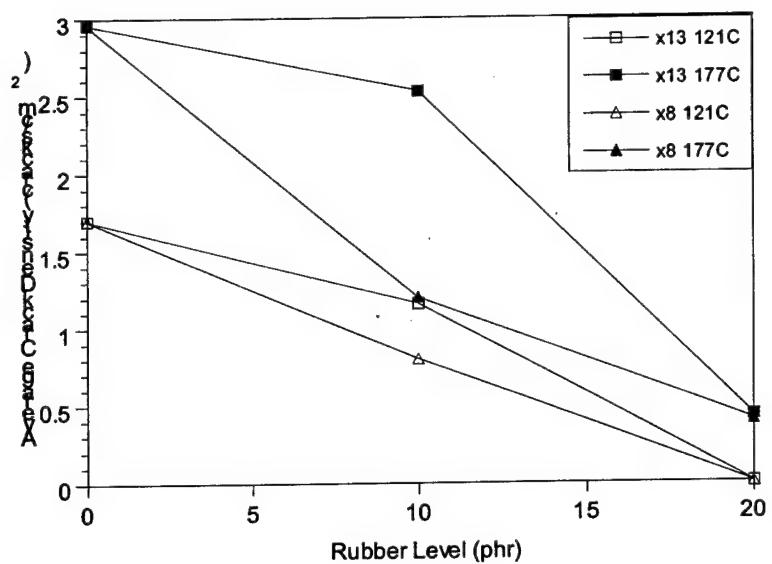
Figure 5-6.   Average final crack density of the cycled laminates

CHAPTER 6: INFLUENCE OF ELASTOMER DISTRIBUTION ON THE CRYOGENIC MICROCRACKING OF CARBON FIBER/EPOXY COMPOSITES

6.1 INTRODUCTION

Liquid rubber tougheners were found to improve the resistance of carbon fiber/epoxy composites to cryogenic microcracking [1]. During cure, these liquid rubbers phase separate and form an evenly distributed second phase which is locked into the matrix upon gelation [2, 3]. The phase separation process is thus significantly affected by the resin components, the cure cycle [4], and the viscosity of the resin system prior to cure initiation [5]. Changes in these variables may drastically affect the microcracking response of the composite. These variables may be eliminated through the selection of toughening materials that are incorporated as preformed particles and remain as distinct particles.

Core-shell rubbers (CSR) enhance the toughness of epoxy resins similar to the use of liquid rubber materials [6, 7]; however, no decrease in glass transition temperature of the epoxy network is observed when core-shell particles are used [6]. Extensive work has been carried out to understand toughening mechanisms in rubber modified epoxies and composites using CSR particles. The major toughening mechanism in the core-shell modified epoxy systems was found to be cavitation of the rubber particles followed by shear yielding of the matrix [7-11]. Yang and co-workers [12] came to the same conclusions using rubber-toughened cyanate ester composites. CSR rubbers typically have an average diameter of 0.2 to 1 μm.

One way to toughen carbon fiber-reinforced polymers is through the modification of the interlayer of the composite using preformed particles [13-15]. This toughening method has been shown to reduce delamination which is one of the greatest causes of composite failure [16, 17]. A significant amount of work has been done to investigate interlayer toughened prepreg systems. While most work has focused on prepregs with epoxy matrices, this engineering approach has also been applied to cyanate ester and bismaleimide systems [18-20]. Materials used for interlayer modifiers have traditionally

been preformed thermoplastic or rubber particles. The most widely used thermoplastics are polyamides [21] but other materials such as polyethersulfones [20] and polyimides [22] have been used. Preformed rubber particles are frequently based on cross-linked butadiene-acrylonitrile, but they sometimes include styrene to increase particle rigidity and glass transition temperatures [23]. The size of these preformed rubber particles is typically found to be between 20 and 50 μm [14, 24]. Hayes et al. [25] provided a review of work that has been done on the use of preformed rubber or thermoplastic particles in high performance thermosetting resins and composite materials.

Other common materials used for the modification of epoxy resins are solid rubbers based on butadiene-acrylonitrile [26, 27]. These elastomers require dissolution in a suitable solvent, such as acetone, for incorporation into the epoxy resin. The solvent can be subsequently removed with heat or under vacuum for hot-melt processing. Nevertheless, due to their high molecular weight and inherent elasticity, the percentage of a dissolved solid rubber in a formulation is usually small. Hayes and co-workers [28] showed that higher quantities of solid carboxyl functionalized rubber could be incorporated in a hot-melt epoxy-based resin if the epoxy/carboxyl esterification is delayed until after the prepreg is developed.

In this chapter, the effects of rubber placement in the polymeric matrix of composites were analyzed in relation to the microcracking response during cryogenic cycling. Composite modification consisted of interlayer toughening using 50 μm average preformed rubber particles, a dispersion of 0.3 μm core shell rubber throughout the entire matrix, and the addition of a rubber interpenetrating network (IPN) to the continuous phase of the matrix. Cross-ply laminates were developed for cryogenic cycling experiments and the microcracking density was quantified for each laminate. Experiments were also performed to determine the effect of these modifiers on the mode I and II fracture toughness, interlaminar shear strength, and flexural properties of the laminates.

6.2 EXPERIMENTAL

6.2.1 Resin Development

The epoxy resin system used in this study consisted of a mixture of equal amounts of diglycidyl ether of bisphenol-A (DGEBA), Epon® 828 from Resolution Performance Products, an epoxy novolac, D.E.N.® 438 from the Dow Chemical Company, and tetraglycidyl methylene dianiline (TGMDA), Araldite® MY 9512 from Vantico Inc. The combination of these epoxy resins provided a high temperature aerospace-grade model resin. To this base resin, 1 phr (parts per hundred parts resin) of fumed silica CAB-O-SIL®TS-720 from Cabot Co., was added to control flow. 0.3 phr of chromium (2%) napthenate, from OMG Americas Inc., was used as an epoxy/carboxyl esterification catalyst.

Preformed rubber particles, core-shell rubber, and solid carboxyl functionalized rubber were used to modify the base resin. The various formulations consisted of combining the three rubber additives separately and in all possible combinations to form a total of eight different resins as shown in Table 1.

The carboxyl functionalized modifiers, supplied by Zeon Chemicals Inc., were Duomod® DP 5045, Duomod® DP 5031, and Nipol 1472, a preformed rubber particle with an average diameter of 50 μm, a CSR particle with an average diameter of 0.3 μm, and a solid crumb rubber, respectively. In each formulation, 6 phr of the rubber material was added to the base resin, so the system with all three modifiers had a total of 18 phr of rubber additives.

The different rubbers were added to the base resin and mixed in an oil bath at 130°C for 1 hour. When the solid carboxyl functionalized rubber was used, it was necessary to alter the procedure slightly. It consisted of combining a portion of the epoxy resins with the acetone rubber solution. After adequate mixing, the resin/rubber solution was placed in a crystallization dish and the acetone was removed under vacuum at 130°C. This rubber-epoxy combination was then transferred to a mixing apparatus with the remaining epoxy. A stoichiometric amount of 4,4'-diamino diphenylsulfone (DDS) from Ciba-Geigy was used to cure the systems. The DDS was melted, added to the resin mixture at 130°C, and mixed for 5 minutes before prepregging.

6.2.2 Processing

The unidirectional prepregs developed in this study consisted of carbon fibers (Toray T300HB 12K epoxy sized fibers), and the previously described epoxy resins. The fibers were impregnated with the epoxy resin using a commercial scale hot-melt prepreg machine [29]. The nominal prepreg grade was set to $145g/m^2$ and the nominal resin content was 35±3 wt% for all the experiments. Resin filming was performed at 62.8°C and the impregnation temperature was 93.3°C. Two 7.62 cm diameter impregnation rollers were used to apply pressure, with the first set at 69 kPa and the second set at 276 kPa. The line speed was 0.91 m/min for all experiments.

Both cross-ply and unidirectional laminates were laid up using the model prepregs. The 12 ply cross-ply laminates consisted of 15 x 15 cm prepreg plies in a $[0_3/90_3]s$ configuration. After every third ply, the prepreg was pre-compacted under vacuum pressure for two minutes during the lay-up before additional plies were positioned. The unidirectional laminates were 20 plies thick, 33 cm long, and had a 5.08 cm FEP crack starter in the midplane of the sample. Unidirectional specimens were cut to a width of 1.27 cm for fracture, short beam shear, and flexure testing. For this second set of laminates, after every two plies, the prepreg was pre-compacted under vacuum pressure for two minutes before another ply was positioned.

The cure cycle for all the laminates consisted of a 2.8°C/min ramp to 177°C followed by a two-hour hold at 177°C and a ramp down to 27°C at a rate of 2.8°C/min. The laminates were manufactured using a total consolidation pressure of 310 kPa and the vacuum bag was vented to the atmosphere when the autoclave pressure reached 103.5 kPa. Once cured, the cross-ply laminates were cut into 3.50 x 1.27 x 0.16 cm (length x width x thickness) samples for cryogenic cycling studies. The edges of the samples were polished prior to cycling in order to view microcracks using optical microscopy.

6.2.3 Analysis

Dynamic mechanical analysis (DMA) experiments were performed on the cross-ply laminates as described in chapter 3.

Interlaminar shear strength (ILSS) of the composite materials was tested as described in chapter 4.

Transverse flexural properties were determined in a three point bend test according to ASTM D 790-98 [30]. For each material five specimens with a length of 70 mm and a width of 12.7 mm were tested. The span to thickness ratio was set to 16 for all of the samples tested.

Mode I interlaminar fracture toughness was measured using the double cantilever beam (DCB) method [31] according to ASTM D 5528-94a [32]. Each specimen was precracked in the mechanical testing apparatus to provide a sharp crack tip before testing. The fracture specimens were pulled apart in tension at 2.54 cm/min until a displacement of 6.35 cm was reached, at which point the crack extension was marked. Five samples were tested and averaged for each reported G_{IC} value. Standard deviations were calculated and are shown as error bars.

Mode II interlaminar fracture toughness was measured using the end notch flexure (ENF) test [31, 33]. A three point bend apparatus with stationary posts set 10.16 cm apart was used to create shear fracture of the specimen down the mid-plane. The crack front was set 2.54 cm from the stationary post and the loading point was set 5.08 cm from the post. All specimens were precracked in the mechanical testing apparatus to provide a sharp crack tip before testing. A displacement rate of 0.254 cm/min was used to load the specimen in flexure until the crack propagated. The crack front was then located with an optical microscope fixture and moved back to 2.54 cm from the stationary post. This was repeated until the sample was cracked down its entire length. Six G_{IIC} values were obtained for each specimen and averaged for the reported G_{IIC} value. Standard deviations were calculated and are shown as error bars.

Scanning electron microscopy (SEM) was used to examine the fracture morphology. The samples were gold sputtered and an accelerating voltage of 15 kV was used with a working distance of 48 mm.

Three cut and polished cross-ply laminates were exposed to the cryogenic cycling procedure outlined in chapter 3.

6.3 RESULTS AND DISCUSSION

In the previous chapter, carboxyl terminated butadiene-acrylonitrile (CTBN) rubber was used as a modifier in the laminates with variations in concentration and acrylonitrile content. The presence and concentration of liquid rubber in the first phase played a significant role in the decrease in microcrack density but it was not clear to what extent the matrix morphology influenced the microcrack response of the laminates. In this work, three different rubber modifiers were used to toughen the composite laminates, i.e. preformed rubber, core shell particles, and solid carboxyl functionalized rubber. These three modifiers were preferred to other additives because different toughening conditions could be achieved. This study focused on the influence of the toughener types on the microcracking response to cryogenic cycling of the composite laminates.

6.3.1 Laminate mechanical properties

The base resin formulation was designed to provide an adequate microcrack response when subjected to cryogenic cycling. The T_g of the unmodified laminate was found to be 204°C, 27°C greater than the cure temperature, which is generally a characteristic of highly cross-linked systems, which are often susceptible to cryogenic microcracking [34]. The T_g of the other specimens were approximately the same as the control laminate except for the laminate made with the resin containing the three different rubbers. It is not surprising that the T_g of this highly modified system fell to 194°C given the extensive level of rubber modification (18 phr).

The interlaminar shear strength (ILSS) of the unmodified laminate was significantly greater than all the modified laminates as shown in Figure 6-1. When the matrices were modified with one type of rubber, the ILSS decreased by about 15% and when two or three rubber additives were used, the decrease in the ILSS values reached 30%. Interlayer particle toughening or rubber modifying the matrix continuous phase played an equivalent role in depressing the ILSS while the ILSS of the laminate modified with the dispersed core shell particles was not decreased as significantly. Regardless of the type of modification, the rubber materials decreased the ILSS value of the laminate, most likely because of the increased concentration of low modulus components in the matrix [35].

Figure 6-2 shows the variation of the transverse flexural strength with the type of rubbers used to toughen the laminates. The only statistically significant increase in the flexural strength was observed when only the solid carboxyl functionalized rubber was present in the laminate. No statistically significant change was seen for all other laminates. The difference in the sample geometries and loading modes between short beam shear and transverse flexural testing might explain the decrease in the ILSS values and the negligible change in the flexural strength of the laminates. The load in the short beam shear test was applied perpendicular to the fiber orientation whereas the loading nose was parallel to the fibers in the transverse flexural testing.

Figure 6-3 shows how the transverse flexural modulus of the composite laminates changed as the type and amount of rubber were varied. The transverse flexural modulus showed a decrease for all the toughened parts when compared to the unmodified laminate. No statistical change could be observed with the variation in rubber type and concentration.

Figure 6-4 shows that the mode I fracture toughness, as measured by G_{IC}, of all the toughened laminates was greater than the control. The most significant increase in G_{IC} was obtained for the laminate modified with the three rubbers, in which case the G_{IC} was three times higher than that of the control. When just one rubber additive was present, the Nipol 1472 modified laminate displayed the largest increase in G_{IC} (approximately 75%). The modification of the matrix continuous phase with the solid carboxyl functionalized rubber may have been responsible for such an increase in the fracture energy. The larger G_{IC} values obtained for the dispersed core shell particle-modified laminate as compared to the interlayer toughened DP 5045-modified sample can be explained by the smaller size of the core-shell rubber particles. With a decreased particle size, a more homogeneous laminate structure was obtained and there was more contact between the crack and the fibers which resulted in fiber influences, increasing the G_{IC} values. If the DP 5045 or the DP 5031 particles were the only modification to the matrix, there was only a slight increase of the mode I fracture toughness of the modified laminate. When the preformed rubber particles and the core-shell rubber were used together, a significant increase was observed, probably due to the greater concentration of

rubber in the crack path, absorbing more energy. Figure 6-4 also shows a clear correlation between the toughness of the material and the amount of rubber present in the matrix. When more rubber additive was used to modify the base resin formulation, a higher G_{IC} value was seen in the laminate.

Scanning electron microscopy was used to characterize the fracture surfaces of the laminates. Figures 6-5 and Figure 6-6 show mode I fracture surfaces for two of the rubber modified laminates. As seen in Figure 6-5, the particles, DP 5045, were torn and/or disbonded during fracture which increased the energy absorption, leaving sections of some of the particles exposed on the surface. Hollow centers of torn particles on the surface can also be observed on Figure 6-5. A higher magnification (5000x) was used in Figure 6-6 because of the average size of the core-shell particles (0.3 μm). It shows a well dispersed phase caused by these particles. Cavitation was most likely the main energy absorbing mechanism explaining the increase in G_{IC} over the unmodified laminate [11].

Figure 6-7 shows the mode II fracture toughness performance of the laminates as measured by G_{IIC}, the critical strain energy release rate. The toughened laminates showed an increased value of G_{IIC} of approximately 30% on average over the control. It appeared that the preformed rubber particles (DP 5045) enhanced the mode II fracture toughness of the laminates most effectively. However, statistically there was very little variation between the rubber-modified samples.

6.3.2   Cryogenic Cycling Analysis

Figure 6-8 shows optical photomicrographs that illustrate examples of the microcrack morphology developed as a result of cryogenic cycling. Microcracks propagated normal to the fibers when viewed along their length through the polymeric matrix beginning at the outer edge of the laminates and ending at the 0°/90° ply interface. The microcrack morphology did not appear to change with the additive type or amount. It must be noted that even though the microcracks appear narrower in the control laminate as shown in Figure 6-8 (a), the spacing between microcracks was much smaller than in the rubber modified laminates.

The effect of the rubber type on the response of the laminates to cryogenic cycling is displayed in Figure 6-9. This figure demonstrates that the microcracking resistance of composites can be greatly improved by including rubber modifiers. Interlayer toughening slightly improved the microcrack resistance of the laminate where the dispersed core shell particles reduced the crack density by 50%. The addition of only the dissolved solid carboxyl functionalized rubber to the matrix resulted in a dramatic reduction in the crack density of the laminate. The presence of Nipol 1472 most likely improved the thermal shock resistance of the laminates, which decreased the level of thermal stresses generated and the resulting average crack density. Because the rubber is present homogeneously in the continuous epoxy phase, it might explain the more effective resistance to microcracking when compared to the rubber particle modified laminates where the particles were more localized or even just present as an interlayer. When the DP 5045 and DP 5031 rubber particles were combined to modify the laminate, a significant drop in the microcrack density was observed. Interestingly, when one of the two Duomod® particle additives was replaced with the Nipol 1472 in the two additive systems, there was no statistical change in the number of microcracks. It seems that at this point, the concentration of rubber additive is a more important factor than the type. The laminate modified with the combined preformed rubber particles, core-shell rubber, and solid carboxyl functionalized rubber did not display microcracking as a response to thermal cycling. This was most likely due to the high concentration of rubber in the matrix.

6.4 CONCLUSIONS

Model carbon fiber/epoxy composite systems toughened with preformed rubber particles, core-shell rubber, and solid carboxyl functionalized rubber were developed to investigate how these additives affect the microcracking response when exposed to cryogenic cycling. A total of eight systems were developed, which included a control, each rubber separately, and every combination. Cross-ply laminates were exposed to cryogenic cycling and most of the laminates formed microcracks in response to the thermal stresses generated by cryogenic cycling. Interlayer toughening did not

significantly reduce the crack density but the dispersed core shell particles reduced the crack density by 50%. The dissolved solid carboxyl functionalized rubber, providing an interpenetrating network, was shown to be the most efficient modifier at reducing the transverse cracking of polymeric composite materials when exposed to cryogenic cycling. The three systems containing pairs of rubber additives resulted in a statistically similar level of microcrack density that was dramatically lower than in the control laminate. The combination of modifiers did not matter as much as the amount of rubber for these laminates. A higher rubber concentration reduced the microcracking. Collectively, this chapter showed that the addition of different types of rubber additives reduced the level of microcracking substantially and totally in some case. The microcrack density was also shown to be dependent on the various distributions of rubber obtained in the composites.

NOTES TO CHAPTER 6

1. Nobelen, M., B.S. Hayes and J.C. Seferis. 2001. Low-temperature Microcracking of Composites: Effects of Toughness Modifier Concentration, *Proceedings of the 33rd International SAMPE Technical Conference*, Seattle, WA, 33: 1619.

2. Riew, C.K., E.H. Rowe and A.R. Siebert; Rubber Toughened Thermosets, *in Toughness and Brittleness of Plastics*, American Chemical Society, Washington, D. C., p. 326.

3. Romanchick, W.A., J.E. Sohn and J.F. Geibel. 1983. Synthesis, Morphology, and Thermal Stability of Elastomer-Modified Epoxy Resins, *in Epoxy Resin Chemistry 2*, American Chemical Society, Washington, D. C., p. 85.

4. Verchere, D., H. Sautereau, J.P. Pascault, S.M. Moschiar, C.C. Riccardi and R.J.J. Williams. 1993. Rubber-modified Epoxies; Analysis of the Phase-separation Process, *in Toughened Plastics I*, American Chemical Society, Washington, D. C., p. 335.

5. Kim, S.C., M.B. Ko and W.H. Jo. 1995. The Effect of the Viscosity of Epoxy Prepolymer on the Generated Morphology in Rubber-toughened Epoxy Resin, *Polymer*, 36(11): 2189.

6. Maazouz, A., H. Sautereau and J.F. Gerard. 1994. Toughening of Epoxy Networks Using Preformed Core-shell Particles or Reactive Rubbers, *Polymer Bulletin*, 33: 67.

7. Qian, J.Y., R.A. Pearson, V.L. Dimonie and M.S. El-Aasser. 1995. Synthesis and Application of Core-shell Particles as Toughening Agents for Epoxies, *Journal of Applied Polymer Science*, 58(2): 439.

8. Becu, L., A. Maazouz, H. Sautereau and J.F. Gerard. 1997. Fracture Behavior of Epoxy Polymers Modified with Core-shell Rubber Particles, *Journal of Applied Polymer Science*, 65(12): 2419.

9. Sue, H.-J., E.I. Garcia-Meitin, and N.A. Orchard. 1991. Toughening of Epoxies via Craze-like Damage, *Journal of Polymer Science, Part B: Polymer Physics*, 31(5): 595.

10. Sue, H.-J., R.E. Jones and E.I. Garcia-Meitin. 1993. <u>Fracture Behavior of Model Toughened Composites Under Mode I and Mode II Delamination</u>, *Journal of Materials Science*, 28(23): 6381.

11. Kim, D.S., K. Cho, J.K. Kim and C.E. Park. 1996. <u>Effects of Particle Size and Rubber Content on Fracture Toughness in Rubber-modified Epoxies</u>, *Polymer Engineering and Science*, 36(6): 755.

12. Yang, P.C., E.P. Woo, S.A. Laman, J.J. Jakubowski, D.M. Pickelman and H.-J. Sue. 1991. <u>Rubber-toughened Cyanate Composites - Properties and Toughening Mechanism</u>, *Proceedings of the 36th International SAMPE Symposium and Exhibition*, Anaheim, CA, 36: 437.

13. Odagiri, N., T. Muraki and K. Tobukuro. 1988. <u>Toughness Improved High Performance Torayca Prepreg T800H/3900 Series</u>, *Proceedings of the 33rd International SAMPE Symposium and Exhibition*, Long Beach, CA, 33: 272.

14. Gilbert, E.N., B.S. Hayes and J.C. Seferis. 1999. <u>Influence of Preformed Rubber Particle Size Distribution on the Structure and Properties of Prepreg Systems</u>, *Proceedings of the 31st International SAMPE Technical Conference*, Chicago, IL, 31: 444.

15. Depase, E.P., B.S. Hayes and J.C. Seferis. 2001. <u>Interlayer Toughened VARTM Composites Using Preformed Particle Toughened Tackifiers</u>, *Proceedings of the 33rd International SAMPE Technical Conference*, Seattle, WA, 33: 1379.

16. Kageyama, K. and I. Kimpara. 1991. <u>Delamination Failures in Polymer Composites</u>, *Materials Science and Engineering A*, 143(1): 167.

17. Sela, N. and O. Ishai. 1989. <u>Interlaminar Fracture Toughness and Toughening of Laminated Composite Materials: A Review</u>, *Composites*, 20(5): 423.

18. Zeng, S., M.A. Hoisington and J.C. Seferis. 1992. <u>Particulate Interlayer Toughening of Dicyanate Matrix Composites</u>, *Polymer Engineering and Science*, 14(6): 458.

19. Recker, H.G., H. Tesch, T. Weber, V. Altstaedt and J.D. Boyd. 1996. <u>Bismaleimide Resin Systems Toughened by Addition of Preformed Functionalized Low Tg Elastomer Particles</u>, U. S. Patent #5,532,296.

20. McGrail, P.T. and S. D. Jenkins. 1993. Some Aspects of Interlaminar Toughening: Reactively Terminated Thermoplastic Particles in Thermoset Composites, *Polymer*, 34(4): 677.

21. Hoisington, M.A. and J.C. Seferis. 1993. Model Multilayer Structured Composites, *SAMPE Quarterly*, 24(2): 10.

22. Boyd, J.D. 1991. Toughened Thermosetting Structural Materials, U. S. Patent #5,037,689.

23. 1990. Gardner, H.C. and R.H. Newman-Evans. 1990. Carboxylated Rubber Particles as Tougheners for Fiber Reinforced Composites, U. S. Patent #4,977,215.

24. Hayes, B.S., E.N. Gilbert and J.C. Seferis. 2000. Modification of Epoxy Based Carbon Fiber Prepregs Through Combined Liquid and Preformed Rubber Materials, *Proceedings of the 45th International SAMPE Symposium and Exhibition*, Long Beach, CA, 45: 67.

25. Hayes, B.S. and J.C. Seferis. 2001. Modification of Thermosetting Resins and Composites Through Preformed Polymer Particles: A Review, *Polymer Composites*, 22(4): 451.

26. Drake, R.S. and A.R. Siebert. 1975. Elastomer-modified Epoxy Resins for Structural Applications, *SAMPE Quarterly*, 6(4): 11.

27. Drake, R.S., D.R. Egan and W.T. Murphy. 1983. Elastomer-modified Epoxy Resins in Coatings Applications, *in Epoxy Resin Chemistry II*, American Chemical Society, Washington, D.C., p. 1.

28. Hayes, B.S. and J.C. Seferis. 2000. Effects of In Situ Esterification on the Performance of Carboxyl Functionalized Rubber-modified Epoxy Film Adhesives, *Journal of Applied Polymer Science*, 76(5): 728.

29. Putnam, J.W., B.S. Hayes and J.C. Seferis. 1996. Prepreg Process-Structure-Property Analysis and Scale-up for Manufacturing and Performance, *Journal of Advanced Materials*, 27(4): 47.

30. 1998. Standard Test Method for Flexural Properties of Unreinforced and Reinforced Plastics and Electrical Insulating Materials, ASTM D 790-98, ASTM: West Conshohocken, PA.

31. Pagano, N.J., Ed. 1989. <u>Interlaminar Response of Composite Materials,</u> Elsevier: New York, Ch. 4.

32. 1994. <u>Standard Test Method for Mode I Interlaminar Fracture Toughness of Unidirectional Fiber-reinforced Polymer Matrix Composites</u>, ASTM D 5528-94a, ASTM: West Conshohocken, PA.

33. 1989, <u>Boeing Material Specification (BMS) 8-276</u>, Boeing Materials Technology, Boeing Commercial Airplane Group, Seattle, WA.

34. Nielsen, L.E. 1969. <u>Cross-linking - Effect on Physical Properties of Polymers,</u> *Journal of Macromolecular Science*, 3(1): 69.

35. Ting, R.Y. 1988. <u>Elastomer-modified Epoxy Resins</u>, *in Epoxy Resins; Chemistry and Technology, 2nd ed.*, Marcel Dekker, Inc., New York, p. 551.

LIST OF TABLES

Table 6-1. Resins developed for composite matrices

Resin	DP 5045	DP 5031	Nipol 1472
Control	-	-	-
DP5045	6 phr	-	-
DP5031	-	6 phr	-
Nipol 1472	-	-	6 phr
DP5045/DP5031	6 phr	6 phr	-
DP5045/Nipol 1472	6 phr	-	6 phr
DP5031/Nipol 1472	-	6 phr	6 phr
3 rubbers	6 phr	6 phr	6 phr

LIST OF FIGURES
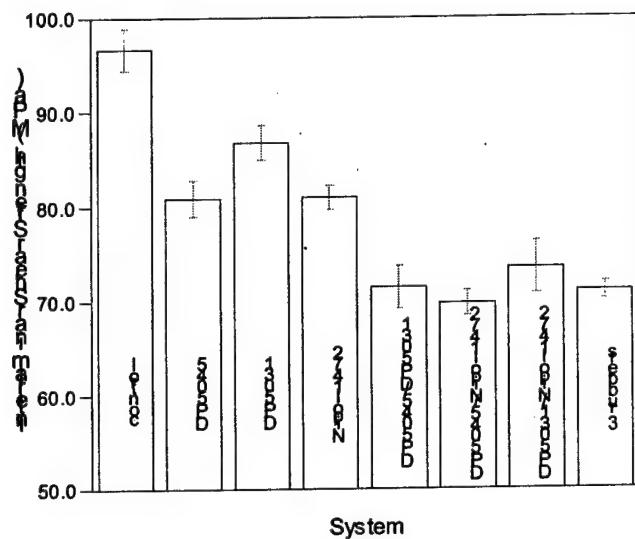
Figure 6-1.　　Interlaminar shear strength (ILSS) of the composite laminates
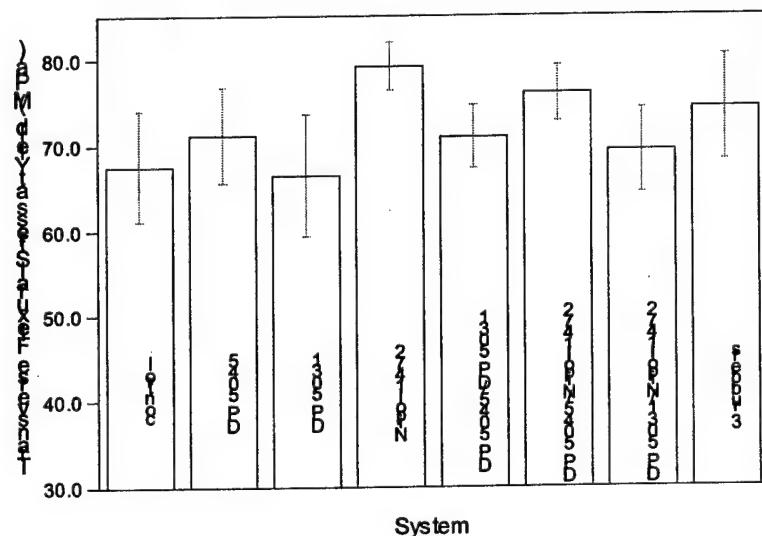
Figure 6-2.　　Transverse flexural strength of the composite laminates
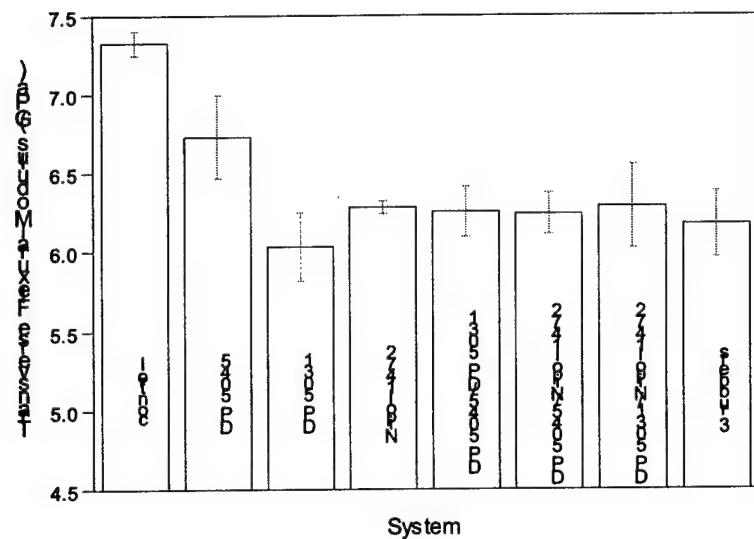
Figure 6-3.   Transverse flexural modulus of the composite laminates
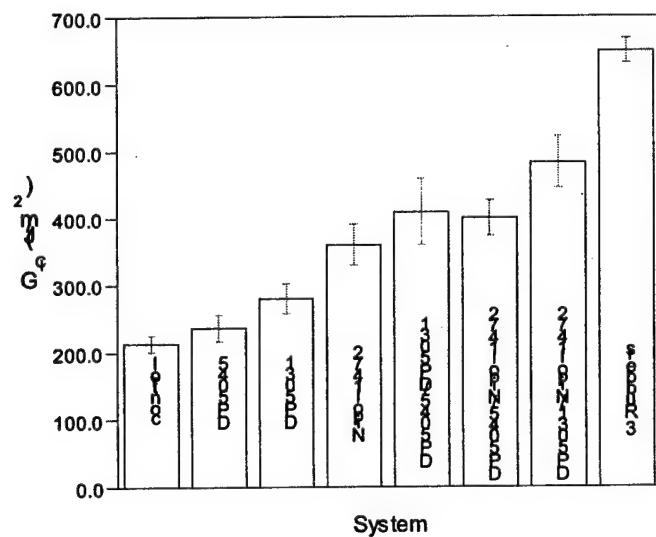
Figure 6-4.   Mode I fracture toughness of the laminates as measured by G_{IC}
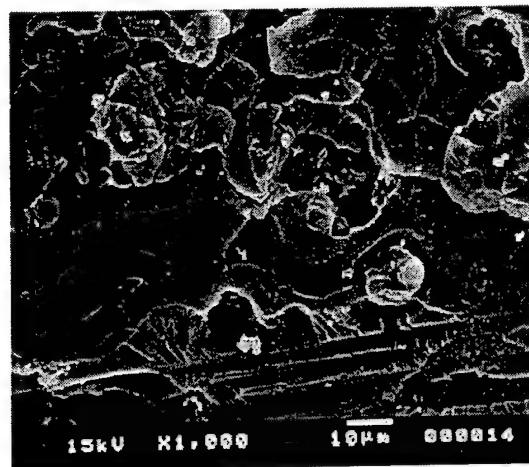
Figure 6-5.   Scanning electron micrograph at 1000x magnification of the mode I fracture surface of the laminate modified with DP 5045
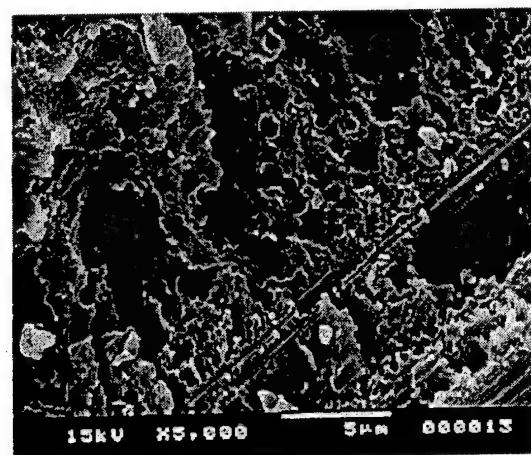
Figure 6-6.   Scanning electron micrograph at 5000x magnification of the mode I fracture surface of the laminate modified with DP 5031
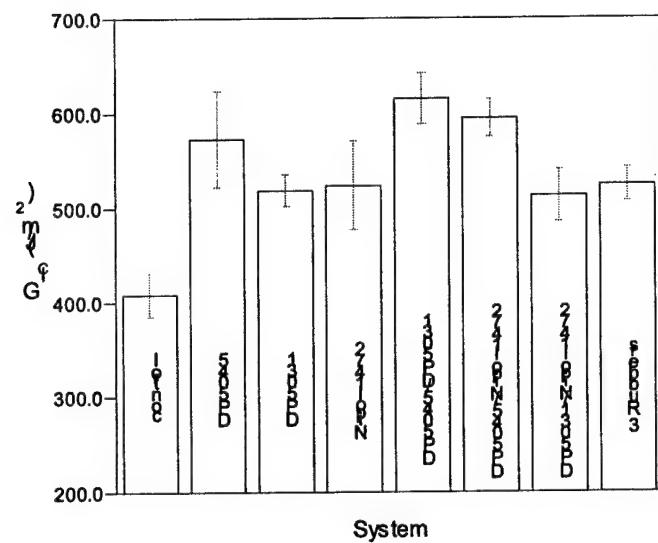
Figure 6-7.   Mode II fracture toughness of the laminates as measured by G_{IIC}

A.)

B.)
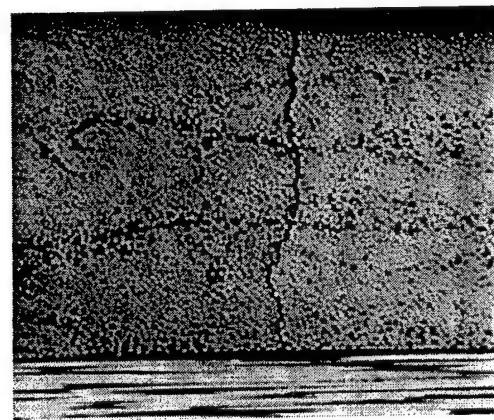
C.)
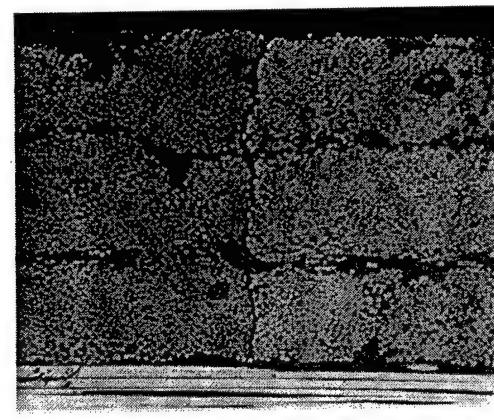
Figure 6-8.   Optical photomicrographs at 100x magnification of cryogenically cycled laminates: (a) control, (b) DP 5031, (c) DP5045/Nipol 1472
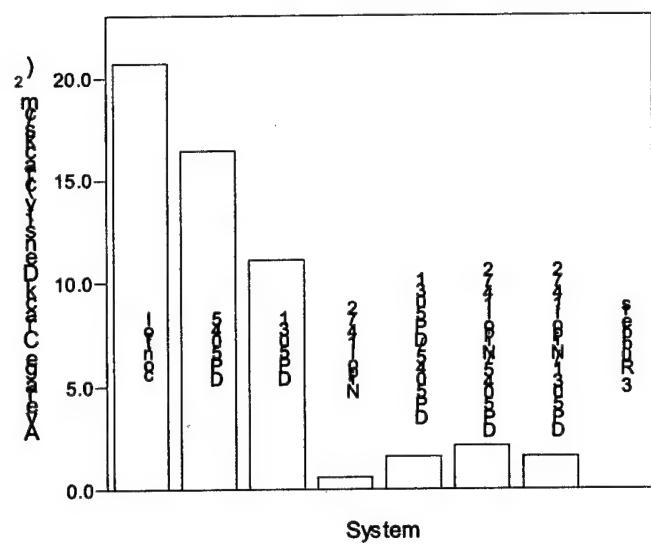
Figure 6-9.   Average crack density of the various systems

CHAPTER 7: CRYOGENIC CYCLING BEHAVIOR OF NANOCLAY MODIFIED POLYMERIC COMPOSITE MATERIALS

7.1 INTRODUCTION AND BACKGROUND

The mechanical, thermal, and chemical properties of polymers and composites can be altered through the use of various kinds of fillers. The dimensions of these fillers typically fall on a macroscopic (1 □ m-1mm) length scale. Fillers of this type increase the stiffness and heat distortion temperature of a polymer, primarily because the filler makes up a significant proportion of the total mass. However, macroscopic fillers usually cause decreases in strength, impact resistance, and processability [1-3].

A new area of composites research has emerged in the last two decades that utilizes nanoparticle fillers to alter the properties of polymers. A widely studied class of nanoparticles is derived from layered aluminosilicate clays, such as montmorillonite, bentonite, and hectorite. These clays are composed of layers of an octahedral metal, usually aluminum or magnesium, complex sandwiched between two sheets of silicate tetrahedrons that are stacked to form the bulk clay [4-7]. Figure 7-1 shows a representation of the structure of montmorillonite. Each layer is approximately 1 nm thick and 500 nm in diameter. In the bulk state the layers are located roughly 1 nm apart. The surfaces of the clay layers develop a negative charge due to defects in the crystal structure and free hydroxyl groups located at the clay surface. Sodium ions in the interlayer region bond to the negative surfaces to create a net zero charge [6, 8, 9].

These layered structures can be dispersed in a polymeric matrix using a process called exfoliation to develop nanocomposite materials. The first step in this procedure involves modifying the interlayer, or gallery, region of the clay with alkyl ammonium compounds in order to create a hydrophobic environment for the polymer. Once this has been done, the polymer or polymer precursor can diffuse into the interlayer region to create what is known as an intercalated structure. Finally, polymerization and/or mechanical processing disperse the clay layers in the polymer, producing an exfoliated nanocomposite [5-8, 10, 11]. A diagram of this process is presented in Figure 7-2.

Definitive results have not yet been achieved for all nanoclay modified polymeric systems, but trends show that when processed properly small amounts ($\leq$ 5 wt. %) of nanoparticle fillers can increase the modulus, strength, toughness, resistance to chemical attack, gas impermeability, resistance to thermal degradation, and dimensional stability of polymeric materials. However, the majority of this work has focused on neat thermoplastics and it is only recently that thermosets have begun to be examined as potential matrices for nanocomposites [5, 7, 12-16].

Inorganic layered nanoparticles have gained acceptance as possible reinforcing structures because of their low cost and ease of fabrication [5, 7]. Some of the earliest work on layered inorganic toughening was performed in 1987 at Toyota. Researchers demonstrated the possibility of functionalizing the surface of layered inorganic silicates to increase their affinity for a polymeric matrix [12]. Usuki et al. polymerized ϵ-caprolactam in the interlayer of an organoclay to form a nanocomposite. This material contained only 4.2 wt. % clay and had a 50 percent increase in strength, an increase in the heat distortion temperature (HDT) of 80°C, a 100 percent increase in tensile modulus, and a 20 percent increase in impact resistance [5]. Many researchers, using a variety of clays and polymeric matrices, have produced similar results to these [8, 14, 16-26].

Toughening using layered inorganic structures is achieved through the high specific surface area and aspect ratio of the filler [18]. These materials are also dominated by the properties of their interfaces as nearly all the polymer in the nanocomposite is near a clay surface. Inhibition of chain rotation by the presence of silicate platelets has also been shown to influence the properties of these materials [26]. Some researchers have suggested that these particles deform under stress to form microvoids that inhibit crack propagation, thus increasing toughness [18, 22, 27]. Zilg et al. demonstrated that exfoliation of the clay particles is central to achieving high performance. If this is not done, an intercalated structure will result that increases stiffness but has no other significant benefits [22, 23]. Pinnavaia et al. showed that manipulation of the surface functionality of the clay particles can tailor the clay surface chemistry to the polymer to maximize exfoliation. They also demonstrated that catalytic

groups could be located in the gallery regions of layered clays to alter the reaction rate inside the clay tactoids [8, 10, 17].

Clays and inorganic reinforcements have been shown to be effective reinforcements in neat polymeric structures, but very little work has been done to examine advanced fiber-reinforced composites that utilize nanocomposite matrices [5, 7]. Hussain reported that matrix reinforcement with nanowhiskers can damage the fibers in composite materials. As such, he incorporated micro and nano-scale Al_2O_3 particles in filament-wound carbon fiber/epoxy composites. He observed an increase in modulus, flexural strength, interlaminar shear strength (ILSS), and fracture toughness when the matrix was filled at 10 vol. % with alumina particles (25 nm diameter). This effect stemmed largely from the large surface area of the filler and the ability of the particles to mechanically interlock with the fibers [28]. Work by Seferis et al. has shown the ability to incorporate nanosized alumina structures in the matrix and interlayer regions of prepreg-based carbon fiber/epoxy composites [29]. Rice et al. incorporated nanoclays in fiber-reinforced materials and found few improvements, but it should be noted that their work was preliminary and many variables were not explored [30].

7.2 RESEARCH MOTIVATION

Nanoparticle reinforcement of continuous fiber reinforced composites has been shown to be a possibility, but much work remains to be performed in order to understand how nanoreinforcement results in dramatic changes in material properties. The understanding of these phenomena will facilitate their extension to the reinforcement of more complicated anisotropic structures and advanced polymeric composite systems. The property and performance enhancements made possible by nanoparticle reinforcement may be of great utility for carbon fiber/epoxy composites that are used for the storage of cryogenic liquids. The structure and properties of these materials can change dramatically when they are exposed to cryogenic temperatures, especially in a cyclical fashion [31-33].

Therefore, the work presented in this chapter investigated the effects of nanoscale matrix modifications on the properties of macro-scale composite materials at low

temperatures. The matrices of carbon fiber/epoxy composites were modified with layered inorganic clays and a traditional filler to determine the effects of particle reinforcement, both micro and nano scale, on the response of these materials to cryogenic cycling. The mechanical properties of the laminates studied were not significantly altered through nanoclay modification of the matrix. The incorporation of nanoclay reinforcement in the proper concentration resulted in cryogenically cycled laminates with microcrack densities lower than those seen in the unmodified or macro-reinforced systems. Lower nanoclay concentrations resulted in a relatively insignificant reduction in microcracking and higher concentrations displayed a traditional filler effect.

7.3 EXPERIMENTAL

7.3.1 Materials and processing

A mixture of commercial epoxy resins was used as the base resin for the polymeric matrix. The resins used were EPON® 828 from Resolution Performance Products and Araldite MY 9512 from Vantico Inc. The details of the chemical structure of these resins are given in chapters 3 and 4, respectively. HT 976, diaminodiphenyl sulfone (DDS), from Ciba was used as a curing agent.

Cloisite® 25A from Southern Clay Products Inc. and 5 μm alumina particles from Buehler Ltd. were used to modify the base matrix formulation. Cloisite® 25A is a layered montmorillonite clay that was treated with a quaternary alkyl ammonium salt to increase the layer spacing and the hydrophobic character of the interlayer region. This material had a cation exchange capacity of 125 meq/100g and a bulk density of 1.87 g/cm^3 [34]. The 25A material was incorporated into the base resin at concentrations of 2, 5, and 8 parts per hundred resin (phr). The alumina particles were used at a concentration of 5 phr. Only one modifier type was present in each resin formulation.

The epoxy resins were combined in a 60:40 ratio by weight of MY 9512: EPON® 828 in an oil bath at 120°C and stirred until they were completely mixed. At this point, the appropriate amount of modifier was added and the material was stirred for two hours. It should be noted that the unmodified resin was also stirred for two hours at 120°C even though no modifier was present. A stoichiometric amount of DDS was melted and added

to the epoxy mixture in the oil bath. The epoxy/modifier/DDS mixture was blended for two minutes in the oil bath at 120°C after which the resin was quenched to room temperature and stored at −10°C until it was prepregged.

Plaques of the resin were cured in an autoclave using a 2.8°C/min ramp to 177°C followed by a two hour hold at 177°C and a ramp down to 27°C at a rate of 2.8°C/min. The total pressure used during cure was 310 kPa.

Unidirectional prepregs were developed consisting of the resins discussed above and Toray 50C T300YC carbon fibers. Epoxy sizing was present on all of the fibers, and the filament count was 12,000 per tow. A hot-melt prepreg machine was used to impregnate the fibers with the epoxy resin [35]. The prepreg fiber areal weight was set to 150 g/m^2 and the nominal resin content was 30±3 weight percent for all of the experiments. The filming and impregnation temperatures were 68°C and 85°C, respectively. Two rollers were used to apply the impregnation pressure. The pressure on the first roller was 69 kPa and the pressure on the second was 241 kPa. The line speed was 0.91 m/min and the doctor blade gap was 0.25 mm.

The resin content of the prepregs was determined in accordance with ASTM D 3171-99 and Boeing Support Standard 7336 using the technique described in chapter 3 [36, 37].

Symmetric cross-ply and unidirectional laminates were laid up using the above prepregs. The symmetric laminates consisted of 12 plies of prepreg in a $[0°_3, 90°_3]s$ configuration, and the unidirectional laminates consisted of 20 plies. After every third ply for the symmetric laminates and every fourth ply for the unidirectional laminates the prepreg stack was precompacted under vacuum pressure for two minutes before additional plies were positioned.

The autoclave cure cycle consisted of a 2.8°C/min ramp to 177°C followed by a 2 hour hold at 177°C and a ramp down to 27°C at a rate of 2.8°C/min. The total consolidation pressure used during cure was 310 kPa. The vacuum bag was vented to the atmosphere when the autoclave pressure reached 104 kPa.

Once cured, the symmetric laminates were cut into 3.49 x 1.27 x 0.16 cm (length x width x thickness) samples for cycling studies and the unidirectional laminates were cut

into 2.54 x 1.27 x 0.32 cm and 15.24 x 1.27 x 0.32 cm (length x width x thickness) samples for interlaminar shear strength and transverse flexure testing, respectively. The edges of the symmetric laminates were polished prior to cycling to facilitate optical microscopy of the surfaces.

7.3.2 Analysis

Differential scanning calorimetry (DSC) analyses were performed on the above resins to determine if the presence of nanoparticles altered the curing behavior of the polymer. A TA Instruments 2910 differential scanning calorimeter was used to perform these experiments. All samples were tested in a nitrogen atmosphere. Each sample was ramped at 5°C/min to 300°C and the peak temperature, onset temperature, and heat of reaction were recorded.

Samples of the unmodified clay, the Cloisite® 25A clay, and cured resin plaques with 2, 5, and 8 phr of nanoclay were subjected to x-ray diffraction experiments. A Siemens D5000 Diffraktometer with 2-15 2Θ, 30 rpm, and a 0.008° step size was used to perform all of the experiments. All of the curves were background corrected and peak smoothed prior to analysis.

Dynamic mechanical analysis (DMA) experiments were performed on single cured symmetric laminates as described in chapter 3 with an amplitude of 0.05 mm.

Interlaminar shear strength (ILSS) and transverse flexural tests were conducted on the unidirectional laminates as described in chapters 4 and 6. Five samples of each material were tested and the average value reported [38, 39].

The unidirectional samples from the flexural tests were used to fabricate 1 x 1 cm samples for the determination of the longitudinal and transverse coefficients of thermal expansion (CTE) of the laminates. Each sample was obtained from a portion of the flexural sample that was not damaged during testing. The coefficient of thermal expansion was determined using a TA instruments 2940 thermomechanical analyzer (TMA) controlled by Thermal Solutions 1.2 J software. A heating rate of 5°C/min from 25°C to 100°C was used with a macro-expansion probe and a force of 0.05 N in a nitrogen environment. The coefficient of thermal expansion was calculated from the

slope of the dimension change with temperature between 25°C and 75°C. Three samples of each material were tested and the average value reported. This technique was performed according to ASTM E 831-93 [40].

Three cut and polished symmetric laminates from each material were exposed to the cryogenic microcracking test procedures described in chapter 3 and the average crack density was recorded. Scanning electron microscopy (SEM) was used to examine the laminate surfaces after they exhibited no further microcracking. All SEM samples were gold sputtered and examined using a working distance of 48 mm with a 15 kV potential.

7.4 RESULTS AND DISCUSSION

7.4.1 Nanocomposite formation

The processing characteristics of the epoxy resins used in this study were not changed by the incorporation of small concentrations of clays or alumina particles. A slight viscosity increase was observed when the clays were blended with the epoxies, but the increase was not sufficient to alter the material processing parameters. DSC analysis showed no change in the heat of reaction, onset temperature, peak temperature, or peak shape when the particle modifiers were blended with epoxy/amine systems.

X-ray diffraction experiments were performed to determine the structural characteristics of the clays used as reinforcements and their distribution in epoxy matrices. It has been shown that this technique can be used to observe how layered nanoparticles are distributed in a polymer and characterize their degree of dispersion [4, 7, 26]. Table 7-1 summarizes the x-ray diffraction data obtained in this study. The modification of the neat clay with a quaternary ammonium salt resulted in an increase in d-spacing as the clay layers were separated. This functionalization of the interlayer region facilitated nanocomposite formation by increasing the gallery spacing and creating a more hydrophobic environment for the epoxy resin and curing agent. It can also be seen that as the concentration of the clay increased, more ordered structures were obtained. No peaks were seen at 2 phr of 25A, indicating an exfoliated or partially exfoliated structure, but as the concentration was increased to 5 and 8 phr smaller peaks appeared and the presence of long range order was observed. These trends can be

observed more clearly in Figure 7-3. At 5 phr a small peak was observed. At 8 phr a similar peak was seen, but an additional shoulder at low 2Θ was also observed. Using the nomenclature of Vaia, these nanocomposites were characterized as disordered intercalated and ordered intercalated, respectively [26]. Intercalated indicates that polymer was located between the clay platelets but some long-range stacking order still remained. The ordered and disordered characterizations refer to the level of order present in the intercalated structures. These results showed that the morphology of the nanocomposites depended on the concentration of the nanoclay.

7.4.2 Composite properties

DMA analysis of the symmetric laminates prepared in this study showed no change in the laminate glass transition temperature (Tg), as determined by the peak in loss modulus, when any of the particle modifiers were present. Therefore, any changes in mechanical properties were due to the physical presence of the modifiers as opposed to changes in the polymeric network structure. Figures 7-4A and B show the results of dynamic mechanical analysis experiments performed on the symmetric laminates used in this study. Figure 7-4A illustrates that the dynamic storage modulus showed a dependence on the type and concentration of the modifier particles below the Tg, while no variation between the samples was seen above the Tg. The largest dynamic storage modulus increase was observed for the alumina modified system. A small dynamic storage modulus increase was seen at 5 phr 25A and no significant change when compared with the control for the 2 phr 25A system was observed. The 8 phr 25A laminate showed a slightly decreased dynamic storage modulus. The high modulus of the alumina particles increased the dynamic storage modulus of the laminates that contained these particles. The well dispersed nanoparticles in the laminate containing 5 phr 25A probably increased the modulus of the matrix. The dynamic storage modulus of the 5 phr 25A modified laminate also remained higher in the vicinity of the Tg than the control and the other clay-modified systems. This was also most likely due to a stiffening of the matrix caused by the well-dispersed nanoparticles. At 2 phr of 25A the nanoparticle concentration was too small to cause a noticeable change in the laminate properties.

Figure 7-4B shows the variation in tan(δ) as different modifiers were used. The width of the tan(δ) peaks at Tg were the same for all the laminates studied, implying that no change in network structure occurred when particle modifiers were incorporated into the matrices of these materials.

Figure 7-5 presents the variation in interlaminar shear strength (ILSS) of the laminates as the concentration and type of particle modification of the matrix were varied. The error bars in this figure represent one standard deviation. A small increase in the ILSS was observed at 2 and 5 phr 25A. This was most likely due to reinforcement of the matrix by the nanoparticles. The largest increase in ILSS was seen when the laminates contained alumina particles. This increase may have resulted from the alumina particles reinforcing the interlayer region. When 8 phr 25A was used the ILSS decreased slightly. It is possible that the more ordered clay particles in this sample acted as flaws or crack initiators instead of reinforcements.

Figure 7-6 shows how the transverse flexural strength of the laminates changed as the concentration and type of particle were varied. One standard deviation is represented by the error bars. When 2 and 5 phr 25A were present in the laminates the flexural strength decreased slightly; however, at 8 phr 25A the strength was the same as the unmodified laminate. When alumina particles were present the strength increased when compared with the control. It has been shown that nanoclay particles will orient themselves preferentially so that the platelets are parallel to the longitudinal axis of the fibers [41]. This effect may have been more pronounced at 2 and 5 phr and could have resulted in orientation effects that caused increases in ILSS and decreases in transverse strength because of the different sample geometries and loading modes in these tests. In the ILSS test the load was applied with the loading nose perpendicular to the fibers, while the loading nose was parallel to the fibers in the transverse flexural testing. The more ordered structures in the laminates containing 8 phr of 25A and the larger, anisotropic particles in the alumina-containing laminates may have made fiber/particle orientation effects less significant. This may have allowed the inclusions to act differently from the more dispersed clay particles and changed their impact on the flexural strength.

Figure 7-7 shows how the transverse flexural modulus changed with the modifier concentration and type. The error bars indicate one standard deviation. The transverse modulus showed no statistical change when the nanoparticle modifiers were incorporated into the matrix at concentrations of 5 and 8 phr. Very slight decreases were observed when alumina and 2 phr 25A were used as modifiers; however, these changes were very small when compared with the variations in the other mechanical tests performed. The modulus was relatively unaffected because of the small concentrations of the modifier particles used. The particles made up a very small fraction of the matrix, and as such, did little to change its stiffness.

Figure 7-8 shows how the transverse CTE of a unidirectional laminate changed as different particle modifiers were used. The error bars in this figure represent one standard deviation. A small initial increase was seen at a nanoclay concentration of 2 phr 25A. After this increase the CTE decreased steadily with increasing nanoclay concentration. No change in CTE when compared with the control was observed when 5 phr alumina was used as a modifier. The increase in CTE at low nanoclay concentrations was unexpected and was most likely due to slight variations in resin content; however, it is possible that orientation of the nanoparticles or nonuniform particle morphologies may have affected the CTE values. Increasing the nanoclay concentration reduced the CTE and demonstrated the possibility that nanoclays could be used to increase the dimensional stability of composite materials. Figure 7-9 demonstrates the difference between the transverse and longitudinal CTEs of the unidirectional laminates tested, with the error bars indicating one standard deviation. The CTE difference values were essentially identical to the transverse CTE values, indicating that the longitudinal CTE was not affected by the presence of a modifier. This suggests that the nanoparticles were preferentially oriented and could be used to customize the thermal expansion properties of composite materials. At concentrations of 2 and 5 phr 25A the nanoparticles were more dispersed and it is possible that this increased the significance of any nanoparticle orientation effects. At a concentration of 8 phr 25A the nanoparticles were more ordered and less dispersed, possibly reducing the impact of any nanoparticle orientation.

7.4.3 Laminate microcracking

Microcracking occurred in all of the laminates studied, and representative optical photomicrographs of the microcracks are shown in Figure 7-10. Scanning electron photomicrographs of the crack surfaces are shown in Figure 7-11. The microcracks propagated towards the interior of the samples normal to the fibers when the fibers were viewed along their length and terminated when the interface between the 0° and 90° ply groups was reached. Figures 7-10B, C, and D along with Figures 7-11A and C show instances in which crack bifurcation was observed and delamination occurred at the $0^{\circ}/90^{\circ}$ interface. Most of the microcracks propagated along the fiber/matrix interface, as shown in Figure 7-11B, but in some cases fiber splitting, which indicates good fiber/matrix adhesion, was observed as shown in Figure 7-10B and indicated with arrows in Figure 7-11A. No significant variation in individual crack morphology was observed as the particle modifier type and concentration were varied.

Significant variations in the crack density were observed as the concentration and type of particle modification were changed. Figure 7-12 demonstrates these variations, with error bars indicating one standard deviation. At 2 phr of 25A the average crack density decreased slightly, but the change was not statistically significant. At 5 phr of 25A the crack density was reduced by 50 percent when compared with the unmodified laminate. When the concentration of 25A was increased to 8 phr the mean crack density increased slightly over the unmodified case, but the change was not statistically significant. Finally, when the micro alumina particles were incorporated into the laminate no change in the microcrack density was observed when compared with the unmodified system. At low nanoclay concentrations the nanoparticles were probably too dispersed to effectively reinforce the matrix and reduce the CTE of the matrix. 5 phr of 25A was a large enough concentration of nanoclay and was dispersed well enough, as shown in the x-ray diffraction data, that the nanoparticles were probably able to reinforce the matrix and lower the thermal stresses present in the laminate by reducing the matrix CTE. When 8 phr of 25A was used the nanoparticles were not as well distributed as shown by the ordered intercalated structure of the nanocomposite matrix. This may have prevented the nanoparticles from providing effective reinforcement in spite of the fact

that they reduced the thermal stresses in the laminates. They may have begun to act like larger structures by serving as flaws and crack initiation sites. The micro alumina particles most likely did not alter the microcrack density because any increase in matrix strength was offset by their ability to concentrate stresses and act as crack initiators.

7.5 CONCLUSIONS

Layered clays were used as nanoparticle fillers in fiber-reinforced polymeric materials. Transverse cracking in symmetric carbon fiber/epoxy laminates as a response to cryogenic cycling was significantly reduced when nanoparticle fillers were used at concentrations much lower than those used for traditional fillers. The concentration of the particles and their distribution in the matrix was observed to be very important in maximizing the benefits of nanoparticle reinforcement. Large concentrations exhibited a typical, macro-scale filler effect and low concentrations showed little or no effect. Exfoliated and disordered intercalated structures provided the best reinforcement, with more ordered intercalated structures offering little benefit. The mechanical properties and processing characteristics of the laminates studied were not adversely influenced by the presence of the nanoparticles and the thermal expansion characteristics were improved. Overall, the work in this chapter showed that nanoclays can be easily used to modify traditional fiber-reinforced composite materials and enhance their resistance to thermal cycling induced stresses.

NOTES TO CHAPTER 7

1. Mallick, P.K. 1993. <u>Fiber Reinforced Composites: Materials Manufacturing and Design</u>, 2nd ed., Marcel Dekker: New York, pp. 566.

2. Rodriguez, F. 1996. <u>Principles of Polymer Systems</u>, 4th ed., Taylor and Francis: Washington D.C., pp. 732.

3. Rosen, S.L. 1993. <u>Fundamental Principles of Polymeric Materials</u>, 2nd ed., John Wiley and Sons, Inc.: New York, pp. 419.

4. Kato, M. and A. Usuki. 2000. <u>Polymer-Clay Nanocomposites</u>, *in Polymer-Clay Nanocomposites*, Wiley: New York, p. 97.

5. LeBaron, P.C., Z. Wang and T.J. Pinnavaia. 1999. <u>Polymer-Layered Silicate Nanocomposites: An Overview</u>, *Applied Clay Science*, 15: 11.

6. Pinnavaia, T.J. and G.W. Beall, Eds. 2000. <u>Polymer-Clay Nanocomposites</u>, John Wiley and Sons: New York, pp. 349.

7. Alexandre, M. and P. Dubois. 2000. <u>Polymer Layered Silicate Nanocomposites: Preparation, Properties and Uses of a New Class of Materials</u>, *Materials Science and Engineering*, 28: 1.

8. Wang, Z., J. Massam and T.J. Pinnavaia. 2000. <u>Epoxy-Clay Nanocomposites</u>, *in Polymer-Clay Nanocomposites*, Wiley: New York, p. 127.

9. Wang, M.S. and T.J. Pinnavaia. 1994. <u>Clay-Polymer Nanocomposites Formed from Acidic Derivatives of Montmorillonite and an Epoxy Resin</u>, *Chemistry of Materials*, 6: 468.

10. Pinnavaia, T.J., T. Lan, P.D. Kaviratna, Z. Wang and S. Hengzhen. 1996. <u>Clay Reinforced Epoxy-Nanocomposites: Synthesis, Properties, and Mechanism of Formation</u>, *ACS Symposium Series*, 622 (nanotechnology): 250.

11. Vaia, R.A. and E.P. Giannelis. 1997. <u>Polymer Melt Intercalation in Organically-Modified Layered Silicates: Model Predictions and Experiment</u>, *Macromolecules*, 30: 8000.

12. Fukushima, Y. and S. Inagaki. 1987. <u>Synthesis of an Intercalated Compound of Montmorillonite and 6-Polyamide</u>, *Journal of Inclusion Phenomena*, 5: 473.

13. Kojima, Y., K. Fukimori, A. Usuki, A. Okada and T. Kurauchi. 1993. Gas Permeabilities in Rubber-Clay Hybrid, *Journal of Materials Science Letters*, 12: 889.

14. Lee, A. and J.D. Lichtenhan. 1999. Thermal and Viscoelastic Property of Epoxy-Clay and Hybrid Inorganic-Organic Epoxy Nanocomposites, *Journal of Applied Polymer Science*, 73: 1993.

15. Gilman, J.W. and T. Kashiwagi. 2000. Polymer-Layered Silicate Nanocomposites with Conventional Flame Retardants, *in Polymer-Clay Nanocomposites*, Wiley: New York, p. 193.

16. Vaia, R.A., H. Ishii and E.P. Giannelis. 1993. Synthesis and Properties of Two-Dimensional Nanostructures by Direct Intercalation of Polymer Melts in Layered Silicates, *Chemistry of Materials*, 5: 1694.

17. Lan, T., P.D. Kavitratna and T.J. Pinnavaia. 1994. Synthesis, Characterization and Mechanical Properties of Epoxy-Clay Nanocomposites, *Proceedings of ACS: Polymeric Materials Science and Engineering*, Washington, D.C., 527.

18. Dietsche, F., Y. Thomann, R. Thomann and R. Mulhaupt. 2000. Translucent Acrylic Nanocomposites Containing Anisotropic Laminated Nanoparticles Derived From Intercalated Layered Silicates, *Journal of Applied Polymer Science*, 75: 396.

19. Rong, M.Z., M.Q. Zhang and Y.X. Zheng. 2000. Irradiation Graft Polymerization on Nano-Inorganic Particles: An Effective Means to Design Polymer-Based Nanocomposites, *Journal of Materials Science Letters*, 19: 1159.

20. Lee, H.B., H.K. Lee, M.J. Shim and S.W. Kim. 1999. Characteristics of Thermal Welding at the Interface of ABS/Bentonite Composite, *Materials Chemistry and Physics*, 58: 264.

21. Chin, I.J., T. Thurn-Albrecht, H.C. Kim and T.P. Russel. 2000. Exfoliation of Montmorillonites in Epoxy, *Polymer Preprints*, 41(1): 591.

22. Zilg, C., R. Mulhaupt and J. Finter. 1999. Morphology and Toughness/Stiffness Balance of Nanocomposites Based upon Anhydride-Cured Epoxy Resins and Layered Silicates, *Macromolecular Chemistry and Physics*, 200(3): 661.

23. Zilg, C., R. Thomann, J. Finter and R. Mulhaupt. 2000. The Influence of Silicate Modification and Compatibilizers on Mechanical Properties and Morphology of Anhydride-Cured Epoxy Nanocomposites, *Macromolecular Materials Engineering*, 280/281: 41.

24. Rong, M.Z., M.Q. Zhang, Y.X. Zheng, H.M. Zeng, R. Walter and K. Friedrich. 2001. Structure-Property Relationships of Irradiation Grafted Nano-Inorganic Particle Filled Polypropylene Composites, *Polymer*, 42: 167.

25. Weimer, M.W., H. Chen, E.P. Giannelis and D.Y. Sogah. 1999. Direct Synthesis of Dispersed Nanocomposites by *in situ* Living Free Radical Polymerization Using a Silicate-Anchored Initiator, *Journal of the American Chemical Society*, 121: 1615.

26. Vaia, R.A. 2000. Structural Characterization of Polymer-Layered Silicate Nanocomposites, *in Polymer-Clay Nanocomposites*, Wiley: New York, p. 229.

27. Huang, Y. and A.J. Kinloch. 1992. The Toughness of Epoxy Polymers Containing Microvoids, *Polymer*, 33(6): 1330.

28. Hussain, M., A. Nakahira and K. Niihara. 1996. Mechanical Property Improvement of Carbon Fiber Reinforced Epoxy Composites by Al_2O_3 Filler Dispersion, *Materials Letters*, 26: 185.

29. Hayes, B.S., M. Nobelen, A.K. Dharia and J.C. Seferis. 2001. Development and Analysis of Nano-Particle Modified Prepreg Matrices, *Proceedings of 33rd International SAMPE Technical Conference*, Seattle, WA, 33: 1050.

30. Rice, B.P., C. Chen, L. Cloos and D. Curliss. 2001. Carbon Fiber Composites Prepared from Organoclay-Aerospace Epoxy Nanocomposites, *Proceedings of 46th International SAMPE Symposium*, Long Beach, CA, 46: 355.

31. Clark, A.F., R.P. Reed and G. Hartwig. 1979. Nonmetallic Materials and Composites at Low Temperatures, *Proceedings of ICMC Symposium on Nonmetallic Materials and Composites at Low Temperatures*, Munich.

32. Engeln, I. and M. Meissner. 1982. Thermal Properties of Crystalline Polymers at Low Temperatures, *Proceedings of Second ICMC Symposium on Nonmetallic Materials and Composites at Low Temperatures*, Geneva, 1.

33. Nguyen, B. 1999. Cryotank Skin/Stringer Bondline Analysis, *Proceedings of 44th International SAMPE Conference*, Long Beach, CA, 44: 856.

34. 2001. Cloisite 25A Physical Properties Bulletin, Southern Clay Products, Gonzales, TX.

35. Putnam, J.W., B.S. Hayes and J.C. Seferis. 1996. Prepreg Process-Structure-Property Analysis and Scale-Up for Manufacturing and Performance, *Journal of Advanced Materials*, 27(4): 47.

36. 1996. <u>Resin Content and Fiber Areal Weight of Prepreg Fabric and Tape, Test Method For</u>, BSS 7336, Boeing Materials Technology, Boeing Commercial Aircraft Group, Renton, WA.

37. 1999. <u>Standard Test Methods for Constituent Content of Composite Materials</u>, ASTM D 3171-99, ASTM: West Conshohocken, PA.

38. 1998. <u>Standard Test Methods for Flexural Properties of Unreinforced and Reinforced Plastics and Electrical Insulating Materials</u>, ASTM D 790-98, ASTM: West Conshohocken, PA.

39. 1995. <u>Standard Test Method for Apparent Interlaminar Shear Strength of Parallel Fiber Composites by Short-Beam Method</u>, ASTM D 2344-84, ASTM: West Conshohocken, PA.

40. 1993. <u>Standard Test Method for Linear Thermal Expansion of Solid Materials by Thermomechanical Analysis</u>, ASTM E 831-93, ASTM: West Conshohocken, PA.

41. Curliss, D. August 2, 2001, Network Symposium II, University of Washington, Seattle, WA. Personal communication.

LIST OF TABLES

Table 7-1. X-ray diffraction data for nanoclays and nanocomposites

| Sample	2Θ	d-spacing (Ang.)	Morphology
Unmodified clay	8.74	10.1	Clay tactoids
Alkylammonium modified clay (25A)	4.65	19	Swollen tactoids
2 phr in resin	No Peak	No Peak	Exfoliated
5 phr in resin	2.51	35.16	Disordered intercalated
8 phr in resin	2.738 5.597	32.23 15.77	Ordered intercalated

LIST OF FIGURES
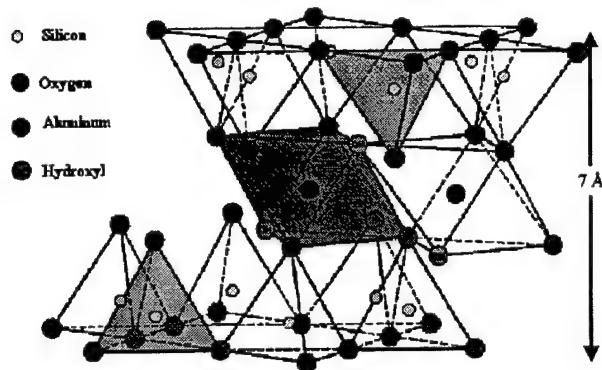
Figure 7-1. Structure of montmorillonite
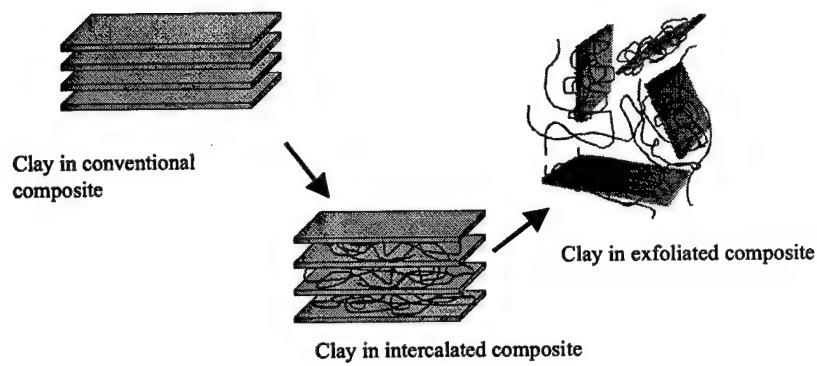

Figure 7-2. Exfoliation of layered clays
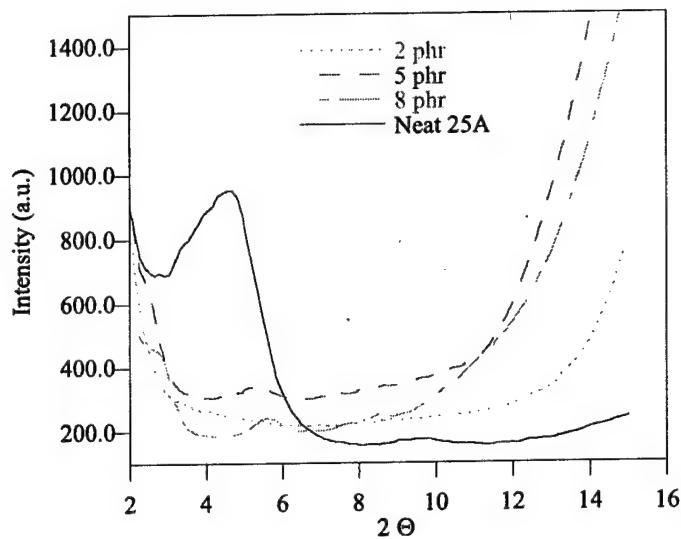
Figure 7-3. X-ray diffraction curves for nanocomposites
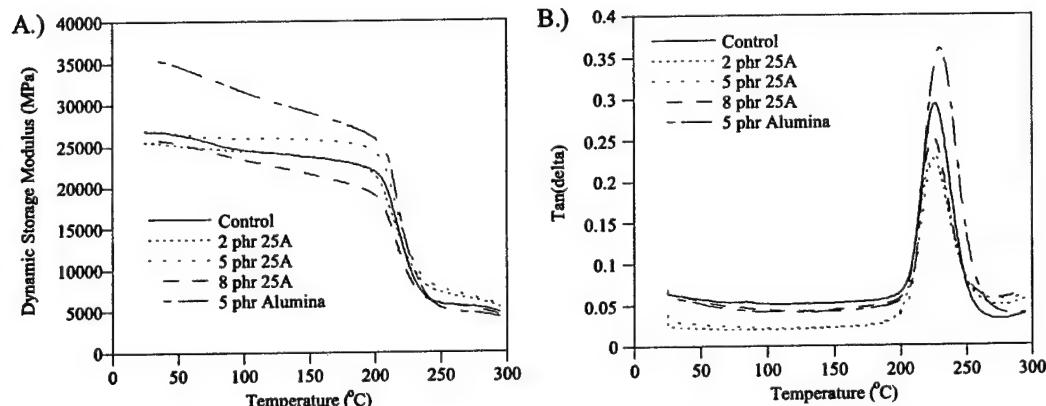
Figure 7-4. Dynamic mechanical property variation with temperature and particle modification. A: Dynamic storage modulus. B: tan(δ)
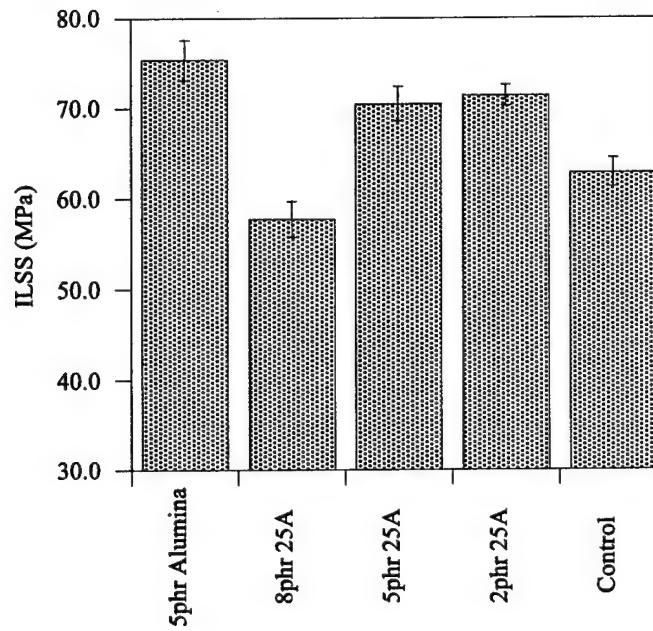
Figure 7-5. Interlaminar shear strength variation with particle modification
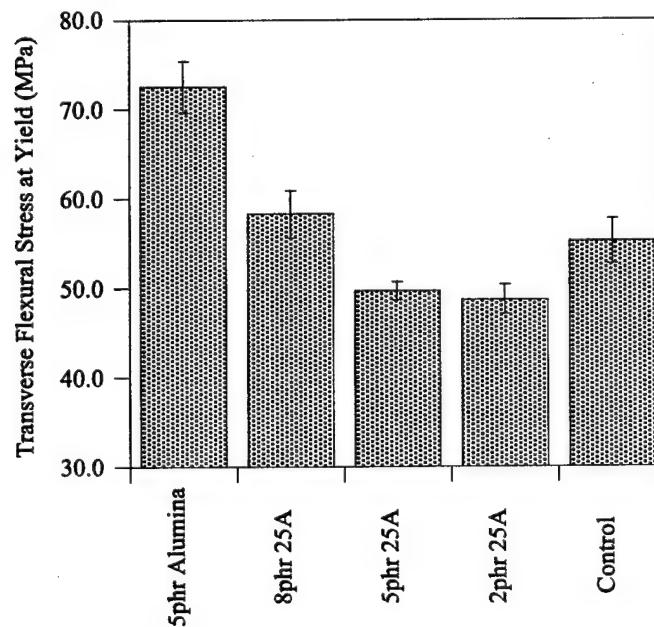
Figure 7-6. Transverse flexural strength variation with particle modification
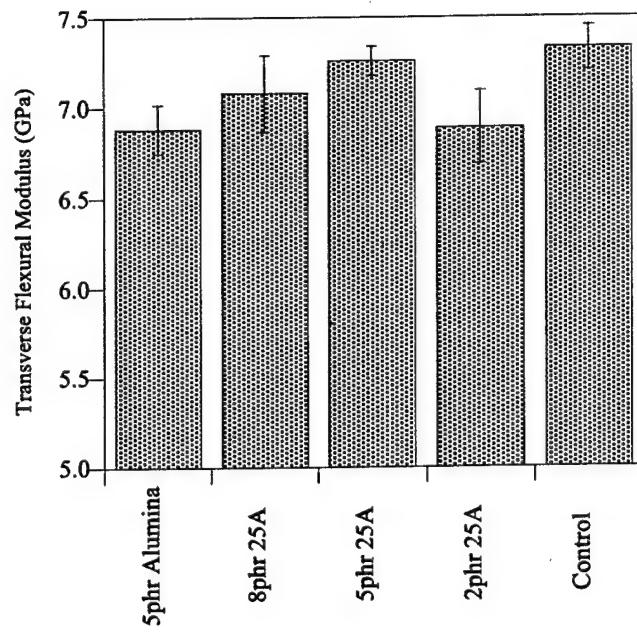
Figure 7-7. Transverse flexural modulus variation with particle modification
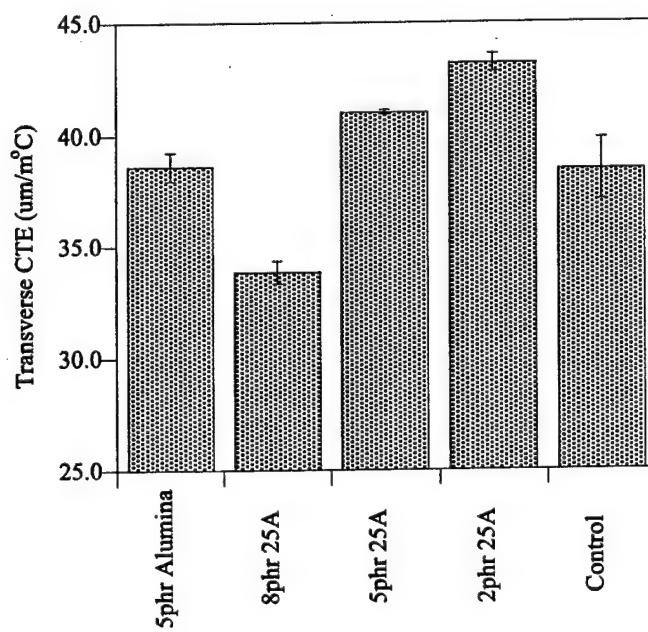
Figure 7-8. Transverse CTE variation with particle modification
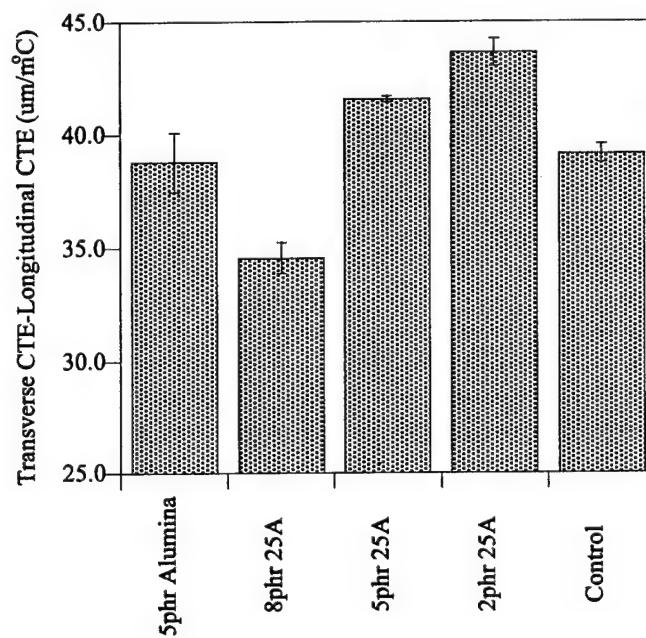
Figure 7-9. Transverse/longitudinal CTE difference variation with particle modification
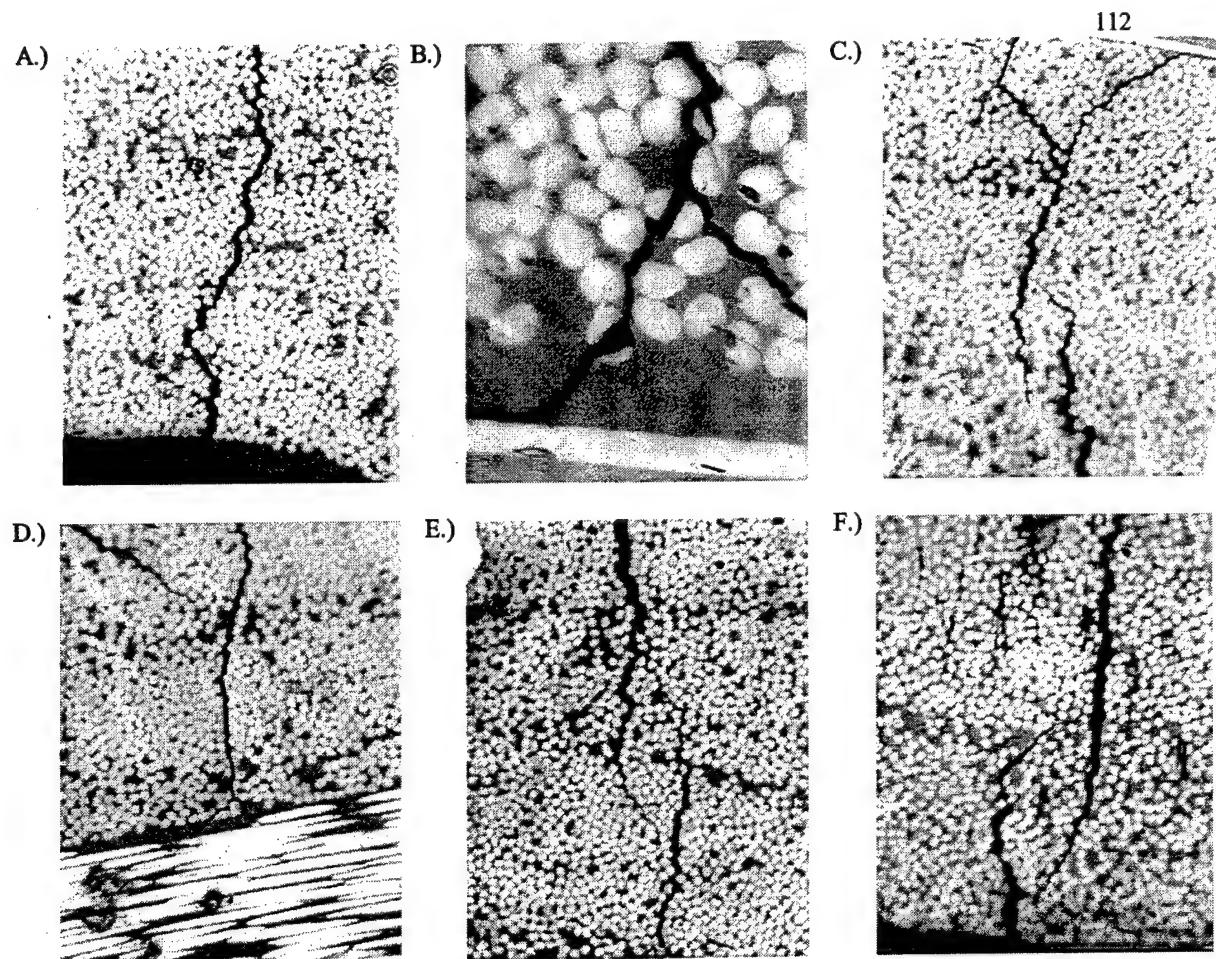
Figure 7-10. Optical photomicrographs of microcracks formed in response to cryogenic cycling. A: Unmodified, 200x, 2cycles. B: Unmodified, 1000x, 1 cycle. C: 2 phr 25A, 200x, 5 cycles. D: 5 phr 25A, 200x, 2 cycles. E: 8 phr 25A, 200x, 2 cycles. F: 5 phr 5μm alumina, 200x, 2 cycles
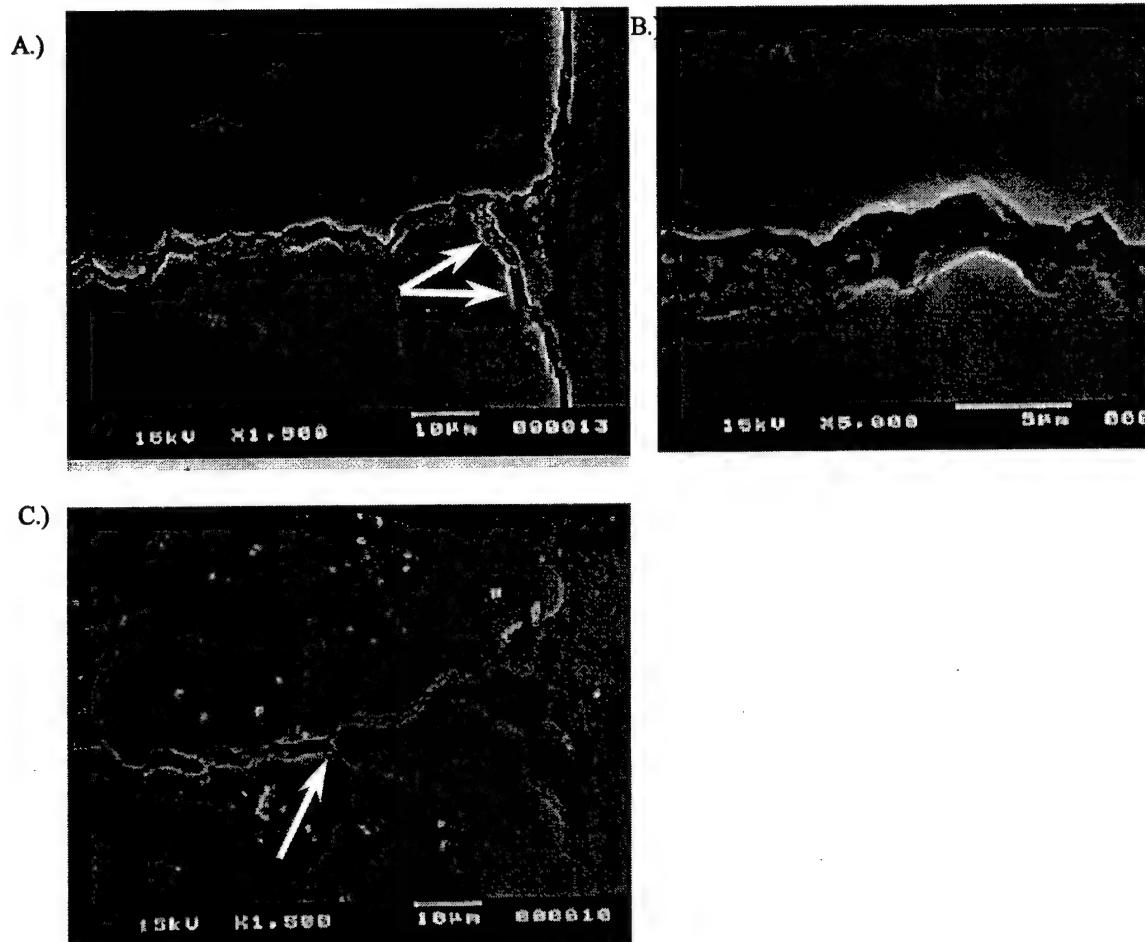
Figure 7-11. Scanning electron micrographs of microcracks formed as a response to cryogenic cycling. A: 8 phr 25A, 1500x. B: 8 phr 25A, 5000x. C: Unmodified, 1500x
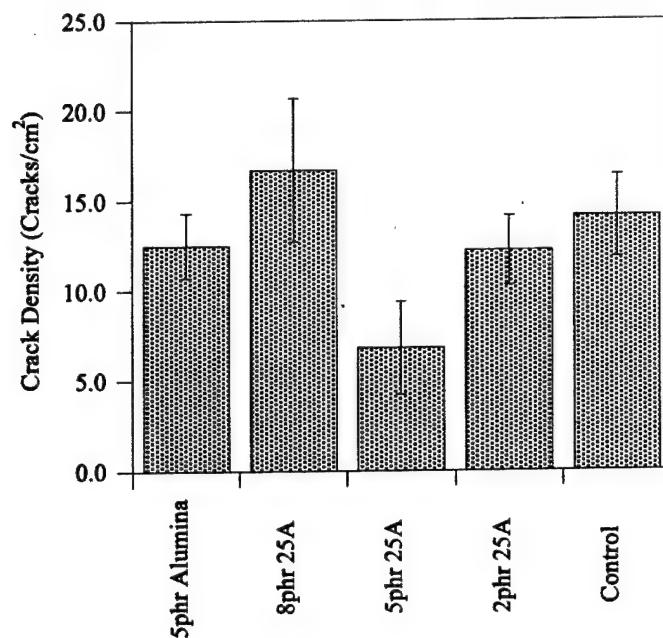
Figure 7-12. Crack density variation with particle modification

CHAPTER 8:   EVALUATION OF MICROCRACKING IN AEROSPACE
COMPOSITES EXPOSED TO THERMAL CYCLING: EFFECT
OF COMPOSITE LAY-UP, LAMINATE THICKNESS, AND
THERMAL RAMP RATE

8.1 INTRODUCTION

Fiber-reinforced composites are currently being used in structural aerospace applications where high strength combined with light weight is of critical importance. In such applications the composites are exposed to extreme environmental conditions. The composites present in the primary structure of airplanes are subjected to cyclic thermal loading during takeoff and landing. These wide variations in temperature cause microcracks to appear in the materials parallel to the fibers [1]. The immediate effect of microcracking is to cause degradation in the mechanical properties of the laminate including changes in moduli, Poisson's ratio, and coefficient of thermal expansion (CTE) [2]. Microcracks can also induce secondary forms of damage such as delamination, fiber breakage and creation of pathways for the ingression of corrosive fluids. Such damage modes may subsequently lead to laminate failure [3, 4].

Thermal cycling involves repeatedly cycling a specimen between two temperatures with a sufficient dwell time at either extreme to allow thermal equilibrium to be attained. Large thermal stresses develop in composite structures due to the anisotropic CTEs and mismatches between the fiber and matrix properties [4]. When the in-plane transverse stresses are sufficiently large, a microcrack appears across the width of a ply-group [5, 6]. A detailed account of the factors affecting the formation of microcracks in carbon fiber composites is given by Spain [7]. Previous work on thermally induced damage was focused on transverse cracking of composites subjected to cyclic thermal loading in the environment of outer space (-157°C to 121°C) [1,8-11].

The long service life requirements of aerospace composite structures and the limited time available for development and evaluation of new materials make accelerated aging characterization necessary. The objective of this research was to study the effect of composite lay-up, thermal ramp rates, and composite laminate thickness on the microcracking performance of a commercially available carbon fiber epoxy system. The

long-term goal of this chapter was to tailor an aging cycle to carbon fiber based composites that produced results in less time than the currently established thermal cycle for Kevlar® based composites.

8.2 EXPERIMENTAL

8.2.1 Laminate Preparation

A commercially available grade 145 carbon fiber prepreg based on unidirectional fibers or 3k-70 PW fibers and Hexcel® F593™ resin was used to fabricate the test laminates. Two sets of composite panels were prepared for this study. The first set of panels consisted of the following orientations: $[0_5/90_5]_s$, $[0/90]_{10}$, 20 ply unidirectional and 20 ply woven. As shown schematically in Figure 8-1 microcracking in the $[0_5/90_5]_s$ and the $[0/90]_{10}$ configurations were observed by looking at two adjacent faces of a single cross-ply laminate. Thus, a total of only four panels were required to study transverse cracking in six configurations. The second set of laminates was prepared to study the effect of laminate thickness and thermal ramp rate on microcracking induced by thermal cycling. The thickness of the panels was varied without changing the ratio of 0° and 90° plies by using the following lay-up schedules: $[90_5/0_5]_s$, $[90_4/0_4]_s$, $[90_3/0_3]_s$ and $[90_2/0_2]_s$. A total of 16 different panels were used to expose each of these configurations to four different ramp rates.

The prepreg was cut into 22.5 x 22.5 cm plies and each ply was vacuum compacted to form a laminate of the required lay-up. The panels were then cured in an autoclave using a standard 177°C cure cycle. The temperature was raised from 27°C to 177°C at a ramp rate of 2.78°C/min with a two-hour hold at 177°C. A pressure of 310 kPa was used during the curing cycle. Vacuum was applied until an autoclave pressure of 103 kPa was reached at which point the vacuum bag was vented to the atmosphere. Each cured laminate was cut into 9 x 9 cm sample specimens.

8.2.2 Thermal Cycling

The first set of laminates was exposed to a previously established thermal cycle for Kevlar® based composites in an environmental chamber (Delta 9039) equipped with

liquid nitrogen cooling and electrical resistance heating. The thermal cycle varied from −53.9°C to 71.1°C at a heating and cooling rate of 10°C/min with a three minute hold at each temperature extreme. Each thermal cycle had a period of 31 minutes [12].

The second set of laminates was exposed to a thermal cycle that varied from −53.9°C to 71.1°C with a three minute hold at each temperature extreme. Four different heating and cooling rates of 2.5°C/min, 5°C/min, 10°C/min and 20°C/min were used.

8.2.3 Microcrack Evaluation

An optical microscope was used to observe microcracks in the sample specimens using 100x magnification. Two adjacent faces of each specimen in the first set and one face of each specimen in the second set were cleaned and polished to enhance microscopic observation. Microcrack density in laminates was calculated by counting the number of transverse cracks present per unit length of the specimen. Cracks per unit length was used as the quantification of microcracking in this case instead of cracks per unit area because the laminate thickness was one of the variables studied. Laminates from the first set were observed at intervals of 400 thermal cycles and the samples from the second set were observed at four cycle intervals until 50 cycles after which observations were made every 10 cycles from 50 to 100 cycles.

8.3 RESULTS & DISCUSSION

The microcrack density of the different laminate configurations used to study the effect of composite lay-up on microcracking is shown in Table 8-1. It was not possible to observe microcracks in the 0° layers since microcracks form parallel to the fibers. Thus microcracks in $[0]_{20}$ unidirectional laminate are not reported. After 1200 thermal cycles the $[90_5/0_5]_s$ side of the symmetric laminate showed extensive transverse microcracking followed by the adjacent $[0_5/90_5]_s$ side of the same laminate and the $[90/0]_{10}$ side of the asymmetric laminate. No microcracks were observed in the unidirectional, woven or the $[0/90]_{10}$ side of the asymmetric laminate. All the microcracks observed in the cross-ply laminates were present on the bag side of the laminate indicating that minor defects present on the bag side induced microcracking. The only difference between the $[90/0]_{10}$

and the $[0/90]_{10}$ asymmetric configuration is that the 90° layer was present on the bag side in case of the $[90/0]_{10}$ and was present on the tool side in case of the $[0/90]_{10}$ configuration. The existence of no microcracks in the $[0/90]_{10}$ configuration after 1200 thermal cycles indicates that tool finish reduces microcracking in laminates. From this initial assessment the $[90_5/0_5]_s$ symmetric laminate was identified as the composite lay-up most susceptible to microcracking and was used in subsequent tests of thickness and thermal ramp rate.

All transverse cracks propagated fully across the thickness of the 90° ply group when first detected (Figure 8-2). The location of the transverse cracks appeared to be random, favoring neither the ends nor the mid-length of the specimen. Some transverse cracks branched into two distinct cracks a few fiber diameters from the adjacent 0° layer (Figure 8-3).

The effect of thickness of the laminate on microcrack density is shown in Figures 8-4 to 8-7. Thinner laminates required more thermal cycles to initiate microcracking (Figure 8-4). $[90_2/0_2]_s$ showed no microcracks after 100 thermal cycles for the four different ramp rates used indicating that thinner laminates had lower stress concentrations. Adams et al. showed that decreasing the percentage of 90° layers increased the transverse tensile stress and microcrack density. In the earlier work no significant difference was detected between laminate configurations having the same percentage of 90° layers and same thickness [6]. However, in this study it was observed that laminates having the same percentage of 90° layers showed differences in microcrack density (Table 9-1 and Figures 8-4 to 8-7). This may possibly have been due to different thermal cycles or different materials used in the two studies. The thermal cycle used in the previous study was much more severe than the one used in this study.

At higher ramp rates (≥5°C/min) it was observed that as the thickness of laminate increases from $[90_2/0_2]_s$ to $[90_4/0_4]_s$ the microcrack density increased. The crack density in the $[90_5/0_5]_s$ was lower than the $[90_4/0_4]_s$ laminate due to the existence of a thermal gradient across the $[90_5/0_5]_s$ laminate. The external layers of the $[90_5/0_5]_s$ laminate were at the same temperature as the surrounding environment while the inner layers remained warmer when the outer temperature reached a minimum and cooler when the outer

temperature reached a maximum. Thus the difference between the material temperature and the stress free temperature was not uniform throughout the laminate. This resulted in lower stress concentrations in the thickest laminate and therefore the crack density was lower than the $[90_4/0_4]_s$ laminate. The inability of a thick laminate to reach thermal equilibrium under thermal cycling is known as the skin core effect. This effect was most obviously displayed in Figure 8-7 when a ramp rate of 20°C/min was used. In all cases, except at a ramp rate of 2.5°C/min, the microcrack density in $[90_5/0_5]_s$ was between $[90_4/0_4]_s$ and $[90_3/0_3]_s$ showing that the skin core effect reduced microcracking in the $[90_5/0_5]_s$. At a ramp rate of 2.5°C/min the microcrack density increased with an increase in thickness of the laminate (Figure 8-4) indicating that that there was no thermal gradients within the in the $[90_5/0_5]_s$ laminate at very low ramp rates. The lower thermal ramp rates allowed thermal equilibrium to be reached in the $[90_5/0_5]_s$ laminate.

The effect of thermal ramp rates on microcrack density after 100 thermal cycles is shown in Figure 8-8. It was observed that as the thermal ramp rates were increased the microcrack density increased in the $[90_3/0_3]_s$, the $[90_4/0_4]_s$ and the $[90_5/0_5]_s$ laminates. Using a faster thermal ramp rate reduced the time of each thermal cycle and appeared to accelerate the thermal aging of the composite. The increase in microcrack density was more dramatic for the $[90_4/0_4]_s$ than the $[90_5/0_5]_s$ and the $[90_3/0_3]_s$ laminates. This shows that for the symmetric lay-up and material used there is a thickness where sensitivity to ramp rate in terms of internal stresses is maximized. There was no effect of thermal ramp rate on the $[90_2/0_2]_s$ laminate showing that a certain minimum thickness of the laminate was required to generate enough internal stress for microcracks to appear.

8.4 CONCLUSIONS

Work was performed on the effect of composite lay-up, laminate thickness and thermal ramp rate on microcracking induced by thermal cycling for a commercially available carbon fiber composite system. The following lay-up schedules were subjected to a previously established thermal cycle for Kevlar® based composites: $[0_5/90_5]_s$, $[0/90]_{10}$, 20 ply unidirectional and 20 ply woven. After 1200 thermal cycles the greatest

microcrack density was found in a symmetric cross-ply laminate on the $[90_5/0_5]_s$ side where the 90° layer contacted the bag. Based on these findings the $[90_5/0_5]_s$, $[90_4/0_4]_s$, $[90_3/0_3]_s$ and $[90_2/0_2]_s$ symmetric laminates were prepared and exposed to a thermal cycle using ramp rates of 2.5°C/min, 5°C/min, 10°C/min and 20°C/min. It was found that a certain minimum thickness of the laminate was required to generate enough internal stress for microcracks to appear. A thermal ramp rate of 2.5°C/min allowed thermal equilibrium to be reached in the thickest panels, but at higher ramp rates a skin core effect was observed that hindered microcracking. The $[90_4/0_4]_s$ laminate appeared to be the ideal cross-ply laminate to study microcracking induced by thermal cycling in this material. Collectively it was shown that for a given composite system subjected to a specific thermal cycle the lay-up and thickness of the laminate can be adjusted to maximize microcrack sensitivity.

NOTES TO CHAPTER 8

1. Park, C.H. and H.L. McManus. 1996. Thermally Induced Damage in Composite Laminates: Predictive Methodology and Experimental Investigation, *Composites Science and Technology*, 56(10): 1209.

2. Tompkins, S.S., J.Y. Shen and A.J. Lavoie. 1994. Thermal Cycling of Thin and Thick Ply Composites, *Proceedings of the 4th International Conference on Engineering, Construction, and Operations in Space*, Albuquerque, NM, 326.

3. Swanson, S.R. 1997. Introduction to Design and Analysis with Advanced Composite Materials, Prentice Hall, Inc., Upper Saddle River, NJ.

4. Mallick, P.K. 1993. Fiber Reinforced Composites: Materials, Manufacturing and Design, 2nd ed., Marcel Dekker: New York, pp. 566.

5. Hancox, N.L. 1998. Thermal Effects on Polymer Matrix Composites: Part 1. Thermal Cycling, *Materials and Design*, 19(3): 85.

6. Henaff-Gradin, C. M., C. Lafarie-Frenot and D. Gamby. 1996. Doubly Periodic Matrix Cracking in Composite Laminates. Part 2: Thermal Biaxial Loading, *Composite Structures*, 36(1-2): 131.

7. Spain, R.G. 1971. Thermal Microcracking of Carbon Fibre/Resin Composites, *Composites*, 2: 33.

8. C. T. Herakovich and M. W. Hyer. 1985. Damage-Induced Property Changes in Composites Subjected to Cyclic Thermal Loading, *Engineering Fracture Mechanics*, 25(5-6): 779.

9. Adams, D.S., D.E. Bowles and C.T. Herakovich. 1986. Thermally Induced Transverse Cracking in Graphite-Epoxy Cross-Ply Laminates, *Journal of Reinforced Plastics and Composites*, 5: 152.

10. McManus, H.L., D.E. Bowles and S.S. Tompkins. 1996. Prediction of Thermal Cycling Induced Matrix Cracking, *Journal of Reinforced Plastics and Composites*, 15: 124.

11. Brown, T.L. and M.W. Hyer. 1996. <u>Effects of Long-Term Thermal Cycling on Microcracking Behavior in Composite Materials</u>, *Proceedings of the 1996 11th Technical Conference of the American Society for Composites*, Atlanta, GA, 476.

12. 1992. <u>BMS 8-341: Surfacing Films for Composites</u>, The Boeing Company, Seattle, WA.

LIST OF TABLES

Table 8-1. Microcrack density (Cracks/cm) as a function of no. of thermal cycles

No. of	Symmetric		Asymmetric		Unidirectional	Woven
Thermal Cycles	$[90_5/0_5]_s$	$[0_5/90_5]_s$	$[90/0]_{10}$	$[0/90]_{10}$	$[90]_{20}$	
400	2.69	1.34	0.38	0	0	0
800	2.69	2.12	0.76	0	0	0
1200	2.84	2.67	1.32	0	0	0

LIST OF FIGURES
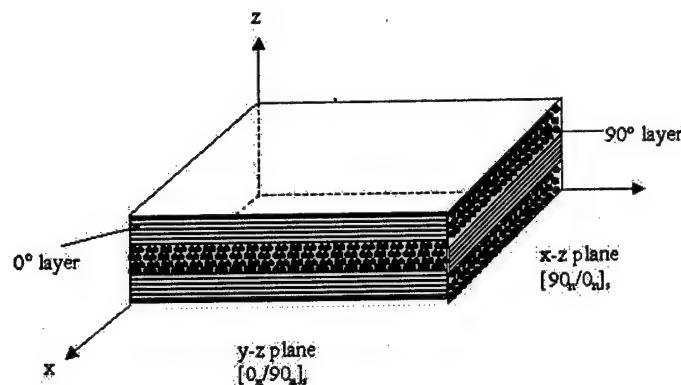
Figure 8-1. Cross-ply laminate showing $[0_n/90_n]_s$ and $[90_n/0_n]_s$ configuration on adjacent faces (Not to scale)
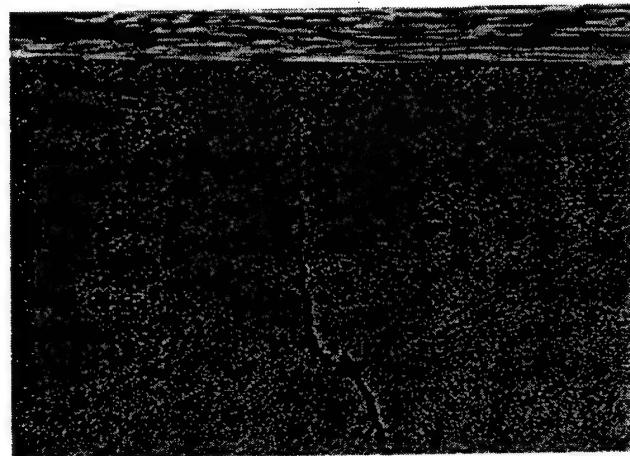
Figure 8-2. Optical micrograph of a $[90_5/0_5]_s$ laminate showing microcracking after 400 thermal cycles (100x)
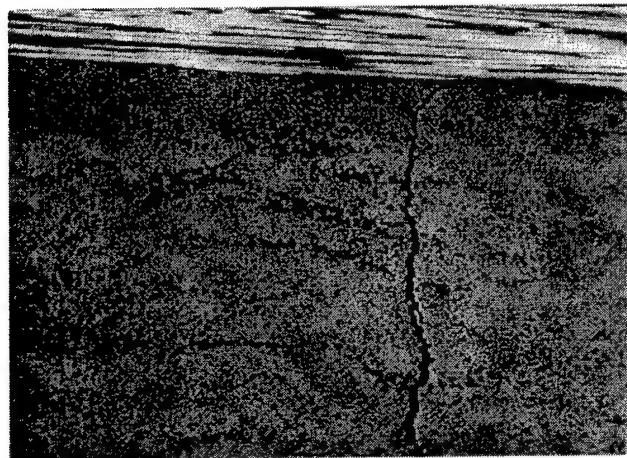
Figure 8-3. Optical micrograph of a [90₅/0₅]ₛ laminate showing branched microcracking after 1200 thermal cycles (100x)
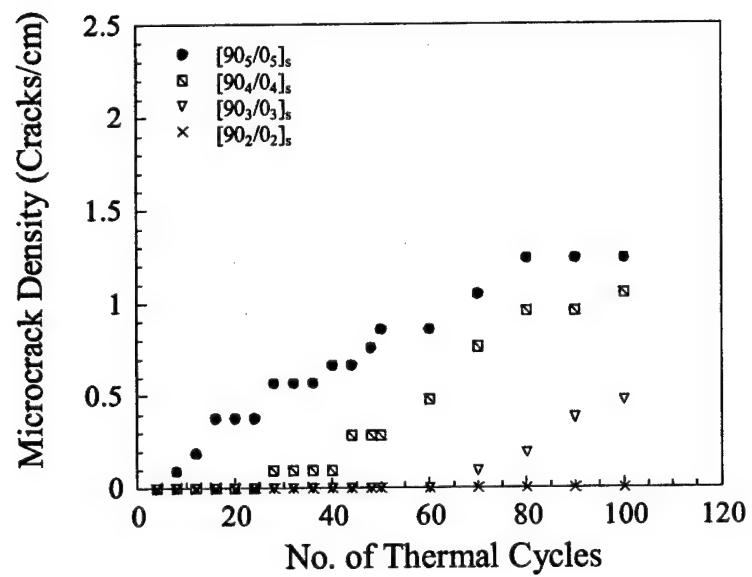
Figure 8-4. Crack density in different thickness symmetric laminates as a function of thermal cycles (Ramp rate of 2.5°C/min)
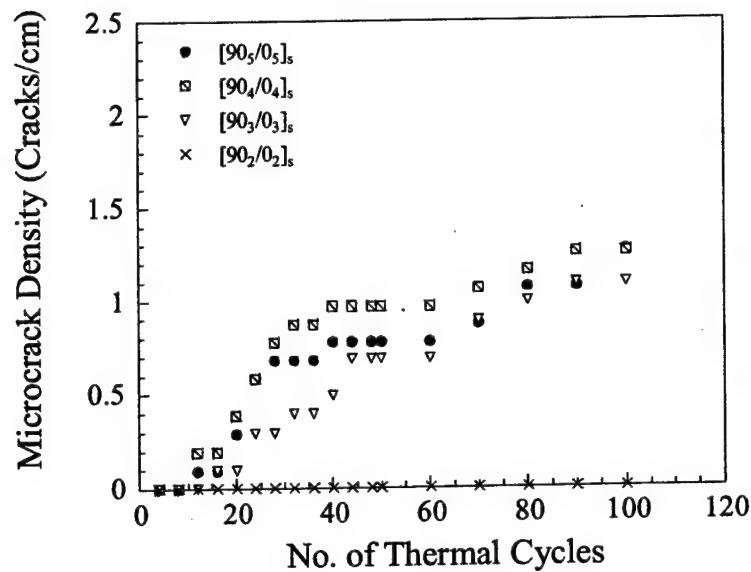
Figure 8-5: Crack density in different thickness symmetric laminates as a function of thermal cycles (Ramp rate of 5°C/min)
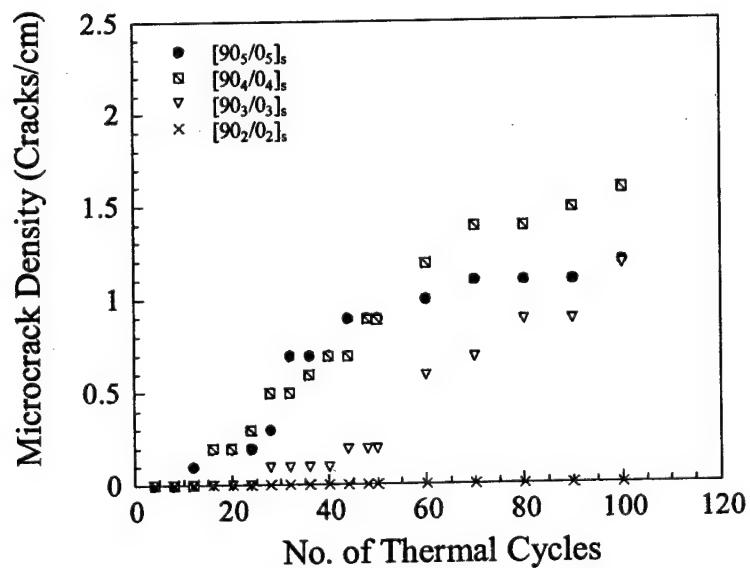
Figure 8-6. Crack density in different thickness symmetric laminates as a function of thermal cycles (Ramp rate of 10°C/min)
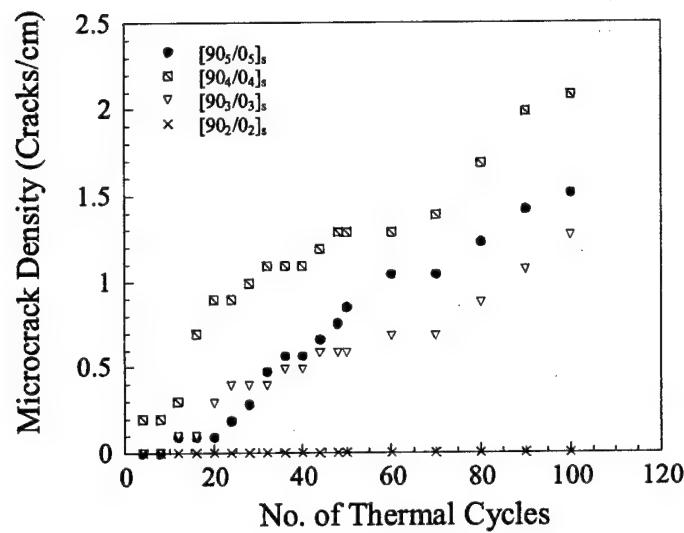
Figure 8-7. Crack density in different thickness symmetric laminates as a function of thermal cycles (Ramp rate of 20°C/min)
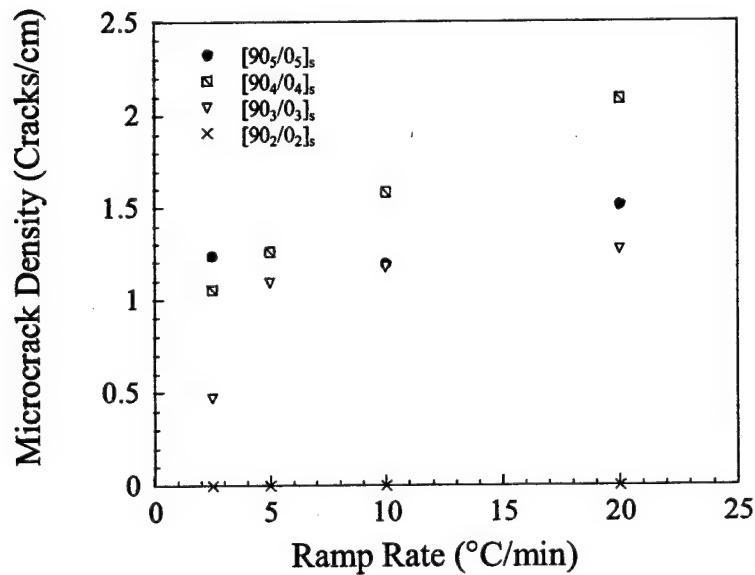
Figure 8-8. Effect of thermal ramp rate on microcrack density in different thickness symmetric laminates (After 100 thermal cycles)

CHAPTER 9: CURE TEMPERATURE EFFECTS ON MICROCRACKING AND INTERNAL STRESS DEVELOPMENT

9.1 INTRODUCTION

Increased thermal stresses are the underlying cause of microcracking in composites at cryogenic temperatures. Residual stresses develop in composite materials during and after cure as the temperature of the material falls below its stress free temperature. Residual stresses are the result of cure shrinkage of the matrix, Poisson's effects, differences in the coefficient of thermal expansion between the fibers and the matrix, and anisotropy in the expansion of the individual plies [1-5]. The amount of thermal stress in a laminate increases as the temperature deviates from the stress free temperature. When the residual stresses in the material become large enough they are relieved through physical processes such as potholing, delamination, and/or microcracking [3-5]. Chung et al. showed that the degradation of composite materials exposed to cryogenic temperatures is increased by thermal cycling between cryogenic and room temperature conditions [6]. Work in the past has shown that the residual stresses in a laminate depend directly on the processing conditions during laminate fabrication. Higher curing temperatures have been shown to cause an increase in the residual stress in a laminate by increasing the stress free temperature [1, 7-9]. However, these studies have not been performed for composite materials used in cryogenic applications.

Understanding the mechanisms behind the generation of residual stresses is key to preventing microcracking and the degradation of composite materials when exposed to cryogenic cycling. The previous chapters focused on a phenomenological approach that evaluated the effects of variations in the components and structure of a composite material on cryogenic microcracking. In this chapter, the effects of processing were evaluated on an experimental and a theoretical level, and a simple model was developed to gain a better understanding of the internal stresses in composite materials at cryogenic temperatures.

A model prepreg system was used to evaluate the effect of cure temperature on microcracking in polymeric composite materials exposed to cryogenic cycling. Symmetric and unsymmetric carbon fiber/epoxy laminates were fabricated to examine the development of thermal stresses and microcracks at cryogenic temperatures. The residual strains and theoretical curvatures of the laminates were calculated from the composite properties and correlated with the microcrack density and experimentally observed curvatures. Higher cure temperatures resulted in higher stress free temperatures and residual strains in the laminates, which corresponded directly to increased levels of microcracking.

9.2 EXPERIMENTAL

9.2.1 Materials and processing

A mixture of commercial epoxy resins was used as the model resin for the polymeric matrix. The resins used were EPON® 828 and EPON® 1031 from Resolution Performance Products and D.E.N. 438 from the Dow Chemical Company. EPON® 828 is described in chapter 3. EPON® 1031 is a tetrafunctional epoxy resin with an aromatic backbone (tetraphenyloethane glycidyl ether). D.E.N. 438 is a multifunctional epoxy novolac resin. Ancamine 2049, 4,4'-methylenebis(2-methyl-cyclohexanamine), a liquid tetrafunctional cycloaliphatic amine from Air Products, was used as a curing agent.

The epoxy resins were combined in a 50:40:10 ratio by weight of D.E.N. 438: EPON® 1031: EPON® 828 in an oil bath at 120°C and stirred until they were completely mixed. The mixture was allowed to cool to 40°C at which point a stoichiometric amount of Ancamine 2049 was added. The resin was then mixed until uniform and immediately prepregged.

Unidirectional prepregs consisting of the resin discussed above and Toray 50C T300YC carbon fibers were developed. Epoxy sizing was present on all of the fibers, and the filament count was 12,000 per tow. A hot-melt prepreg machine was used to impregnate the fibers with the epoxy resin [10]. The prepreg fiber areal weight was set to 150 g/m^2 and the nominal resin content was 30±2 weight percent for all of the experiments. The filming and impregnation temperatures were 55°C and 65°C,

respectively. Two rollers were used to apply the impregnation pressure. The pressure on the first roller was 69 kPa and the pressure on the second was 276 kPa. The line speed was 1.53 m/min. The resin content of the prepregs was determined in accordance with ASTM D 3171-99 and Boeing Support Standard 7336 using the technique described in chapter 3.

Symmetric, unsymmetric, and unidirectional 15.24 x 15.24 cm laminates were laid up using the above prepregs. The symmetric laminates consisted of 12 plies of prepreg in a $[0°_3, 90°_3]_s$ configuration, the unsymmetric laminates consisted of 4 plies in a $[0°_2, 90°_2]$ configuration, and the unidirectional laminates contained 20 plies of prepreg. After every third ply for the symmetric and unidirectional laminates and every ply for the unsymmetric laminates the prepreg stack was precompacted under vacuum pressure for two minutes before additional plies were positioned.

The autoclave cure cycle consisted of a 2.8°C/min ramp to the cure temperature followed by a hold at the cure temperature and a ramp down to 27°C at a rate of 2.8°C/min. The total consolidation pressure used during cure was 310 kPa. The vacuum bag was vented to the atmosphere when the autoclave pressure reached 104 kPa. Several curing temperatures were investigated, and the different curing temperatures necessitated different curing times to achieve a high degree of cure. Table 9-1 shows the curing times and temperatures used in this study.

Once cured, the symmetric laminates were cut into 3.49 x 1.27 x 0.16 cm (length x width x thickness) samples for cycling studies. The edges of the symmetric laminates were polished prior to cycling to facilitate optical microscopy of the surfaces. Geometric considerations were used to measure the curvature of the unsymmetric laminates, and the unsymmetric laminates were then cut into 1 x 20 cm (width x length) samples for three point bend testing. The unidirectional laminates were cut into 11 x 1.2 x 0.3 cm (length x width x thickness) samples for flexural tests.

9.2.2 Analysis

Differential scanning calorimetry (DSC) was performed on the matrix resin to determine the amount of residual cure present when different curing times and

temperatures were used. The same instrument described in chapter 5 was used for this investigation. All samples were tested in a nitrogen atmosphere. Each sample was ramped at 2.8°C/min to a cure temperature (70, 80, 100, 120, 140, 160, or 180°C), held for a specified time, and cooled to room temperature at 2.8°C/min before being subjected to a 5°C/min ramp to 350°C. The percentage cure was found by comparing the heat evolved during the cure cycle to the exotherm when an untested sample was ramped at 5°C/min to 350°C.

The resin content of the prepregs was determined in accordance with ASTM D 3171-99 and Boeing Support Standard 7336 [11, 12] using the technique described in chapter 3.

Dynamic mechanical analysis (DMA) experiments were performed on the cured symmetric laminates using the same instrument and experimental techniques outlined in chapter 3. The cured unsymmetric laminates were tested with the DMA described in chapter 3 using a three point bending apparatus in a controlled force mode. The samples were exposed to a 2°C/min ramp to 250°C with an applied force of 0.005 N. The stress free temperature of each sample was reported as the temperature at which each laminate displayed zero curvature.

The flexural modulus and strength of the unidirectional laminates in the transverse and longitudinal directions were determined through three point bend testing as described in chapter 6, with a span to thickness ratio of 60 for the longitudinal tests [13]. Five samples from each material were tested and the average value reported

The unidirectional samples from the flexural tests were used to fabricate 1 x 1 cm samples for the determination of the longitudinal and transverse coefficients of thermal expansion of these materials. Each sample was obtained from a portion of the flexural sample that was not damaged during testing. The coefficient of thermal expansion was determined using a TA instruments 2940 thermomechanical analyzer (TMA) with subambient temperature capability controlled by Thermal Solutions 1.2 J software. A heating rate of 5°C/min from 0°C to 100°C was used with a macro-expansion probe and a force of 0.1 N in a nitrogen environment. The coefficient of thermal expansion was calculated from the slope of the dimension change with temperature between 10°C and

60°C. This technique was performed according to ASTM E 831-93 [14]. Three samples from each material were tested and the average value reported.

Three cut and polished symmetric laminates from each material were exposed to the cryogenic microcracking test procedures described in chapter 3 and the average crack density was recorded.

9.2.3 Modeling approach

Bailey et al. used the model developed by Brand and Backer to show that the longitudinal strain, $\varepsilon_{tl}{}^{th}$, that develops in the transverse plies of a 0°/90°/0° composite upon cooling to a temperature T_2 below the stress-free temperature T_1 is given in the following equation [8, 15].

$$\varepsilon_{tl}^{th} = \frac{E_1 b (\alpha_t - \alpha_l)(T_1 - T_2)}{E_1 b + E_t d} \tag{9-1}$$

E_1 and E_t are the Young's moduli of the unidirectional plies parallel to the fibers and perpendicular to the fibers, respectively. Similarly, α_l and α_t are the longitudinal and transverse linear coefficients of thermal expansion of the unidirectional plies. *b* and *2d* are the 0° and 90° ply group thicknesses. An extension of the above analysis showed that the radius of curvature, ρ, of a $[0°_b\ 90°_d]$ laminate can be calculated using the following equation [8, 9, 15].

$$(\alpha_t - \alpha_l)(T_1 - T_2) = \frac{b+d}{2\rho} + \frac{E_1 b^3 + E_t d^3}{6\rho(b+d)}\left(\frac{1}{E_1 b} + \frac{1}{E_t d}\right) \tag{9-2}$$

This model is based on compound beam theory and assumes that the materials obey Hooke's law of elasticity, the number of 0° and 90° plies in the unsymmetric laminate are the same, the laminate cross-section is rectangular, and the radius of curvature of the unsymmetric laminate is much greater than the thickness of the laminate [15].

The above equations were used to calculate the longitudinal thermal strains in the transverse plies of $[0°_3 \, 90°_3]_s$ laminates and the curvature of $[0°_2 \, 90°_2]$ laminates cured at different temperatures. When the number of $90°$ plies equals the number of $0°$ plies in this geometry, as is the case in this study, it can be shown that the strains are of the same magnitude in the $0°$ and $90°$ plies [8, 15].

9.3 RESULTS AND DISCUSSION

9.3.1 Internal stress observation and prediction

In this study carbon fiber/epoxy laminates were cured at 70, 80, 100, 120, 140, 160, and 180°C. Curing times were adjusted so that all of the laminates showed approximately 5% residual cure as determined by differential scanning calorimetry. The anisotropy in expansion between the $0°$ and $90°$ plies in an unsymmetric laminate resulted in stresses that manifested themselves as curvature in the laminate [2]. Higher curing temperatures caused increased residual stresses in the laminates that were observed as larger curvatures of the unsymmetric laminates. Figure 9-1 shows the variation in curvature with cure temperature. Theoretical curvature values were determined from the mechanical properties of the laminates using Equation 9-2. These predicted curvatures are compared with the experimentally determined values in Figure 9-2. The error bars on the predicted curvatures represent one standard deviation. In nearly all of the cases, the predicted curvature was larger than the experimental curvature. This was probably due to the fact that the model approximated the laminates as being perfectly elastic, when they actually acted viscoelastically.

Controlled force dynamic mechanical analysis was used to determine the temperature at which the curvature of the unsymmetric laminates became zero. This method of determining the stress free temperature of a laminate has been shown to be an effective technique, taking into account both thermal and cure shrinkage effects [1, 16]. Figure 9-3 shows how the stress free temperatures of the laminates varied with cure temperature.

At lower cure temperatures the stress free temperature was significantly higher than the cure temperature, but as the cure temperature was increased the stress free

temperature began to approach a constant value. This may have been the result of an increase in the temperature of the laminate above the autoclave temperature because of an exotherm. It is also possible that at higher cure temperatures the ultimate glass transition temperature of the resin system was approached. At this point free volume changes would become smaller and a reduced dependence of the laminate properties on cure temperature would be seen.

Equation 9-1 was used to calculate the residual thermal strains in the symmetric laminates at cryogenic temperatures. Figure 9-4 shows how the predicted residual strains changed with cure temperature. The error bars represent one standard deviation. The residual strains increased with cure temperature and leveled off at the high and low end of the temperature range studied. This paralleled the increase in stress free temperature shown in Figure 9-3.

9.3.2 Composite properties

Crasto et al. showed that the ratio of the difference between the stress free temperature (SFT) and the cure temperature (Tcure) to the difference between the stress free temperature and the use temperature (TLN$_2$) is a measure of the percent of the total stresses that may be attributed to cure shrinkage [1]. The use temperature was considered to be that of liquid nitrogen (-195.6°C) in this study as it was primarily concerned with thermal stresses at cryogenic temperatures. Figure 9-5 shows the percentage of shrinkage stress in the laminates at cryogenic temperatures.

Some small variations in the percent of stress resulting from cure shrinkage were present at low cure temperatures and were most likely due to the longer curing times and slightly lower degree of cure when the laminates were cured at 70 and 80°C. When cure temperatures above 100°C were used the percent shrinkage stress decreased regularly with increasing cure temperatures.

The cure temperature affected the glass transition temperature (T$_g$) of the laminates as obtained by the peak in the loss modulus from dynamic mechanical analysis. Figure 9-6 demonstrates the effect of cure temperature on the laminate glass transition temperature. The T$_g$s of the laminates increased with cure temperature. When higher

cure temperatures were used the polymeric network was formed at a higher temperature, and as such, the glass transition temperatures were higher.

9.3.3 Laminate microcracking

All of the laminates in this study formed microcracks as a response to cryogenic cycling. The density, distribution, and morphology of the microcracks varied with the cure temperature. Figure 9-7 is an optical photomicrograph of a representative microcrack in one of the laminates after thermal cycling at cryogenic temperatures.

Microcracks began at the outer edge of the sample and propagated towards the interior, transverse to the fibers as shown in Figure 9-7. Higher cure temperatures caused the formation of microcracks that were more tortuous and wider than those in the laminates cured at lower temperatures. The laminates with cure temperatures above 140°C exhibited some delamination at the 0°/90° ply interface, which can be seen in Figure 9-7. This phenomenon became more widespread as the cure temperature increased. Laminates with higher cure temperatures were also more prone to the formation of networks of cracks rather than individual cracks as shown in Figure 9-8. Larger thermal stresses were generated in the laminates when cured at higher temperatures. Fracture processes relieved these stresses in the laminates and manifested themselves as more delamination, wider microcracks, and greater crack network formation during thermal cycling relative to laminates cured at lower temperatures.

The microcrack density in the ambient/cryogenic thermally cycled laminates, shown in Figure 9-9, exhibited a dependence on the cure temperature. The error bars represent one standard deviation. It should be noted that no statistical difference in the flexural modulus, flexural stress at yield, or coefficient of thermal expansion was observed in the unidirectional laminates cured at different temperatures. This suggested that any dependence of microcrack density on cure temperature was due to different levels of stress and not a variation in the mechanical properties of the laminates. Higher curing temperatures caused an increase in the microcrack density by elevating the level of thermal stress present in the laminates. There was no statistical difference in the microcrack density between the laminates cured at 140, 160, and 180°C. However,

within this series of cure temperatures the microcrack tortuosity, width, and presence of crack networks increased. These phenomena could have increased the amount of stress relieved without increasing the microcrack density. The microcrack density was also shown to be affected by the stress free temperature of the laminate. When the stress free temperature became larger the level of thermal stress in the laminate increased and the release of more energy was necessary to relieve the stresses [2]. Figure 9-10 presents the relationship between the microcrack density and the stress free temperature of the laminates, with the error bars representing one standard deviation. Predicted values of residual strain in the laminates parallel the stress free temperature and correlate with the microcrack density. Figure 9-11 shows how the microcrack density varied with the calculated thermal strains in the laminates, with the error bars representing one standard deviation. The microcrack density increased with higher stress free temperatures and the resulting larger thermal strains but reached a constant value as differences in microcrack distribution and morphology began to outweigh the formation of more microcracks.

9.4 CONCLUSIONS

The research presented in this chapter examined the effects of cure temperature on the response of carbon fiber/epoxy composite materials to cryogenic cycling. Theoretical predictions of the development of thermal strains in composite materials were shown to correlate with experimental observations. Microcracking occurred in all of the laminates tested, but significant variations in the number and morphology of the microcracks existed between the laminates cured at different temperatures. Higher curing temperatures resulted in higher stress free temperatures, residual thermal strains, and glass transition temperatures of the laminates. The larger stress free temperatures corresponded to increased microcrack densities and larger levels of residual thermal strain. Laminates cured at high temperatures also showed a greater propensity to delaminate, contain wider and more tortuous cracks, and form networks of cracks. Collectively, this chapter showed that the development of thermal stresses in composite

materials at cryogenic temperatures could be modeled and was enhanced by higher cure temperatures.

NOTES TO CHAPTER 9

1. Crasto, A.S. and R.Y. Kim. 1993. On the Determination of Residual Stresses in Fiber-Reinforced Thermoset Composites, *Journal of Reinforced Plastics and Composites*, 12: 545.

2. Mallick, P.K. 1993. Fiber Reinforced Composites: Materials Manufacturing and Design, 2nd ed., Marcel Dekker: New York, pp. 566.

3. Nguyen, B. 1999. Cryotank Skin/Stringer Bondline Analysis, *Proceedings of 44th International SAMPE Conference*, Long Beach, CA, 44: 856.

4. Jang, B.Z., Y.K. Lieu, S. Chang and L.R. Hwang. 1987. Cryogenic Failure Mechanisms of Fiber-Epoxy Composites for Energy Applications, *Polymer Composites*, 8(3): 188.

5. Bobrov, E.S., J.E.C. Williams and W. Iwasa. 1985. Experimental and Theoretical Investigation of Mechanical Disturbances in Epoxy-Impregnated Superconducting Coils. Part 2. Shear-Stress-Induced Epoxy Fracture as the Principle Source of Premature Quenches and Training - Theoretical Analysis, *Cryogenics*, 25(6): 307.

6. Chung, K., J.C. Seferis and J.D. Nam. 1998. Accelerated Aging of Polymer Composites Through Environmental Cycling Effect, *Microstructural Science*, 25: 247.

7. Brinkman, M.R. and H. Sarrazin. 1995. Effects of Processing Temperature and Layup on Matrix Cracking, *Journal of Reinforced Plastics and Composites*, 14: 1252.

8. Bailey, J.E., P.T. Curtis and A. Parvizi. 1979. On the Transverse Cracking and Longitudinal Splitting Behavior of Glass and Carbon Fibre Reinforced Epoxy Cross Ply Laminates and the Effect of Poisson and Thermally Generated Strain, *Proceedings of the Royal Society of London, Series A*, 366: 599.

9. Simpson, M., P.M. Jacobs and F.R. Jones. 1991. Generation of Thermal Strains in Carbon Fibre-Reinforced Bismaleimide (PMR-15) Composites Part 1: The Determination of Residual Thermal Strains in Cross-Ply Laminates, *Composites*, 22(2): 89.

10. Putnam, J.W., B.S. Hayes and J.C. Seferis. 1996. Prepreg Process-Structure-Property Analysis and Scale-Up for Manufacturing and Performance, *Journal of Advanced Materials*, 27(4): 47.

11. 1996. Resin Content and Fiber Areal Weight of Prepreg Fabric and Tape, Test Method For, BSS 7336, Boeing Materials Technology, Boeing Commercial Aircraft Group, Renton, WA.

12. 1999. Standard Test Methods for Constituent Content of Composite Materials, ASTM D 3171-99, ASTM: West Conshohocken, PA.

13. 1998. Standard Test Methods for Flexural Properties of Unreinforced and Reinforced Plastics and Electrical Insulating Materials, ASTM D 790-98, ASTM: West Conshohocken, PA.

14. 1993. Standard Test Method for Linear Thermal Expansion of Solid Materials by Thermomechanical Analysis, ASTM E 831-93, ASTM: West Conshohocken, PA.

15. Brand, R.H. and S. Backer. 1962. Mechanical Principles of Natural Crimp of Fiber, *Textile Research Journal*, 32: 39.

16. Pagano, N.J. and H.T. Hahn. 1977. Evaluation of Composite Curing Stresses, *in Composite Materials: Testing and Design*, ASTM STP 617, ASTM: Philadelphia, p. 317.

LIST OF TABLES

Table 9-1. Laminate cure times and temperatures

Cure Temperature (°C)	Cure Time (hr)
70	18
80	5
100	3
120	2
140	2
160	2
180	2

LIST OF FIGURES
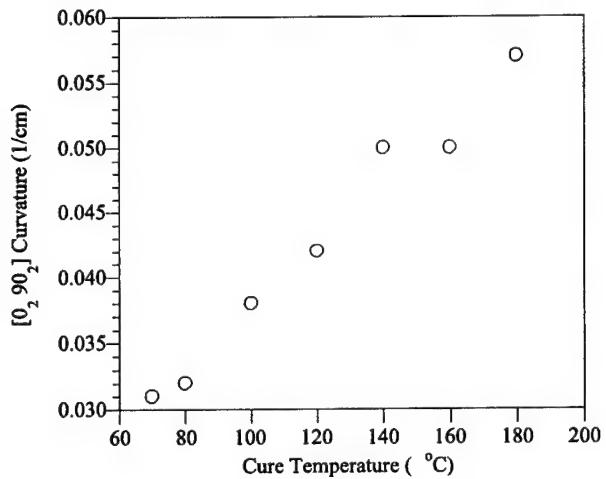
Figure 9-1. Variation in laminate curvature with cure temperature
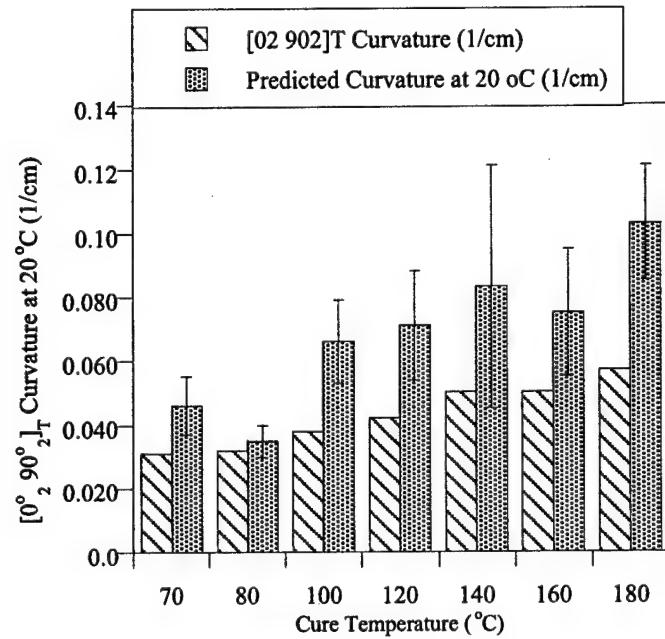
Figure 9-2. Predicted and experimental laminate curvatures at 20°C
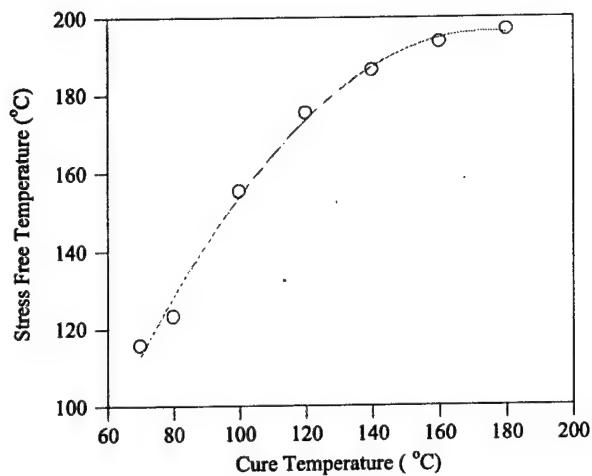
Figure 9-3. Variation in stress free temperature with cure temperature
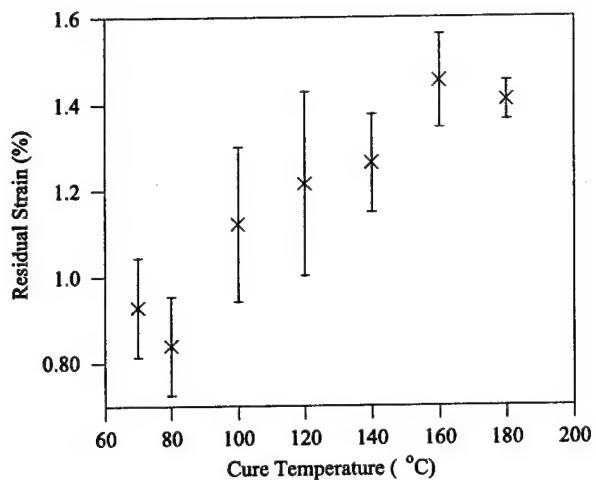
Figure 9-4. Variation in predicted residual thermal strains transverse to the plies in a
[0^{o}_{b} 90^{o}_{2d} 0^{o}_{b}] laminate with cure temperature at -195.6^{o}C
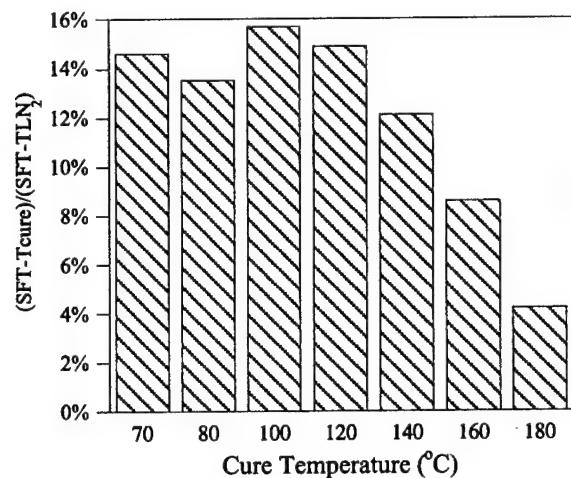
Figure 9-5. Variation in percent shrinkage stress with cure temperature
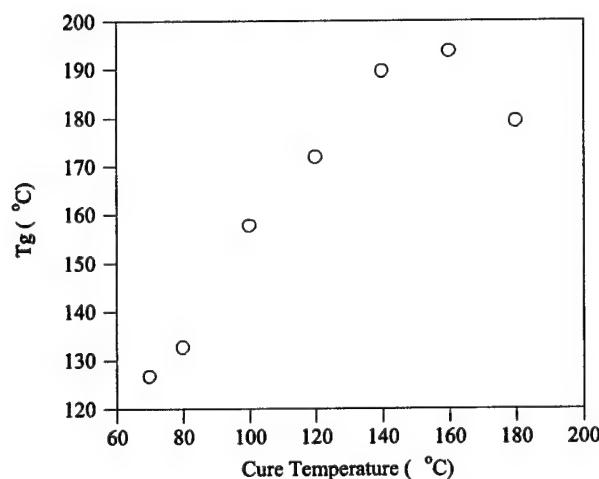
Figure 9-6. Variation in laminate glass transition temperature (from dynamic loss modulus) with cure temperature
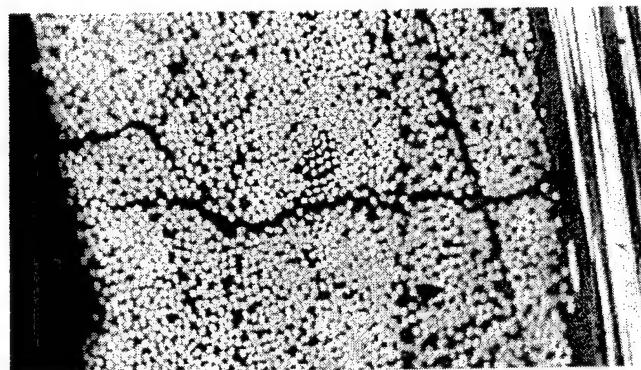
Figure 9-7. Optical photomicrograph of microcrack in a cured laminate (160°C) after 2 cycles in liquid nitrogen. 200x magnification
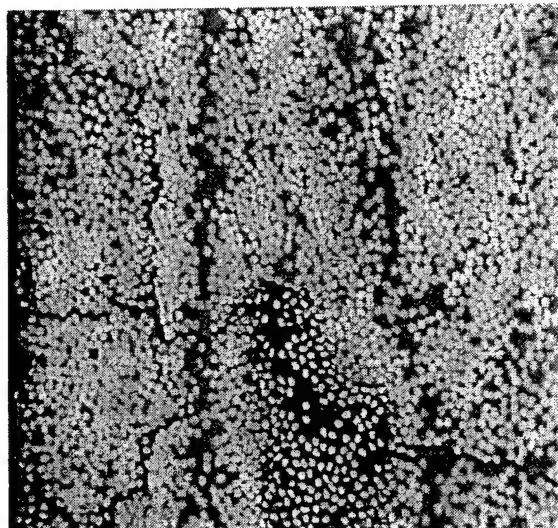
Figure 9-8. Optical photomicrograph of crack network in a cured laminate (180°C) after 3 cycles in liquid nitrogen. 200x magnification
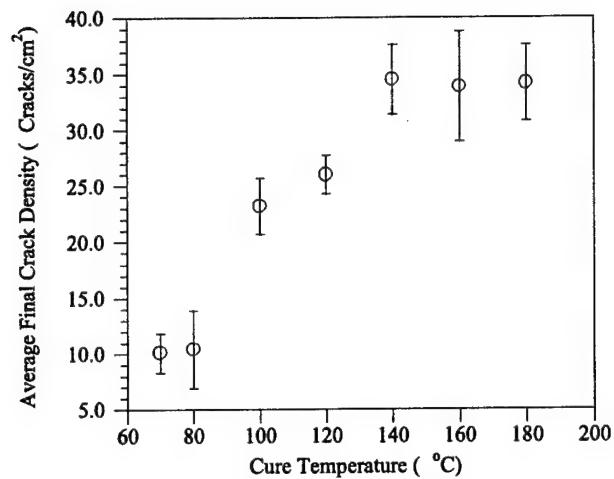
Figure 9-9. Variation in microcrack density with cure temperature
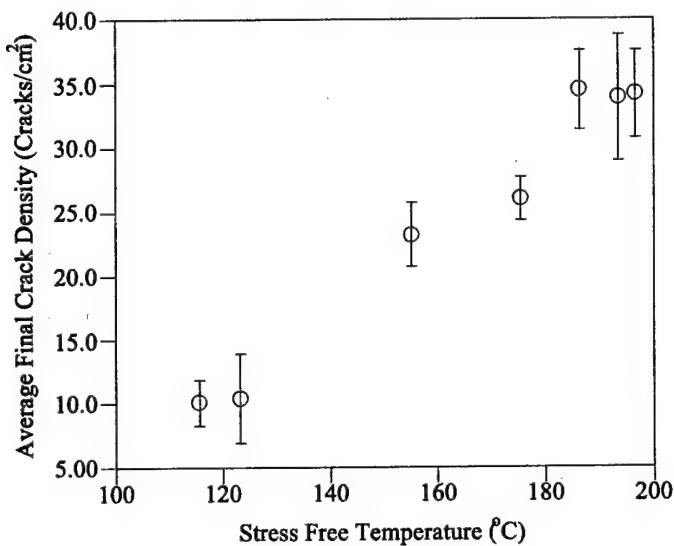
Figure 9-10. Variation in microcrack density with stress free temperature
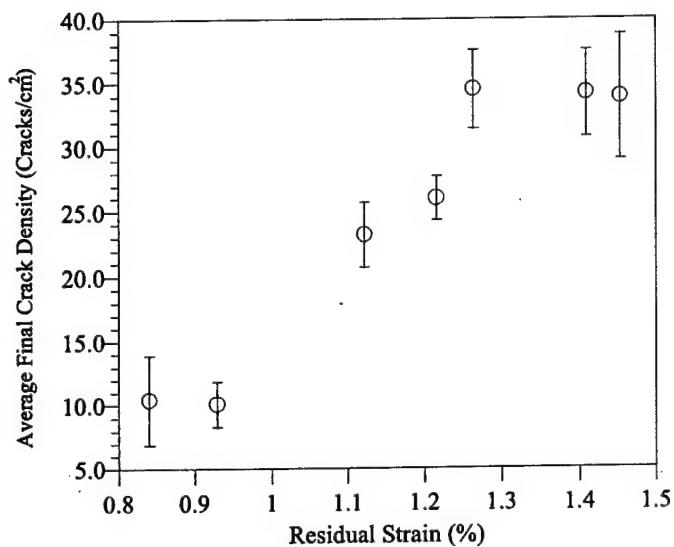
Figure 9-11. Variation in microcrack density with predicted residual thermal strains transverse to the plies in a $[0^{\circ}_b \, 90^{\circ}_{2d} \, 0^{\circ}_b]$ laminate at $-195.6^{\circ}C$

CHAPTER 10: PREDICTIVE MODELING OF MICROCRACKING IN CARBON FIBER/EPOXY COMPOSITES AT CRYOGENIC TEMPERATURES

10.1 INTRODUCTION

10.1.1 Background

As discussed in the previous chapters, the failure of composite cryogenic liquid storage structures is serious concern [1-8]. Because of this issue, many attempts have been made to predict the generation of thermal stresses in composite materials, the onset of microcracking, and the distribution and origination of microcracks during failure. Shear lag analyses, variational and strain energy release rate approaches, Monte-Carlo simulations, and *in situ* strength analyses are among the approaches that have been used to address this problem [9-14]. Varying degrees of success have been achieved by these analyses, but they are often unnecessarily complex and fail to account for the change in material properties with temperature. The strength and modulus of the laminate and its components, particularly the viscoelastic polymeric matrix, will be altered when exposed to significant decreases in temperature, resulting in stress generation and failure criteria that are different from those at room temperature [1, 15-19].

In this chapter, the temperature at which microcracking occurred in symmetric cross-ply carbon fiber/epoxy composite materials was predicted using a yield stress-based failure model. A fracture mechanics analysis of the *in situ* strength of the ply groups in a composite material was combined with a compound beam determination of thermal stress development to create the predictive model. This approach, unlike many other models, incorporated the change in material properties with temperature by using the room temperature properties of the laminate to predict the low temperature behavior of the ply groups. Dynamic mechanical analysis was used to assess microcracking at cryogenic temperatures through the observation of discontinuities in material properties during failure. Four different material systems were studied, and the model accurately predicted the onset temperature for microcracking in three of the four cases. It was shown that the room-temperature properties of a fiber reinforced polymeric composite laminate, appropriately modified to account for property variation at low temperatures, could be used to predict transverse microcracking as a response to thermal stresses at cryogenic

temperatures.

10.1.2 Model Development

Brand and Backer developed a compound beam analysis that can be adapted to describe the generation of thermal stresses in laminated materials. The advantage of this approach is that it takes into account stress relaxation during curing and cooling. The foundation of the compound beam analysis involves considering the ply groups as individual elastic entities and calculating the stresses that result from thermal expansion and contraction [20, 21]. The transverse tensile thermal stress in the central plies of a symmetric cross-ply laminate (σ_{tl}^{th}) was derived using compound beam theory and can be described by the following equation. It should be noted that Equation 10-1 was modified from Equation 9-1 to account for the change in material properties with temperature.

$$\sigma_{tl}^{th} = \frac{-E_t(T)E_l(T)\int\limits_{T_{SFT}}^{T_{Use}}[(\alpha_t(T)-\alpha_l(T))dT]}{E_l(T)+E_t(T)} \tag{10-1}$$

T_{Use} is the use temperature of the laminate ($^{\circ}$C), T_{SFT} is the stress free temperature ($^{\circ}$C), E_l and E_t, are the longitudinal and transverse Young's moduli (Pa) of a unidirectional laminate with the same thickness as the central ply group expressed as a function of temperature, and α_l and α_t are the longitudinal and transverse linear coefficients of thermal expansion expressed as a function of temperature ($^{\circ}$C^{-1}). It is proposed that microcracking will occur at the temperature that sets the thermal transverse tensile stress in the central ply group equal to the *in situ* yield strength. Past work by Wang et al. and Laws et al. showed that the yield strength of this ply group (Y_t) can be expressed as follows [12, 22].

$$Y_t = \frac{\sqrt{G_{IC}(T)E_t(T)}}{F_I\sqrt{a}} \tag{10-2}$$

Note that the original expression has been modified to account for the variation in material properties with temperature. G_{IC} is the critical strain energy release rate (N/m), E_t is the transverse modulus of the ply group in a plane stress condition, F_I is a factor derived from fracture mechanics, and a is the initial half crack length (m). The $F_I(a)^{1/2}$ term can be expressed as a constant, C ($m^{1/2}$). The following expression was produced from the combination of Equations 10-1 and 10-2 and can be solved to obtain the temperature at which failure will first occur.

$$\frac{\sqrt{G_{IC}(T)E_t(T)}}{C} = \frac{-E_t(T)E_l(T)\int\limits_{T_{SFT}}^{T_{Use}}[(\alpha_t(T)-\alpha_l(T))dT]}{E_l(T)+E_t(T)} \qquad (10\text{-}3)$$

A model laminate system was developed to determine the constant C and describe the temperature dependence of the material properties. The thermal stress in the laminate at the first failure event was calculated from the observed material parameters and the experimentally determined microcracking onset temperature. The thermal stress at failure was then set equal to the yield stress and Equation 10-3 was solved to determine C. This value of C was used in the model prediction for all subsequent materials.

10.2 EXPERIMENTAL

10.2.1 Material development

Four different unidirectional, prepreg-based carbon fiber/epoxy composite systems were used to determine the model parameters and validate its effectiveness. Three of these prepregs (referred to as prepregs 1 to 3) were prepared in the laboratory and one (prepreg 4) was supplied from an outside industrial source. The industrial material was used to assess the performance of the model in relation to a material with a less well known composition and processing history. The four prepregs are outlined in Table 10-1. The numbers in parentheses in Table 10-1 indicate standard deviations.

A mixture of commercially available epoxy resins formed the base of the polymeric matrix for the prepregs prepared in the laboratory. The resins used were

EPON® 828 and 1031 from Resolution Performance Products and D.E.R. 661 from the Dow Chemical Company. EPON® 828 and D.E.R. 661 are described in more detail in chapter 3, and the structure of EPON® 1031 is discussed in chapter 9. HT 976, 4,4'-diaminodiphenyl sulfone (DDS), from Ciba and 1-cyanoguanidine (dicy), Amicure® CG 1400 from Pacific Anchor Chemical Co., accelerated with 3-(3,4-dichloro-phenyl)-1,1-dimethyl urea (diuron) from Aldrich Chemical Co. were used as the curing agents.

The epoxy resins were combined in the weight ratios shown in Table 10-1 in an oil bath at 120°C and stirred until they were completely mixed. For prepreg systems 1 and 2, a stoichiometric amount of DDS was melted and added to the epoxy mixture in the oil bath. The epoxy/DDS mixture was blended for two minutes in the oil bath at 120°C after which the resin was cooled to 80°C and prepregged. For prepreg system 3, half of the 828 was set aside and blended with 5 parts per hundred resin (phr) dicy and 2 phr diuron in a high shear mixer to form a curing paste. The epoxy mixture was blended and allowed to cool to 80°C, at which point the curing paste was added. After blending the paste with the epoxies, the mixture was prepregged.

Unidirectional prepregs were developed consisting of the resins discussed above and epoxy sized Toray 50C T300YC carbon fibers. The filament count for all of the fibers was 12,000 per tow. A hot-melt prepreg machine was used to impregnate the fibers with the epoxy resin [23]. The prepreg fiber areal weight and the nominal resin content for the different prepregs are shown in Table 10-1. The filming and impregnation temperatures were 82°C and 93°C, respectively. Two rollers were used to apply the impregnation pressure. The pressure on the first roller was 69 kPa and the pressure on the second was 138 kPa. The line speed was 1.5 m/min and the gap height for resin filming was 0.30 mm.

The resin content of the prepregs was determined in accordance with ASTM D 3171-99 and Boeing Support Standard 7336 using the technique described in chapter 3 [24, 25].

Symmetric, unsymmetric, and unidirectional 10.16 x 10.16 cm laminates and unidirectional 33.02 x 12.7 cm laminates were laid up using the above prepregs. The symmetric laminates consisted of 12 plies of prepreg in a $[0^o_3, 90^o_3]_s$ configuration. The

unsymmetric laminates consisted of four plies in a $[0^o_2, 90^o_2]$ configuration. The 10.16 x 10.16 cm unidirectional laminates consisted of 6 plies and the 33.02 x 12.7 cm unidirectional laminates consisted of 16 plies with a 5.08 cm fluorinated ethylene propylene copolymer (FEP) crack starter placed in the midplane.

The laminates described above were exposed to an autoclave cure cycle that consisted of a 2.8°C/min ramp to 93°C, a one hour hold at 93°C, a ramp at 2.8°C/min to 177°C, a two hour hold at 177°C, and a ramp to 25°C at 2.77°C/min. The total consolidation pressure used during cure was 310 kPa. The vacuum bag was vented to the atmosphere when the autoclave pressure reached 104 kPa.

Once cured, the symmetric laminates were cut with a diamond saw into 3.49 x 1.27 cm (length x width) samples for cycling studies and the 6-ply unidirectional laminates were cut into 5.08 x 1.27 cm (length x width) transverse and longitudinal samples for modulus determination. The unsymmetric laminates were cut into 20.0 x 1.27 cm (length x width) samples for the determination of the stress free temperature and the 16-ply unidirectional laminates were cut into 33.02 x 1.27 cm (length x width) samples for fracture toughness testing. The edges of the cycling and modulus samples were polished prior to testing to facilitate optical microscopy of the surfaces.

10.2.2 Testing and analysis

Mode I interlaminar fracture toughness, G_{IC}, was measured using the double cantilever beam (DCB) method as described in chapter 6 [26]. For each laminate, five samples were tested. The longitudinal and transverse tensile moduli of the 6-ply unidirectional samples were determined using a Seiko SII 6100 dynamic mechanical spectrometer (DMS) controlled by Exstar 6000 version 6.0 software. The samples were exposed to a 2.5 N load for 10 seconds and then held at zero load for 10 seconds. This process was repeated as the samples were heated at 5°C/min from −120°C to 170°C. From the resulting position/load data, modified to account for thermally induced dimension changes in the samples, the modulus during each loading cycle could be determined. The dependence of the modulus on temperature was quantified using these data. The samples were examined using optical microscopy before and after testing to

ensure that no cracks or failure sites were formed during testing.

The cured unsymmetric laminates were tested as described in chapter 9 to determine the stress free temperature.

The unidirectional samples from the G_{IC} tests were used to fabricate 1.0 x 1.0 cm samples for the determination of the longitudinal and transverse coefficients of thermal expansion of the laminates. Each sample was obtained from a portion of the fracture toughness specimen that was not damaged during testing. The coefficient of thermal expansion was determined using the instrument and technique described in chapter 9. The dependence of the coefficient of thermal expansion on temperature was determined from the slope of the dimension change with temperature between -100°C and 170°C.

The cut and polished symmetric laminates were allowed to equilibrate at 22°C and were then cooled to a specified temperature and held for 10 minutes in the DMS 6100 described earlier. The microcracking onset temperature was determined by lowering the hold temperature in 5°C increments between runs until microcrack formation was observed. During cycling the laminates were deformed at a frequency of 1 Hz with an oscillation amplitude of 10 μm to identify changes in dynamic mechanical behavior at low temperatures and as microcracking occurred. It should be noted that previous experiments showed that deformation of this type and duration did not change the microcracking behavior of these samples.

Optical microscopy was used to observe and document the microcracking onset temperature and the response of the samples to cryogenic exposure as described in chapter 3. Five samples from each laminate were tested to determine the onset temperature for microcracking.

10.3 RESULTS AND DISCUSSION

10.3.1 Microcracking

Dynamic mechanical analysis of the symmetric laminates at cryogenic temperatures revealed information about the low temperature properties of composite materials and the effects of microcracking on their response to dynamic loads. The storage modulus (E′) and tan(δ) during exposure to sub-ambient temperatures are shown

in Figure 10-1 for a symmetric cross ply laminate made from prepreg 2. Figure 10-1A demonstrates that the storage modulus of the laminate increased as the temperature decreased, establishing that the properties of the laminates studied changed significantly at low temperatures. Therefore, the temperature dependence of material properties must be accounted for in a predictive model of microcracking at cryogenic temperatures.

The sharp, discontinuous decrease in the storage modulus seen in Figure 10-1A and the spike in tan(δ) shown in Figure 10-1B corresponded with the onset of microcracking in the laminate. Examination of the laminate after cycling revealed the formation of a microcrack spanning the interior ply group of face 2 of the laminate as defined in Figure 3-1. It should be noted that a similar E' and tan(δ) response appeared in all of the laminates where microcracking was observed. It was seen that microcrack formation decreased the stiffness of the laminate and caused a momentary increase in the phase lag. Microcracking debonded the fibers from the matrix and prevented efficient load transfer, reducing the modulus of the sample and increasing the ability of the laminate to dissipate energy at the fiber/matrix interface, causing an increase in tan(δ) [27, 28].

Microcracking was observed in the laminates made from prepregs 1, 2, and 4 as a response to cryogenic cycling. The majority of the microcracks spread across the entire width of the central plies in face 2 and propagated through the laminate. When the microcracks reached the interface between the 0° and 90° ply groups delamination was observed in some cases. Figure 10-2 presents optical photomicrographs of representative microcracks formed during cryogenic cycling. Figure 10-2A shows the microcrack formed during the thermal cycle in Figure 10-1. Figures 10-2B and 10-2C illustrate the formation and extension of a small crack during exposure to progressively lower temperatures. In some cases, as seen in Figure 10-2A, microcracks formed effectively instantaneously and propagated through the sample, at other times, demonstrated in Figures 10-2B and 10-2C, small cracks formed initially and gradually extended through the sample.

The microcracks propagated along the fiber-matrix interface and demonstrated considerable variation in width and morphology. Irregularities in crack size and shape

introduced significant error into the prediction of the number and distribution of microcracks as one large, tortuous crack may have dissipated as much energy as the formation of two smaller cracks. It is for this reason that the objective of this study was to predict the onset of microcracking and not the specific number or distribution of failure events.

10.3.2 Model predictions

The important material properties, specifically the coefficients of thermal expansion and the longitudinal and transverse tensile moduli, varied with temperature to different extents, ranging from effectively constant to depending strongly on temperature. The linear and transverse coefficients of thermal expansion did not exhibit temperature dependence between -100°C and 170°C for the carbon fiber/epoxy laminates studied. The longitudinal tensile modulus showed a small linear increase with decreasing temperature, with a typical increase of 0.08% after cooling from 25°C to -120°C. The transverse tensile modulus, which played a key role in the development of transverse tensile stresses, showed a significant linear increase with decreasing temperature, increasing on average 25% from 25°C to -120°C. The fracture toughness (G_{IC}) as a function of temperature was unknown and unable to be determined; therefore, an additional factor to account for changes in fracture behavior at low temperature was grouped into the constant C in Equation 10-3.

The average onset temperature for microcracking (T_{Use}), T_{SFT}, $E_l(T)$, $E_t(T)$, $\alpha_l(T)$, $\alpha_t(T)$, and G_{IC} for the laminates made from prepreg 1 were used to solve Equation 10-3 for the constant C. C was calculated to be $0.036 \text{ m}^{1/2} \pm 0.0062$. Once C was determined, the model could be applied to other material systems.

Figure 10-3 illustrates the effectiveness of the model in predicting the microcracking onset temperature, with the error bars indicating one standard deviation. It should be noted that the error bars are relatively large due to the variation in microcrack size and shape between each failure event. Error bars are not present on the observed microcracking temperature for prepregs 3 and 4 because less than 3 out of 5 samples formed microcracks and a standard deviation could not be calculated. The microcracking

temperatures were essentially the same for prepregs 1 and 2, which was consistent with their similar composition. The use of dicy/diuron as the curing agent in prepreg 3 increased the microcracking temperature, which was consistent with the results in chapter 3. The model correctly predicted the onset of microcracking for laminates made from prepregs 1-3. In the case of prepreg 4, the model predicted microcracking between –140°C and -60°C, while microcracking actually occurred at –190°C.

The microcracking temperature may have been underpredicted for prepreg 4 due to the fact that it was supplied by an industrial source. The properties of this material were known less accurately than those of the prepregs that were produced in the laboratory. It was also possible that the longitudinal and transverse coefficients of thermal expansion were no longer temperature-independent or the dependence of the tensile moduli on temperature deviated from linearity as the temperature approached the microcracking temperature ($\approx$-200°C). Instrumental limitations prevented the recording of data below –120°C; therefore, the property variation with temperature trends in the –100°C to 0°C temperature range were extended to lower temperatures.

10.4 CONCLUSIONS

Symmetric, cross-ply carbon fiber/epoxy laminates were produced and exposed to sub-ambient temperatures to determine the microcracking onset temperature. These data were then compared with the predictions of a stress-based compound beam model in which fracture mechanics was used to determine the *in situ* yield strength of the ply groups in the laminates and the variation in material properties at low temperatures was accounted for. The model correctly predicted the failure temperature for most of the materials tested. In addition, it showed that accurate predictions of thermal stress-induced failure can be made using the room temperature properties of a laminate, appropriately modified to account for low temperature property variation. Microcracking changed the dynamic mechanical properties of the composite materials studied, and it was shown that dynamic mechanical analysis could be used to assess the formation of microcracks.

NOTES TO CHAPTER 10

1. Wigley, D.A. 1985. <u>Basic Cryogenics and Materials</u>, NASA-CR-177932, NASA.

2. Toth, J.M., Jr., W.J. Bailey and D.A. Boyce. 1985. <u>Fiberglass Epoxy Laminate Fatigue Properties at 300 and 20 K</u>, p. 163.

3. Toth, J.M., W.J. Bailey and D.A. Boyce. 1985. <u>Fatigue at Low Temperatures</u>, *in ASTM Stp 857*, ASTM: Philadelphia, p. 163.

4. Ambur, D.R., J. Sikora, J.F. Maguire and P.M. Winn. 1996. <u>Development of a Pressure Box to Evaluate Reusable-Launch-Vehicle Cryogenic-Tank Panels</u>, NASA-TM-11406, AIAA Paper 96-1640, NASA.

5. Nelson, K.M. 1999. <u>Composites in Cryogenic Fuel Tank Applications</u>, Boeing Materials Technology - Phantom Works, Seattle, WA.

6. Liokhman, V.V., L.N. Kopsitskaya and V.M. Muratov. 1997. <u>Stress-Strained State of Cryogenic Vessel Under Cyclic Loading With Internal Pressure</u>, *Khimicheskoe I Neftyanoe Mashinostroenie*, 6: 22-24.

7. Nguyen, B. 1999. <u>Cryotank Skin/Stringer Bondline Analysis</u>, *Proceedings of 44th International SAMPE Symposium*, Long Beach, CA, 44: 856.

8. Wood, C. and W. Bradley. 1996. <u>A New Technique to Study the Interfacial Strength and Transverse Cracking Scenario in Composite Materials</u>, *In Fiber Matrix and Interface Properties, ASTM STP 1290*, ASTM: Philadelphia, p. 132.

9. Mcmanus, H.L., D.E. Bowles and S.S. Tompkins. 1996. <u>Prediction of Thermal Cycling Induced Matrix Cracking</u>, *Journal of Reinforced Plastics and Composites*, 15: 124.

10. Nairn, J.A. 1989. <u>The Strain Energy Release Rate of Composite Microcracking: A Variational Approach</u>, *Journal of Composite Materials*, 23: 1106.

11. Michii, Y. and H.L. Mcmanus. 1997. <u>Prediction of Microcracking Distributions in Composite Laminates Using a Monte-Carlo Simulation Method</u>, *Journal of Reinforced Plastics and Composites*, 16(13): 1220.

12. Wang, J. and B.L. Karihaloo. 1996. <u>Optimum *In Situ* Strength Design of Composite</u>

Laminates. Part I: *In Situ* Strength Parameters, *Journal of Composite Materials*, 30(12): 1314.

13. Wang, J. and B.L. Karihaloo. 1996. Optimum *In Situ* Strength Design of Composite Laminates. Part II: Optimum Design, *Journal of Composite Materials*, 30(12): 1338.

14. Takeda, N. and S. Ogihara. 1994. *In Situ* Observation and Probabilistic Prediction of Microscopic Failure Processes In CFRP Cross-Ply Laminates, *Composites Science and Technology*, 52: 183.

15. Mallick, P.K. 1993. Fiber Reinforced Composites: Materials Manufacturing and Design, 2nd ed., Marcel Dekker: New York, pp. 566.

16. Rodriguez, F. 1996. Principles Of Polymer Systems, 4th ed., Taylor and Francis: Washington D.C., pp. 732.

17. Markley, F.W., J.A. Hoffman and D.P. Muniz. 1986. Cryogenic Compressive Properties of Basic Epoxy Resin Systems, *Advances in Cryogenic Engineering*, 32: 119.

18. Schaffer, J.P., A. Saxena, S.D. Antolovich, T.H. Sanders, Jr. and S.B. Warner. 1995. The Science and Design of Engineering Materials, Irwin: Chicago, pp. 842.

19. Nettles, A.T. and E.J. Biss. 1996. Low Temperature Mechanical Testing of Carbon-Fiber/Epoxy-Resin Composite Materials, NASA-TP-3663, NASA.

20. Bailey, J.E., P.T. Curtis and A. Parvizi. 1979. On the Transverse Cracking and Longitudinal Splitting Behavior of Glass and Carbon Fibre Reinforced Epoxy Cross Ply Laminates and the Effect of Poisson and Thermally Generated Strain, *Proceedings of the Royal Society of London, Series A*, 366: 599.

21. Brand, R.H. and S. Backer. 1962. Mechanical Principles of Natural Crimp of Fiber, *Textile Research Journal*, 32: 39.

22. Laws, N. and G.J. Dvorak. 1987. Effect of Fiber Breaks and Aligned Penny-Shaped Cracks on the Stiffness and Energy Release Rates in Unidirectional Composites, *International Journal of Solids and Structures*, 23(9): 1269.

23. Putnam, J.W., B.S. Hayes and J.C. Seferis. 1996. Prepreg Process-Structure-Property Analysis and Scale-Up for Manufacturing and Performance, *Journal of Advanced Materials*, 27(4): 47.

24. 1999. Standard Test Methods for Constituent Content of Composite Materials,

ASTM D 3171-99, ASTM: West Conshohocken, PA.

25. 1996. <u>Resin Content and Fiber Areal Weight of Prepreg Fabric and Tape, Test Method for</u>, BSS 7336, Boeing Materials Technology, Boeing Commercial Aircraft Group, Renton, WA.

26. Pagano, N.J., Ed. 1989. <u>Interlaminar Response of Composite Materials</u>, Elsevier: New York, Ch. 4.

27. Kennedy, J.M., D.D. Edie, A. Banerjee and R.J. Cano. 1992. <u>Characterization of Interfacial Bond Strength by Dynamic Analysis</u>, *Journal of Composite Materials*, 26(6): 869.

28. Adams, D.S., D.E. Bowles and C.T. Herakovich. 1986. <u>Thermally Induced Transverse Cracking in Graphite-Epoxy Cross-Ply Laminates</u>, *Journal of Reinforced Plastics and Composites*, 5: 152.

LIST OF TABLES

Table 10-1. Prepreg characteristics

| Prepreg | Carbon Fiber | | | Prepreg Resin | Prepreg Fiber Areal |
	Type	Epoxy Formulation	Curing Agent	Content (wt. %)	Weight (g/m^2)
1	T300 YC	3:1 1031:828	DDS	54.7 (0.77)	124.0 (2.26)
2	T300 YC	3:2 1031:828	DDS	45.3 (0.65)	129.9 (1.60)
3	T300 YC	2.4:2:1 828:661:1031	Dicy/Diuron	47.0 (1.00)	144.5 (2.40)
4	T-50S	-	-	47.7 (0.021)	100.0

LIST OF FIGURES
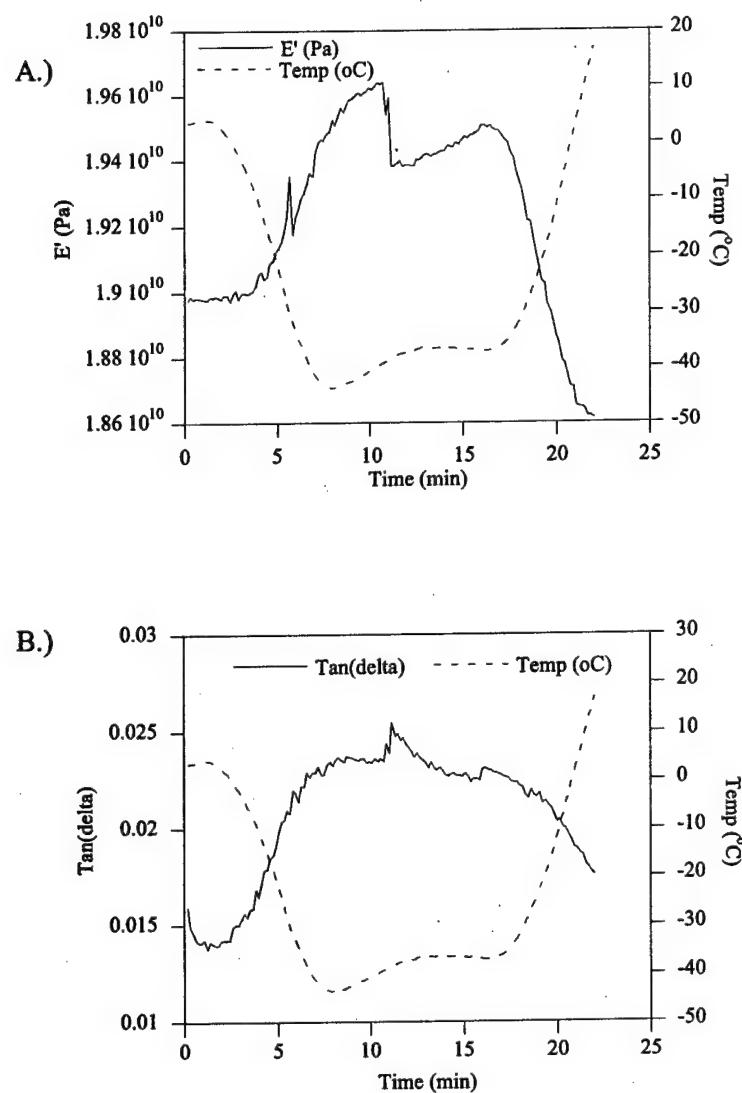
Figure 10-1. Effects of cryogenic temperatures and microcracking on the dynamic
mechanical properties of symmetric laminates. A.) Storage modulus B.)
tan(δ)
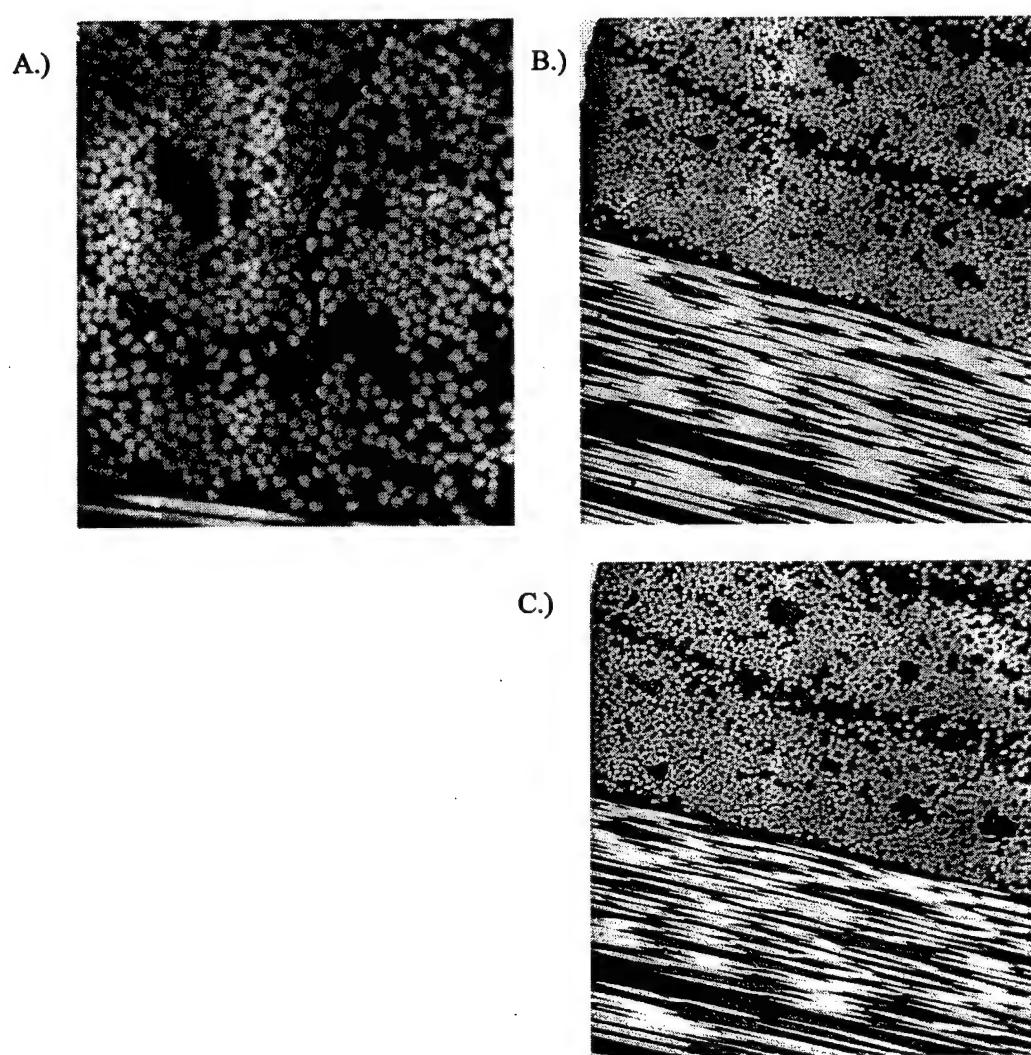
Figure 10-2. Optical photomicrographs of microcracks. A.) Prepreg 2, 200x, -40°C, B.) Prepreg 1, 100x, -40°C, C.) Prepreg 1, 100x, -60°C, extension of crack in B
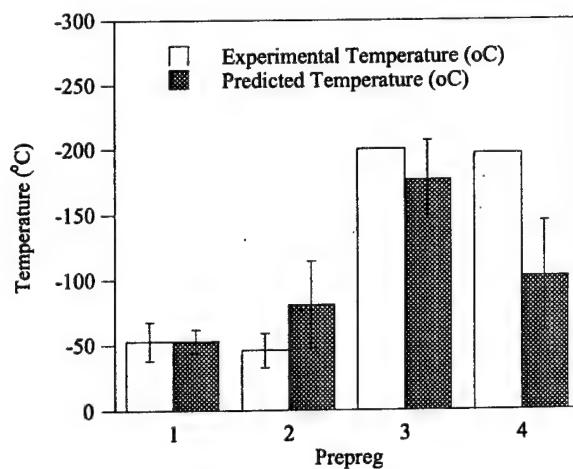
Figure 10-3. Comparison of predicted and experimental microcracking onset temperatures

CHAPTER 11: CONCLUSIONS AND RECOMMENDATIONS

11.1 CONCLUSIONS

In this work the behavior of carbon fiber/epoxy composites at low temperatures was investigated. Of particular interest was the generation of internal stresses during thermal cycling between cryogenic and ambient temperatures. These stresses reached a level at which failure of the composite occurred through the formation of transverse microcracks and delamination between ply groups. These phenomena were analyzed using a process-structure-property methodology. This approach allowed the effects of the components of a composite material, the fibers and the matrix, to be investigated along with the interface between the matrix and the fibers, the processing conditions during laminate fabrication, and the nature of the thermal cycle. Understanding the links between the processing and structure of a composite material facilitated the development of a fundamental knowledge base on how these parameters influenced the performance of composite materials at low temperatures. The majority of this work used a phenomenological approach to identify the important variables in matrix microcracking during cryogenic cycling. Once these variables had been identified, a model was developed to predict the thermal strains generated in composite materials at low temperatures and the temperature at which microcrack formation occurred.

The first set of variables to be explored was the structure of the matrix and fibers used in the composite materials studied. It was found that the type of fibers and the polymeric matrix used in the composites played a large role in determining the propensity for microcracking as well as the microcrack morphology in symmetric cross-ply carbon fiber/epoxy composites. The microcrack density increased and larger cracks were formed when fibers with larger tensile moduli and longitudinal coefficients of thermal expansion were used. Increased flexibility of the polymeric matrix decreased the glass transition temperatures of the laminates studied and caused an increase in the microcrack density. The response of composite materials to cryogenic cycling was found to be influenced by the type of curing agent used. A curing agent that led to stiffer and more regular network structures resulted in a decrease in microcrack density. The presence of a rubber

interpenetrating network toughener prevented the formation of microcracks in all of the laminates studied. It was shown that the fibers and the matrix used in a composite altered the thermal stresses present in a material as well as the ability of the material to resist thermal stresses, and therefore, had a direct influence on matrix microcracking at cryogenic temperatures.

The second set of variables to be investigated was the interaction between the fibers and the matrix in the interfacial region. Symmetric cross-ply carbon fiber-reinforced polymeric composite materials were prepared using fibers with different surface chemistries. Variations in the fiber surface chemistry changed the fiber-matrix adhesion in laminates containing these fibers. The fiber-matrix adhesion had a direct impact on the microcrack density in composite materials after cryogenic cycling. The laminates with good adhesion exhibited lower microcrack densities than the laminates with poor adhesion. Surfactant sized fibers outperformed traditional epoxy sized fibers by yielding composites with improved mechanical properties and resistance to microcracking.

The effect of rubber type and concentration was investigated to understand how traditional toughening techniques performed at cryogenic temperatures. Variations in rubber amount (10 and 20 phr) and compatibility (two different acrylonitrile contents) with the model resin provided different levels of phase separation in the laminates. Five resin systems were developed and impregnated into unidirectional carbon fibers to be cured at two different temperatures. Both the glass transition temperature and the interlaminar shear strength of the parts were depressed due to the addition of rubber, especially when the more compatible rubber (higher acrylonitrile content) was used. Symmetric cross-ply laminates were exposed to cryogenic cycling and all but the most highly rubber modified of the composite materials formed microcracks in response to the thermal stresses generated during exposure to low temperature. A higher rubber concentration gave a greater crack resistance by most likely increasing the toughness of the matrix. It was shown that an increase in reactive liquid polymer concentration in carbon fiber/epoxy based laminates led to a decrease in the microcrack density resulting from cryogenic cycling.

After the effectiveness of liquid rubber in decreasing the microcrack density in cryogenically cycled composites was studied, the influence of the rubber type and distribution was investigated. Three different rubbers were used. Cross-linked carboxyl functionalized preformed rubber particles, carboxyl functionalized core-shell particles, and solid carboxyl functionalized rubber were used to modify the prepreg matrices in order to obtain various distributions: Interlayer toughening, dispersion throughout the matrix, and an interpenetrating network, respectively. The eight different systems developed included a control, each rubber separately, and every combination. The same cryogenic cycling procedure was applied to these laminates and most of the laminates formed microcracks in response to the thermal stresses generated by cryogenic cycling. Interlayer toughening did not significantly reduce the crack density, but the dispersed core-shell particles reduced it by 50%. The dissolved solid carboxyl functionalized rubber, providing an interpenetrating network, was shown to reduce the microcracking the most efficiently. It was shown that the level of microcracking in an inherently brittle system could be reduced substantially by the addition of various types of rubber additives; furthermore, it was shown that the microcrack density was highly dependent on the distribution and amount of rubber added to the system.

Modification of the polymeric matrix on the nano and micro scale and its effects on microcracking was studied using layered clays as nanoparticle fillers and alumina particles as microfillers in fiber-reinforced polymeric materials. When nanoparticle fillers were used at concentrations much lower than those used for traditional fillers a significant reduction in cryogenic microcracking was observed. The concentration of the particles and their distribution in the matrix were important parameters in the optimization of the benefits of nanoparticle reinforcement. A typical, macro-scale filler effect was seen at large concentrations of nanoclay, and low concentrations showed little or no effect. The best reinforcement was provided by exfoliated and disordered intercalated structures, with more ordered intercalated structures, which were seen at large clay concentrations, offering little benefit. The mechanical properties and processing characteristics of the laminates studied were not adversely influenced by the presence of the nanoparticles and the thermal expansion characteristics were improved.

It was shown that the resistance of traditional fiber-reinforced composite materials to microcracking during cryogenic cycling could be enhanced using nanoparticle modification.

After studying the effects of the composite components on cryogenic microcracking, work was performed on the effects of composite lay-up, laminate thickness, and thermal ramp rate. The following lay-up schedules were subjected to a previously established thermal cycle for Kevlar® based composites: $[0_5/90_5]_s$, $[0/90]_{10}$, 20 ply unidirectional and 20 ply woven. After 1200 thermal cycles the greatest microcrack density was found in a symmetric cross-ply laminate on the $[90_5/0_5]_s$ side where the 90° layer contacted the bag. Based on these findings, $[90_5/0_5]_s$, $[90_4/0_4]_s$, $[90_3/0_3]_s$ and $[90_2/0_2]_s$ symmetric laminates were prepared and exposed to a thermal cycle using ramp rates of 2.5°C/min, 5°C/min, 10°C/min and 20°C/min. It was found that a certain minimum thickness of the laminate was required to generate enough internal stress for microcracks to appear. A thermal ramp rate of 2.5°C/min allowed thermal equilibrium to be reached in the thickest panels, but at higher ramp rates a skin core effect was observed that hindered microcracking. The $[90_4/0_4]_s$ laminate appeared to be the ideal cross-ply laminate to study microcracking induced by thermal cycling in this material. For a given composite system subjected to a specific thermal cycle, the lay-up and thickness of the laminate can be adjusted to maximize microcrack sensitivity.

The last variable explored was the processing conditions, namely the cure temperature, of a composite material. A theoretical and experimental analysis was performed on carbon fiber/epoxy symmetric cross-ply laminates to investigate microcracking and the development of thermal stresses at low temperatures. Experimental results correlated with the theoretical predictions of the development of thermal strains in composite materials. Microcracking occurred in all of the laminates tested, but the number and morphology of the microcracks was strongly dependent on the cure temperature. Higher stress free temperatures, residual thermal strains, and glass transition temperatures of the laminates were all the results of elevated cure temperatures. The larger stress free temperatures corresponded to increased microcrack densities and larger levels of residual thermal strain. Larger cure temperatures resulted in laminates

with a greater propensity to delaminate, contain wider and more tortuous cracks, and form networks of cracks when cycled between ambient and cryogenic temperatures. The development of thermal stresses in composite materials at cryogenic temperatures was modeled and the levels of these stresses were enhanced by higher cure temperatures.

The investigation of the role of the cure temperature in thermal stress generation was extended to develop a model that predicted the onset temperature for microcracking in symmetric cross-ply carbon fiber/epoxy laminates based on the thermal stresses in a laminate and the yield strengths of the ply groups in a laminate at sub-ambient temperatures. The fact that the model accounted for the change in material properties at cryogenic temperatures by predicting the low temperature behavior of the ply groups in a laminate based on the room temperature properties of the plies made it unique. It was also found that microcrack formation caused a discontinuity in material properties that could be detected using dynamic mechanical analysis. Four different material systems were studied, and the model was found to accurately predict the onset temperature for microcracking in three of the four cases. It was shown that microcracking resulting from thermal cycling and thermal stresses could be predicted based on the room-temperature properties of a laminate, with appropriate modifications for property variation at low temperatures.

Taken as a whole, this work comprised a phenomenological and theoretical investigation of cryogenic microcracking in composite materials. The results presented here furthered the understanding of the causes and mechanisms of cryogenic microcracking and will be of utility in the development of composite materials and structures that operate at low temperatures.

11.2 RECOMMENDATIONS FOR FUTURE WORK

The studies that have been performed so far have characterized microcracking in fiber-reinforced composites at cryogenic temperatures and predicted the onset temperature for crack formation. However, the distribution and number of microcracks and the formation of microcracks in an already cracked material have not been satisfactorily predicted. It is proposed that a model that could predict how the low

temperature properties of a composite material changed with microcrack formation would be very useful for the design of composite structures and would facilitate a deeper understanding of cryogenic microcracking [1-3]. If the variation in properties with microcracking was known, it could be incorporated into a model similar to the one presented in this work and used to predict additional microcracking after the first failure event. An understanding of the changes in the local stress state of a composite material with microcracking could be used to gain a deeper knowledge of how thermal stresses develop in a microcracked material and how microcracks are distributed during failure.

Composite structures that are used for the storage and transportation of cryogenic liquids are exposed to a dynamic environment that was not accounted for in previous studies of microcracking. Future work will investigate the effects of the frequency and amplitude of loads applied to a composite specimen during cryogenic cycling. These loads will alter the stress state in a material and have the potential to change the microcracking behavior of cryogenically cycled materials.

Recent work on the modification of the matrix in fiber-reinforced composite materials has shown that microcracking can be reduced by the incorporation of toughening agents into the matrix. Second phase liquid rubber tougheners have been used to reduce microcracking, as have nanoclay particles [4]. It has been shown that rubber/clay nanocomposites can be formulated and that they can exhibit improved properties over the neat rubber [5, 6]. It is proposed that modifying the dispersed rubber phase with nanoclay structures could improve the properties of a traditionally toughened composite material. Stiffening of the second phase may prevent the decrease in glass transition temperature and matrix stiffness that is often associated with rubber tougheners. Alignment or preferential orientation of the nanoparticles at the interface between the phases could also result in improved properties of the bulk composite. Much work remains to be done to understand how toughening agents reduce microcracking and how nanoparticles interact with larger, macro-sized structures in composite materials.

NOTES TO CHAPTER 11

1. Nairn, J.A. 1989. The Strain Energy Release Rate of Composite Microcracking: A Variational Approach, *Journal of Composite Materials*, 23: 1106.

2. McManus, H.L., D.E. Bowles and S.S. Tompkins. 1996. Prediction of Thermal Cycling Induced Matrix Cracking, *Journal of Reinforced Plastics and Composites*, 15: 124.

3. Michii, Y. and H.L. McManus. 1997. Prediction of Microcracking Distributions in Composite Laminates Using a Monte-Carlo Simulation Method, *Journal of Reinforced Plastics and Composites*, 16(13): 1220.

4. Nobelen, M.J-K., B.S. Hayes and J.C. Seferis. 2002. Cryogenic Cycling of Carbon Fiber/Epoxy Composites: Effects of Matrix Modification, *Proceedings of 47th International SAMPE Symposium*, Long Beach, CA, 47: 1539.

5. Kojima, Y., K. Fukimori, A. Usuki, A. Okada and T. Kurauchi. 1993. Gas Permeabilities in Rubber-Clay Hybrid, *Journal of Materials Science Letters*, 12: 889.

6. Okada, A., K. Fukimori, A. Usuki, Y. Kojima, N. Sato, T. Kurauchi and O. Kamigaito. 1991. Rubber-Clay Hybrid - Synthesis and Properties, *Polymer Preprints (American Chemical Society, Division of Polymer Chemistry)*, 32(3): 540.